STURCTURE AND CHEMISTRY OF DEFECT PASSIVATION AT THE INTERFACE BETWEEN SILICON DIOXIDE AND SILICON CARBIDE

by

YI XU

A dissertation submitted to the

Graduate School-New Brunswick

Rutgers, The State University of New Jersey

In partial fulfillment of the requirements

For the degree of

Doctor of Philosophy

Graduate Program in Chemistry and Chemical Biology

Written under the direction of

Eric L. Garfunkel and Leonard C. Feldman

And approved by

_____

_____

_____

_____

New Brunswick, New Jersey

October, 2014

ABSTRACT OF THE DISSERTATION

STURCTURE AND CHEMISTRY OF DEFECT PASSIVATION AT THE INTERFACE BETWEEN SILICON DIOXIDE AND SILICON CARBIDE

By YI XU

Dissertation Director:

Eric L. Garfunkel and Leonard C. Feldman

Silicon carbide (SiC) is a wide bandgap semiconductor which has material properties well-suited for high-power, high-temperature electronics applications. The performance of SiC transistors is limited by electrical defects formed at the SiO_2/SiC interface under high temperature oxidation. A central goal of this work is to improve our atomic level understanding of electrical defects in SiC devices, and to further develop methods to minimize defects. Introduction of interfacial nitrogen (N) or phosphorus (P) reduces the interface (charge) trap density, increases the SiC charge mobility (in the semiconductor channel), and thus device performance.

This dissertation is focused on the chemistry of the SiO_2/SiC interface, the critical interface in future SiC-based devices. We address issues of composition, structure,

chemical bonding, and reaction behavior of N and P that we have used to improve device performance.

We report photoemission and ion scattering studies to determine the concentrations of N and P passivating agents at the SiO_2/SiC interface, and develop a more complete understanding of the mechanism and kinetics for the passivation processes on different crystallographic surfaces. The study shows that N (and P) passivated SiO_2/SiC structures have a thin oxy-nitride (oxy-phosphide) interface dielectric layer that cannot be removed by a buffered HF etchant. The same dielectric structures are completely etched when formed on Si. Atomic scale modeling, combined with our experimental observations, results in the suggestion of likely bonding structures of N and P at the SiO_2/SiC interface. The depth profile of N and P at SiO_2/SiC interface has also been established and provides further insights into the nature of N and P as surface passivating additives.

DEDICATION

To my mentors:

Prof. Eric L. Garfunkel, who taught me about Surface Science

Prof. Torgny Gustafsson, who taught me about the Physics of Ion Scattering

and

Prof. Leonard C. Feldman, who taught me everything about SiC and wide band gap semiconductors and guided me through the dissertation work.

To my beloved family and friends

ACKNOWLEDGEMENTS

First, I would like to express my deepest gratitude to my dissertation advisor Professor Eric L. Garfunkel and co-advisor Professor Leonard Feldman, for introducing the world of surface science and semiconductor materials to me, for bringing out my potential, for their support, guidance, encouragement, and patience.

I would also like to thank my dissertation committee members, Prof. Jane Hinch, Prof. Tewodros Asefa, and Prof. Jing Li for taking time off of their busy schedule to review my dissertation and participate in my defense.

I could not have come this far without the help of the many people I met and interacted with since my arrival at Rutgers. They gave me essential assistance in my graduate studies as well as my research. My research program is the result of collaboration between several groups at Rutgers as well as multiple universities and institutes.

My thanks go to Drs. Chien-Lan Hsueh and Ozgur Celik who taught me about doing research with ultrahigh vacuum systems and guide me through the process of designing and building my own equipment. This has benefited me in many different aspects. They also taught me about atomic layer deposition (ALD) and semiconductor etching for MEMS (microelectromechanical systems). These two projects, as well as work on ZnO (including two published papers to which I contributed), have not been included in this thesis. I would also like to thank Dr. Xingguang Zhu for helping me start with this project, Dr. Gang Liu for electrical measurement and collaborating with me during the last three years, Dr. Leszek Wielunski for all the RBS and NRA measurements, Dr. Tian Feng, Mr. Can Xu, Dr. Hang Dong Lee, Dr. Samir Shubeita for

MEIS measurements and other help, Dr. Alan Wan for discussions during his time in Rutgers and SIMS measurement during his time at the Evans Analytical Group. My thanks also go to the essential help on sample preparation, electrical measurement and many valuable discussions with Prof. Sarit Dhar, Prof. Ayayi C. Ahyi, Dr. Yogesh Sharma, Mr. Aaron Modic, Mr. Chunkun Jiao, Ms. Tamara Isaacs-Smith and Prof. John R. Williams from Auburn University, and Prof. Zengjun Chen at Tuskegee University. I would also like to thank Prof. Blair R. Tuttle from Pennsylvania State University – Erie, Dr. Xiao Shen and Prof. Sokrates T. Pantelides from Vanderbilt University for the theoretical calculations, which bring our experimental work to another level. Many thanks also go to Prof. Torgny Gustafsson, Dr. Sylvie Rangan and Prof. Robert A. Bartynski for their advice and guidance.

My thanks also go to my colleagues, Dr. Lei Yu, Mr. Daniel Mastrogiovanni, Dr. Lauren Klein, Dr. Ning Wu and Dr. Joseph Bloch, my collaborators Dr. Ziqing Duan, Dr. Jeren Ku, Dr. Pavel Ivanoff Reyes, Mr. Yang Zhang, Mr. Rui Li, Mr. Wen-chiang Hong, Mr. Tengfei Xu, Mr. Robert Lorber, Prof. Warren Lai, Prof. Jaeseok Jeon and Prof. Yicheng Lu, for their kind help to the work not included in this dissertation.

This work has been supported by U.S. Army Research Laboratory (W911NF-07-2-0046), the II-VI foundation block-gift program cooperative research initiative and NSF (DMR -1006740, -0907385, -1106070, -1206793, -1206655, and -1206256). During my first years at Rutgers I was also supported in part by a grant from Qualcomm (on a MEMS project).

TABLE OF CONTENTS

LIST OF FIGURES

LIST OF TABLES

Chapter 1. Introduction

1.1. General introduction

This dissertation is focused on the chemistry of the SiO_2/SiC interface, the critical interface in future SiC based devices. We address issues of composition, structure, chemical bonding, and reaction behavior of nitrogen and other potential "passivating" species used to improve the device electrical properties.

Chapter 1 includes a general analysis of group IV semiconductors that are relevant to electronics applications, especially SiC, including some aspects of their history, crystallography and applications. SiO_2/SiC interface issues and passivation approaches are also reviewed.

Chapter 2 briefly introduces the main techniques that used in this research, which include X-ray photoemission spectroscopy (XPS), Rutherford backscattering (RBS), nuclear reaction analysis (NRA), medium energy ion scattering (MEIS), secondary ion mass spectrum (SIMS), and capacitance-voltage (CV) electrical measurements.

The addition of nitrogen is the preferred method of lowering the density of electrical defects and improving device performance of SiC-based devices. In chapter 3, we quantify the areal density, establish the depth profile and study the chemical environment of nitrogen that is introduced by several different chemistries to the SiO_2/SiC interface.

In chapter 4, the kinetics of N incorporation at the SiO_2/SiC interface is investigated for different crystal orientations of 4H-SiC, including the C-face, Si-face and a-face (see below, page 9).

In chapter 5, we examine phosphorus passivation of SiO_2/SiC interface (as an alternative to N). In additional to quantifying and determining the depth distribution of P, we determine its chemical behavior, which is somewhat distinct from N.

1.2. Some properties of group IV semiconductors

Table 1.1. Comparison of some basic properties of group IV semiconductors.

	Diamond	Si	Ge	4H-SiC
Dielectric constant ($\varepsilon_S/\varepsilon_0$)	5.5	11.8	16	10
Bandgap (eV)	5.45	1.12	0.66	3.26
Intrinsic carrier concentration (cm^{-3})		1.45×10^{10}	2.4×10^{13}	5×10^{-9}
Electron mobility ($cm^2/V\ s$)		1450	3900	900//c-axis 800 ⊥ c-axis
Hole mobility ($cm^2/V\ s$)		480	1900	115
Break down field (MV/cm)		0.3	0.1	2.2
Electron Saturation velocity (10^7 cm/s)		1	3	2
Native oxide	none	SiO_2	GeO_2 (water soluble)	SiO_2

Silicon-based semiconductor devices have played the central role in the development of the microelectronics industry over the past 50+ years, and Si remains the

dominant semiconductor in most electronic devices. In addition to its low cost, one of the main reasons for the longevity of Si is that its native oxide, SiO_2, is very stable and yields an SiO_2/Si interface that has very few electrical defects. This latter property is essential for device electrical performance. Over the past 5+ decades the semiconductor industry has developed a very thorough set of fabrication processes involving Si that make it hard to be replaced. Nevertheless, for certain special applications, other group IV elements can be employed as more suitable semiconductors. A comparison of some basic properties of group IV semiconductors is shown in Table 1.1.

Table 1.2. Comparison of some basic properties of wide band gap semiconductor

	4H-SiC	GaN (wurtzite)
Dielectric constant ($\varepsilon_S/\varepsilon_0$)	10	9.0
Bandgap (eV)	3.26	3.39
Intrinsic carrier concentration (cm^{-3})	5×10^{-9}	2×10^{-10}
Electron mobility ($cm^2/V\ s$)	900//c-axis 800 $\perp$ c-axis	500
Hole mobility ($cm^2/V\ s$)	115	80
Break down field (MV/cm)	2.2	3
Saturation e velocity (10^7 cm/s)	2	1
Native oxide	SiO_2	Ga_2O_3

There has been an increasing demand for higher power and higher temperature devices; unfortunately Si cannot fully satisfy the need due to its own thermal and

electrical limitations. In order to reduce the energy loss during operation, for some applications we need power devices which can be operated at high switching speeds and work at voltages of up to 20kV.[1-3] The main approach to realizing this new class of power devices is to use a wide band gap semiconductor.[4]

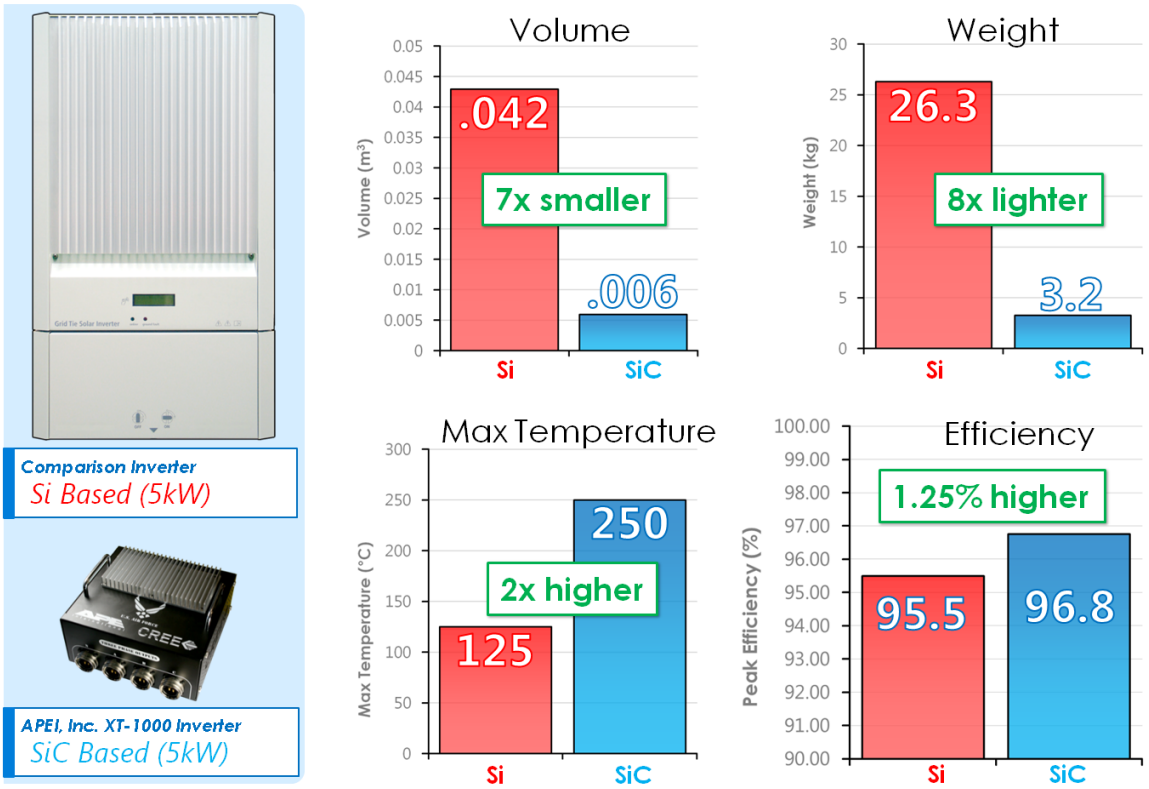

Fig. 1.1. System comparison of Si-based and SiC-based inverter (an electronic device that converts direct current to alternating current). Adapted from A. Agarwal and M. Sofos, 2013.[5]

Silicon carbide (SiC) and gallium nitride (GaN) are the two most studied materials that researchers and industry are exploring to replace Si in high power applications. A comparison of basic physical and electrical properties of SiC and GaN is shown in Table 1.2. A comparison of Si-based and SiC-based inverters, which convert direct current to

alternating current, also one of the first and most immediately desired high power applications of SiC, is shown in Fig. 1.1. It is important to note that SiC is also the only material that has the same native oxide as Si, which makes it possible to adopt many well-developed Si fabrication techniques for SiC metal-oxide-semiconductor (MOS) devices. In addition, some of SiC's other properties also make it superior to other semiconductors, such as its wide band-gap, low dielectric constant, high critical field and high thermal conductivity. All of these properties make SiC an excellent candidate for high power, high temperature and radiation-tolerant devices applications, especially for power MOS devices, which is the main technological motivation of this work.

1.3. Introduction to SiC history and applications

Silicon carbide is a compound semiconductor with a 1:1 ratio of silicon and carbon atoms. The material was first discovered in nature by Moissan in a meteorite in 1893 and named Moissanite after him in 1905.[6] The first recorded scientific study of SiC dates to 1824 by Jöns Jacob Berzelius,[7] where he proposed a possible bond between Si and C. Then at around 1885, E.G. Acheson started to manufacture the material in an electric smelting furnace.[8] The crystalline products that Acheson made were found to have great hardness, refractabiliy and chemical inertness.[8] Later, a process for growing high quality SiC crystals was developed by Lely in 1955.[9] In 1978, a new process using a seeded sublimation for substrate growth was introduced by Tairov and Tsvetkov.[10] This discovery helped draw attention back on to the development of SiC technology. The growth of single crystal SiC on a Si substrate was later demonstrated by Matsunami et al[11] in 1981. Recently high quality 4 inch and 6 inch SiC wafers have become

commercially available. In 1998 Cree developed a process to manufacture gem quality SiC. Because of its hardness and excellent optical properties, SiC (Moissanite) is now also sold as an alternative to diamond, and has a high hardness on the Mohs scale (9.5, diamond is 10.0).

The first application of SiC in electronic devices was in light emitting diodes (LEDs); the first SiC LED was made as early as 1907.[12] The main current uses of SiC are as a structural material and a semiconductor material. In addition to being used as abrasives and cutting materials, SiC is also a favorite material for heating elements, ceramic membrane and mechanical parts.

As a semiconductor material, SiC is used as a substrate for power devices, such as ultra-fast Schottky diodes and metal-oxide-semiconductor field effect transistors (MOSFET). Silicon carbide is also widely used in blue light emitting diodes (LED) as a substrate on which gallium nitride is grown.

1.4. SiC crystallography

There are many different crystal structures known to exist for SiC, however, each is composed of the same tetragonal structural units (similar to the diamond structure of pure C), with each silicon atom surrounded by four carbon atoms and vice versa, as shown in Fig. 1.2. The distance between each Si and C atom is 1.89 Å, and the distance between two neighboring silicon (or carbon) atoms is approximately 3.08 Å.[13]

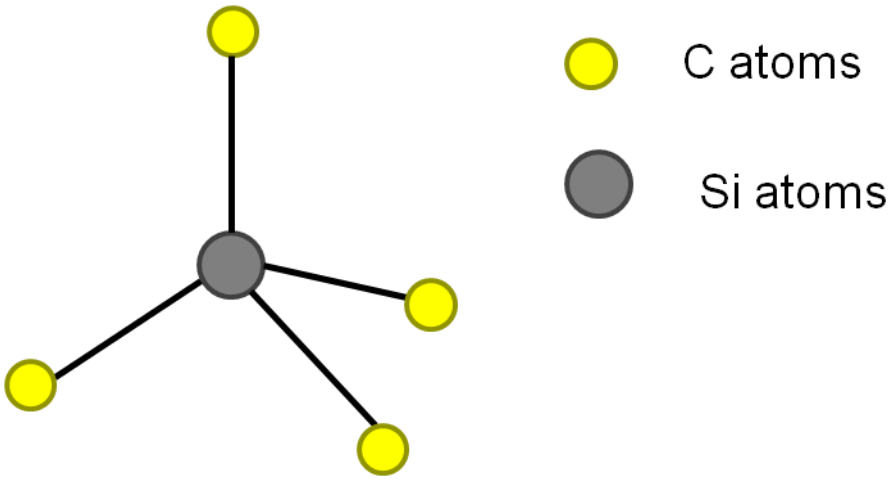

Fig. 1.2. The local tetragonal structure around each atom in the SiC crystal.

One of the most significant characteristics of the silicon carbide crystal is that is can occur in various polytypes. A polytype is a sub-class of polymorphs (which described different atomic/molecular structures for an otherwise compositional equivalent compound) in which the structure varies by changing the stacking in one dimension. The polytype structures of SiC are Si and C double layers that stack with different repeating sequences, with each repeating sequence ranging from two to several hundreds of bi-atom layers. At present, there are more than 200 known polytypes of SiC,[14] each with a different bi-atom layer stacking sequence with the exact same stoichiometry. The various polytypes have distinctively different physical and electrical properties; only a few polytypes are commonly used as electronic semiconductors.

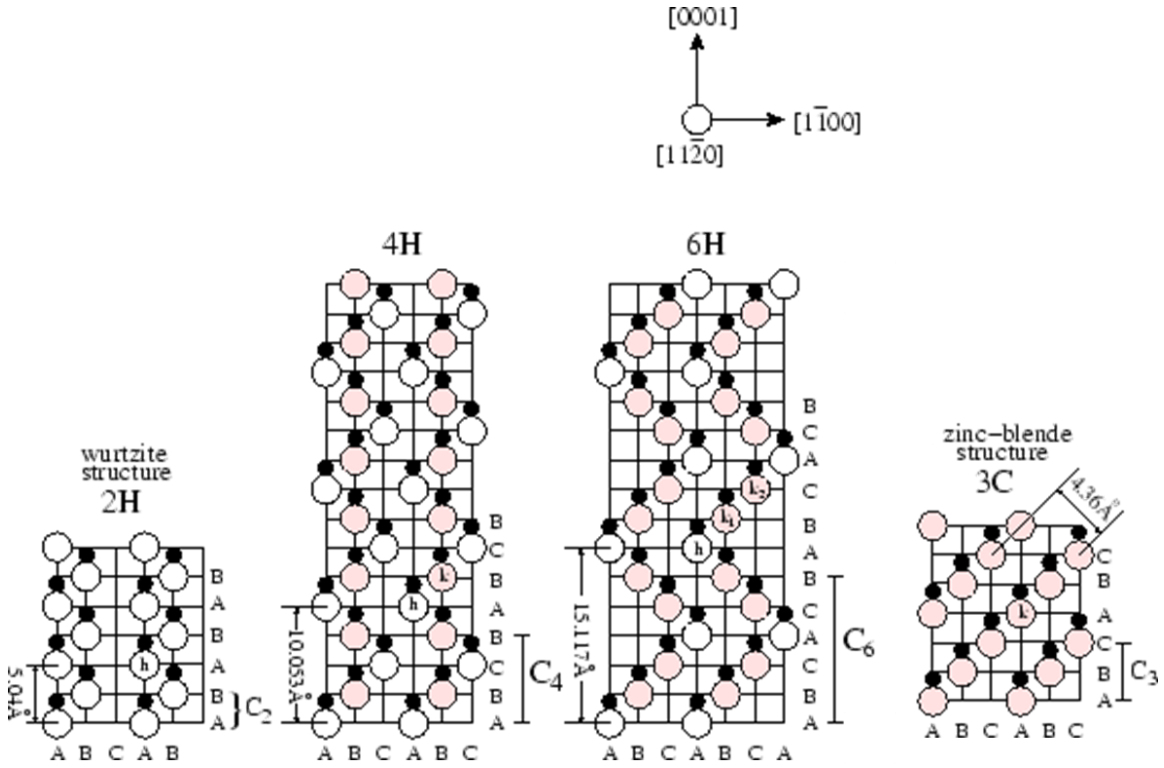

Fig. 1.3. Stacking sequence for common SiC crystalline polytypes. (Adapted from Ayalew, 2004)[15]

The most common polytypes used in electronic applications are cubic SiC (3C), rhombohedral SiC (15R), and hexagonal SiC (4H and 6H). Their stacking sequences are shown in the Fig. 1.3. Each Si and C double layer projects onto one of the lattice positions, labeled A, B and C, with different stacking sequence.

Among the hundreds of polytypes, the cubic (zinc-blende) and hexagonal (wurtzite) crystalline structures are most commonly seen. 3C-SiC is the only known form of SiC with a cubic crystal lattice structure. The rest of the polytypes are hexagonal, also referred as α-SiC. For the hexagonal structure, the most commonly used polytypes are 2H, 4H, and 6H.

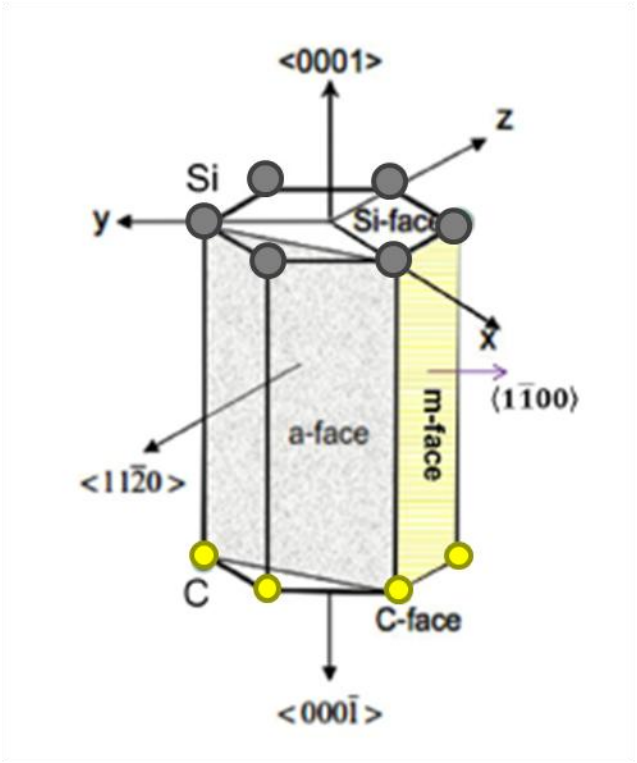

Fig. 1.4. Different crystal faces of 4H-SiC.

Hexagonal SiC are anisotropic materials, hence even within the same polytypes, physical properties, electrical properties and fabrication approaches vary for the different crystal faces. Device researchers are particular interested in 4H-SiC due to the fact that it has the highest bandgap of all polytypes. The research in this dissertation explores the chemistry and device behavior of different crystal faces of 4H-SiC.

1.5. MOSFETs and dielectric-semiconductor interface

The SiC MOSFETs performance to date is still far from satisfactory (a very crude schematic of an FET device structure is shown in Fig. 1.5). SiO_2 is the native (natural, and most simple) oxide that grows on SiC. This greatly facilitates SiC device processing as it enables one to use many of the well-developed processes originally devised for SiO_2

on Si. Unfortunately, the poor quality of the as-grown SiO_2/SiC interface (relative to SiO_2/Si) limits the performance of SiC MOSFETs and hence the development of the entire field. For example, there appears to be a thin transition layer (~ 1-15 nm) that exists between SiO_2 and SiC that is different from either pure component;[16] this is rather different from the abrupt lower defect density interface observed for SiO_2/Si. As a result, there appears to be more and different kinds of defects, including near-interface charged traps, extra carbon, and other defects. This high interface trap density results in low inversion layer mobility, and poor device reliability. At present, efforts are underway worldwide by scientists and engineers to solve these problems, some of which are discussed in later chapters of this thesis.

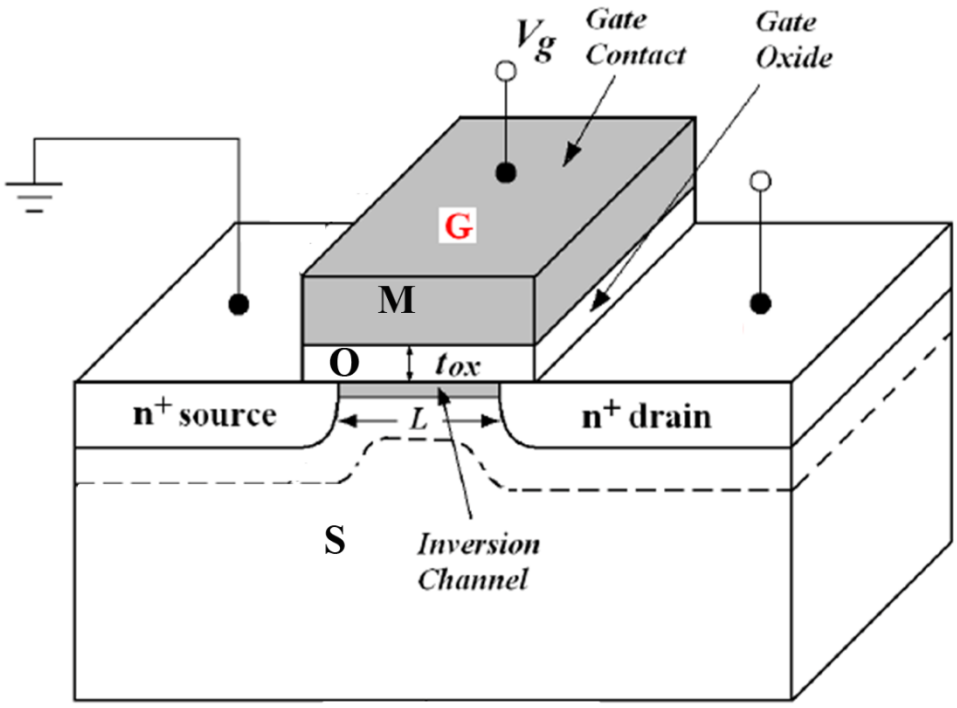

Fig. 1.5. Scheme of generic MOSFET structure

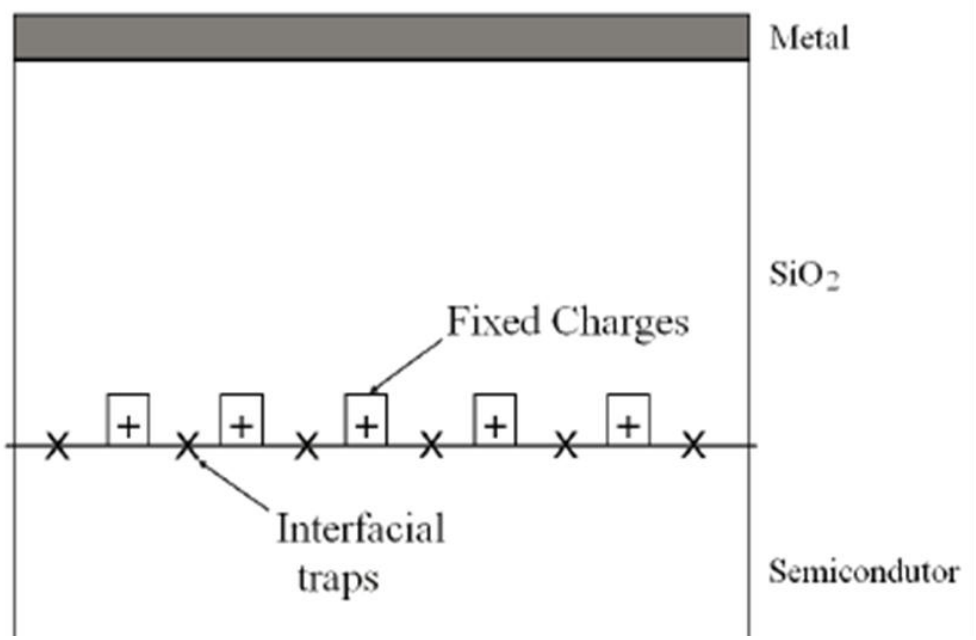

Fig. 1.6. Nature and location of different oxide and interface traps in thermally grown SiO_2. (Adapted from Deal, B.E., 1980) [17]

One major factor responsible for the non-ideal MOSFET performance is the existence of various types of defects and charged traps at the oxide/semiconductor interface or in the near-interfacial region of the oxide.[18] Their locations in the oxide and interface are shown in Fig. 1.6. These charged traps can lead to very severe problems for MOS device performance.[17]

Fixed oxide charges that appear in the near (a few nanometer) interface oxide are usually positive, they are fixed in space (thus their name), and they do not move with high temperature or bias stress. The origin of fixed charge near the interface is related to the SiC thermal oxidation conditions. These conditions include oxidation temperature, gas ambient, cool down procedure and crystal orientation of the SiC.

Charged traps at the interface, described collectively by the concept of an 'interface trap density', can be quantified using electrical measurements. The origin of interface trapped charges is not well understood, but is likely related to silicon or carbon dangling bonds, carbon clusters, carbon dimmers at the interface, and/or oxygen vacancies in the near interface oxide.[19] Interfacial traps can create localized energy levels at the interface – surface states in the SiC band gap. Depending on the nature of the traps, the bulk Fermi energy, and the surface potential, the charge of these traps can be positive or negative. These interfaces traps can capture electrons and holes from the channel. In addition, charged traps are also Columbic scattering centers that can limit the channel charge mobility in a MOSFET.

1.6. SiO_2/SiC interface issue

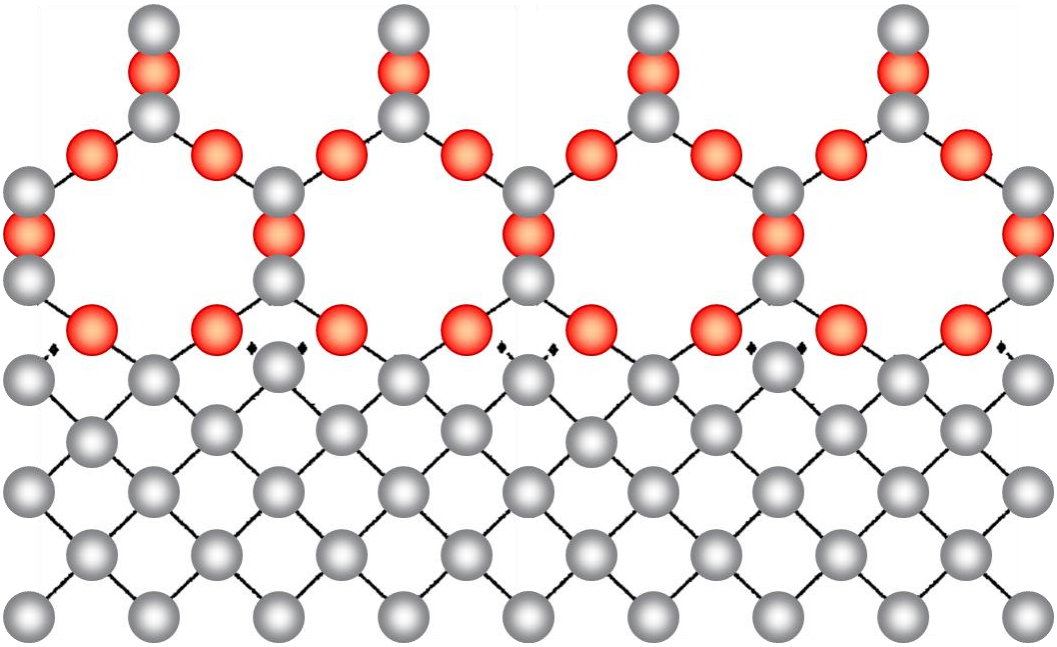

Fig. 1.7. Simplified scheme of an ordered dielectric-semiconductor (Si) interface

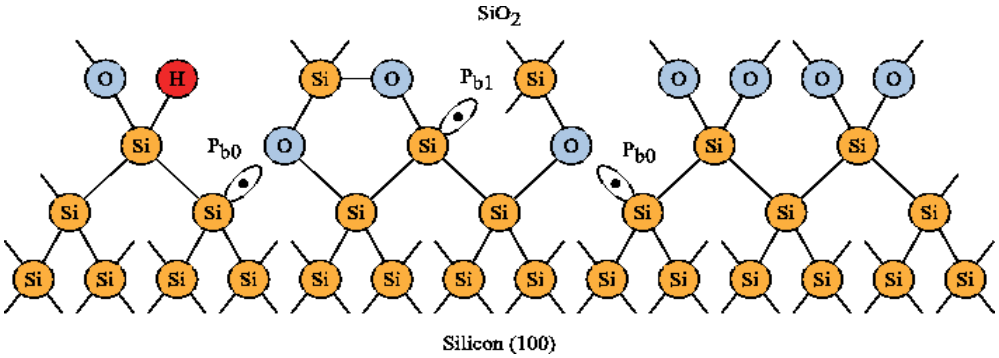

Fig. 1.8. Scheme of a non-ideal dielectric-semiconductor (Si) interface with several type of defects. (Adapted from C. R. Helms and E. H. Poindexter, 1994)[20]

An ideal oxide-semiconductor interface would show all (surface) atoms on each side of the interface coupled to ones on the other side, bonding in a manner such that all orbitals are doubly occupied, stable, and located in positions that do not stress either material. Such a structure for the SiO_2/Si(100) interface is shown in Fig. 1.7, with all semiconductors atoms appropriately bonded to others the oxide. Fig. 1.8 shows a non-ideal oxide-semiconductor interface with some of the bonds of Si "unsatisfied". Those unsatisfied bonds are available to trap carriers, becoming charged scattering centers at the interface.

The density of the interface traps can be very low, of order $10^{11}/cm^2$ or less, far below the detection limit of physical characterization methods. The best way to quantify them is to use electrical measurements.

1.7. SiO_2/SiC interface passivation

The oxidation of SiC is very different from the oxidation of Si,[21, 22] as it involves an extra element, carbon (C). The liberation of carbon as carbon monoxide during

oxidation makes the process more complicated. Interface traps formed during the oxidation due to silicon dangling bonds, carbon dangling bonds, carbon clusters and oxygen vacancies, can create extra energy levels in the band gap.[19, 23-26] Carbon forms complex structures and exists in the SiC bulk crystal as interstitials.[27, 28] Unlike the SiO_2/Si interface, the SiO_2/SiC interface is not abrupt.[29] The band gap of 4H-SiC (3.26 eV) is three times larger than that in Si (1.12 eV), and this energy range enables a wider range of traps to exist within the semiconductor band-gap.[30-32] This leads to a much higher interface trap density near the SiC conduction band edge for the n-MOS devices.[33, 34] For an unpassivated 4H-SiC MOS capacitor, the interface trap density at 0.2 eV below the conduction band edge is of the order of 10^{13}/eV cm^2. [35]

In the field, the term "passivation" is used to describe methods that lower the interface trap density. Some of the more common passivation techniques to reduce interface trap density involve post-oxidation anneals in NH_3, H_2, N_2O or NO. At the SiO_2/Si interface, most of the interface traps are related to Si dangling bonds, and a hydrogen (or "forming" gas) anneal is a well-known, effective method to passivate these traps, presumably by forming Si-H bonds at the interface.[36-38] The hydrogen passivation technique is widely used as a standard fabrication procedure for Si-based devices. Hydrogen passivation has also been explored for SiO_2/SiC structures,[39] although for SiC there is usually not any measurable improvement observed. N_2 anneals also do not result in any device benefits. However, there are a few methods that can be applied and do work.

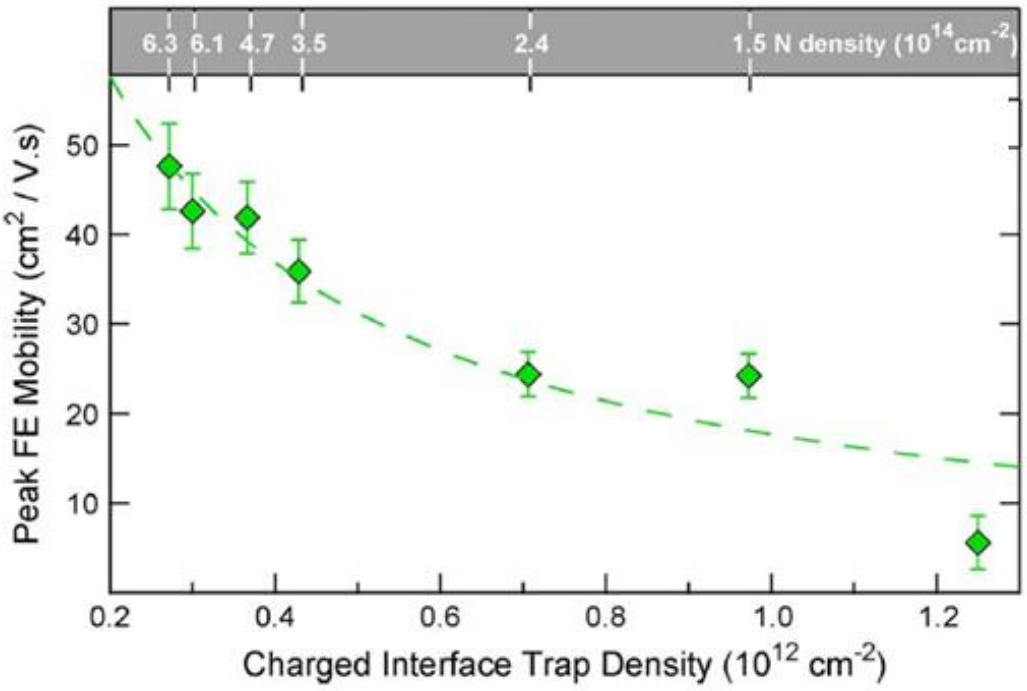

Fig. 1.9. Interfacial nitrogen coverage scaling with density of interface states and inversion layer mobility. (Adapted from Rozen et al, 2011)[40]

One of the most widely used fabrication processes to reduce the interface trap density in the silicon carbide industry is a nitric oxide (NO) anneal. This process was first reported to effectively passivate the SiO_2/SiC interface by Li et al, on 6H-SiC[41] and Chung et al, on 4H-SiC.[42, 43] For 4H-SiC, especially n-type, it has been observed that adding an NO (g) anneal step after the standard dry O_2 oxidation process can significantly reduce the interface trap density, increase the channel mobility, improve oxide reliability, and enhance device performance.[42-45]

Rozen, et al reported results from the Si-face of SiC after a nitric oxide (NO) post-oxidation anneal.[40] They correlated NO annealing time with N coverage, interface trap density (D_{it}) (reduced the Dit to $1\times10^{11}/cm^2$ eV at 0.2 eV below the conduction band

edge), and field-effect mobility (increasing μ_{FE} up to ~ 40 cm^2/V-s).[40] As shown in Fig. 1.9, an NO anneal is an effective and well controlled interface passivation process.

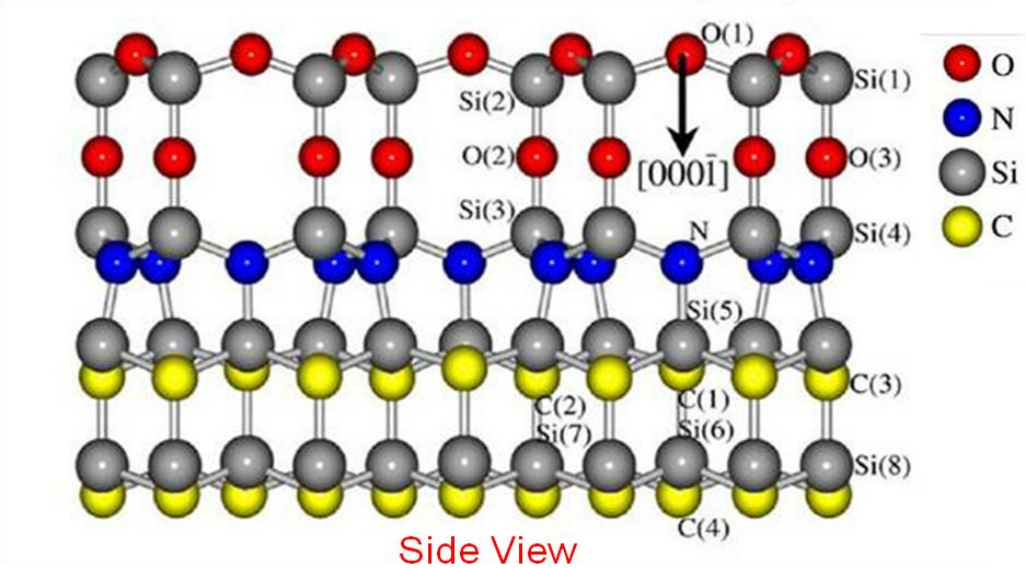

Fig. 1.10. A model epitaxial interface structure for an NO annealed SiO_2/SiC structure with N atoms passivating dangling bonds. (Adapted from Shirasawa et al, 2007)[46]

The mechanism by which the post oxidation anneal affects the SiO_2/SiC interface is not very clear, but a possible explanation (described in more detail in subsequent chapters) is that at high temperature (1100~1120^oC), the NO gas molecules diffuse to the interface and then dissociate into N atoms and O atoms. The O atoms oxidize the SiC at the interface (analogous to what might occur with O_2 or H_2O as the O source) forming SiO_2 and CO, which eventually diffuses out leaving into the gas phase. The N atoms will likely compete with O in bonding with Si. One does not observe Si_3N_4 formation. N incorporation lowers the defect concentration (likely by passivating dangling bonds), and

may also bond with the excess C atoms (and C clusters).[41] This is supported by experimental evidence and theoretical calculations, with one proposed epitaxial interface structure shown in Fig. 1.10.[26, 46-48] The NO (g) anneal successfully reduces interface trap density by an order of magnitude close to the conduction band edge, and increases channel mobility from about 5 cm^2/V s to 35~40 cm^2/V s, which makes this process widely used for most of the current 4H-SiC MOS device fabrication schemes.[41-43] Several other hypotheses explaining how N might enhance device properties are also discussed below.

In addition to nitrogen passivation, improved performance can also be achieved by introducing phosphorous to the SiO_2/SiC interface.[49-52] It is shown that under certain conditions phosphorus passivation (P-passivation) can be even more effective than NO passivation in reducing interface trap density and channel mobility.[49-52] The peak mobility of the P passivated 4H-SiC MOSFET is approximately 85 cm^2/V s.[53] But phosphorus processing unfortunately causes another instability in the device which we believe is due to conversion of SiO_2 into a phosphosilicate glass (PSG), a rather polar material.[49, 50, 52] Sharma et al, reported the improved stabilization of P-passivated SiC MOSFET devices by switching the gate oxide from a “bulk” PSG film to a very thin PSG layer capped with deposited SiO_2.[51] This modified P-passivation process appears to stabilize the device while keeping most of the beneficial passivating effects of P. The peak field effect mobility obtained using this approach is around 72cm^2/V s.[51] The mechanism by which phosphorus improves interface quality and device performance is also discussed in chapter 5.

References

[1] R. H. Lasseter and P. Paigi, "Microgrid: a conceptual solution," in *Power Electronics Specialists Conference, 2004. PESC 04. 2004 IEEE 35th Annual*, 2004, pp. 4285-4290 Vol.6.

[2] N. Hatziargyriou, H. Asano, R. Iravani, and C. Marnay, "Microgrids," *Power and Energy Magazine, IEEE,* vol. 5, pp. 78-94, 2007.

[3] Q. C. Zhang, R. Callanan, M. K. Das, S. H. Ryu, A. K. Agarwal, and J. W. Palmour, "SiC Power Devices for Microgrids," *Ieee Transactions on Power Electronics*, vol. 25, pp. 2889-2896, Dec 2010.

[4] S. E. Saddow and A. K. Agarwal, *Advances in silicon carbide processing and applications*: Artech House, 2004.

[5] A. Agarwal and M. Sofos, "Title," unpublished|.

[6] H. Moissan, "Etude du siliciure de carbone de la meteorite de canon diablo," *Comptes rendus Acad. sci,* vol. 140, pp. 405-506, 1905.

[7] J. Berzelius, "Investigation of Hydrofluoric Acid and Its Most Remarkable Compounds," *Ann. Physik Chem.(Pogg.)*, vol. 1, pp. 1-48, 1824.

[8] E. G. Acheson, *Engl. Pat*, p. 17911, 1892.

[9] J. A. Lely, *Berichte der Deutschen Keramischen Gesellschaft,* vol. 32, p. 229, 1955.

[10] Y. M. Tairov and V. F. Tsvetkov, "Investigation of growth processes of ingots of silicon carbide single crystals," *Journal of Crystal Growth,* vol. 43, pp. 209-212, 1978.

[11] H. Matsunami, S. Nishino, and H. Ono, "IVA-8 heteroepitaxial growth of cubic silicon carbide on foreign substrates," *Electron Devices, IEEE Transactions on,* vol. 28, pp. 1235-1236, 1981.

[12] H. J. Round, "A note on carborundum," *Electrical world,* vol. 49, p. 309, 1907.

[13] W. Knippenberg, "Philips Research Reports," vol. 18, ed: Philips research Laboratory, Eindhoven, Netherlands, 1963, pp. 161-274.

[14] H. Baumhauer, *Zeit. Krist.*, vol. 50, pp. 33-39, 1912.

[15] T. Ayalew, "SiC Semiconductor Devices Technology, Modeling, and Simulation," Ph. D., Institute for Microelectronics, TU Vienna., 2004.

[16] J. A. Taillon, J. H. Yang, C. A. Ahyi, J. Rozen, J. R. Williams, L. C. Feldman, T. S. Zheleva, A. J. Lelis, and L. G. Salamanca-Riba, "Systematic structural and chemical characterization of the transition layer at the interface of NO-annealed 4H-SiC/SiO_2 metal-oxide-semiconductor field-effect transistors," *Journal of Applied Physics,* vol. 113, Jan 28 2013.

[17] B. E. Deal, "Standardized terminology for oxide charges associated with thermally oxidized silicon," *Electron Devices, IEEE Transactions on,* vol. 27, pp. 606-608, 1980.

[18] B. E. Deal, "The Current Understanding of Charges in the Thermally Oxidized Silicon Structure," *Journal of The Electrochemical Society,* vol. 121, pp. 198C-205C, June 1, 1974 1974.

[19] V. V. Afanas'ev, M. Bassler, G. Pensl, and M. Schulz, "Intrinsic SiC/SiO2 interface states," *Physica Status Solidi a-Applications and Materials Science,* vol. 162, pp. 321-337, Jul 16 1997.

[20] C. R. Helms and E. H. Poindexter, "The Silicon Silicon-Dioxide System - Its Microstructure and Imperfections," *Reports on Progress in Physics,* vol. 57, pp. 791-852, Aug 1994.

[21] M. Di Ventra and S. T. Pantelides, "Atomic-scale mechanisms of oxygen precipitation and thin-film oxidation of SiC," *Physical Review Letters,* vol. 83, pp. 1624-1627, Aug 23 1999.

[22] J. M. Knaup, P. Deak, T. Frauenheim, A. Gali, Z. Hajnal, and W. J. Choyke, "Theoretical study of the mechanism of dry oxidation of 4H-SiC," *Physical Review B,* vol. 71, Jun 2005.

[23] J. L. Cantin, H. J. von Bardeleben, Y. Shishkin, Y. Ke, R. P. Devaty, and W. J. Choyke, "Identification of the carbon dangling bond center at the 4H-SiC/SiO2 interface by an EPR study in oxidized porous SiC," *Physical Review Letters,* vol. 92, Jan 9 2004.

[24] F. Devynck, F. Giustino, P. Broqvist, and A. Pasquarello, "Structural and electronic properties of an abrupt 4H-SiC(0001)/SiO2 interface model: Classical molecular dynamics simulations and density functional calculations," *Physical Review B,* vol. 76, Aug 2007.

[25] F. Devynck and A. Pasquarello, "Semiconductor defects at the 4H-SiC(0001)/SiO2 interface," *Physica B-Condensed Matter,* vol. 401, pp. 556-559, Dec 15 2007.

[26] F. Devynck, Z. Sljivancanin, and A. Pasquarello, "Electronic properties of an epitaxial silicon oxynitride layer on a 6H-SiC(0001) surface: A first-principles investigation," *Applied Physics Letters,* vol. 91, p. 061930, Aug 6 2007.

[27] X. Shen, M. P. Oxley, Y. Puzyrev, B. R. Tuttle, G. Duscher, and S. T. Pantelides, "Excess carbon in silicon carbide," *Journal of Applied Physics,* vol. 108, Dec 15 2010.

[28] X. Shen and S. T. Pantelides, "Oxidation-Induced Epilayer Carbon Di-Interstitials as a Major Cause of Endemically Poor Mobilities in 4H-SiC/SiO_2 Structures," *Materials Science Forum,* vol. 717-720, pp. 445-448, 2012.

[29] G. L. Harris, *Properties of Siliocn Carbide*. IEEE INSPEC: IEEE INSPEC, 1995.

[30] F. Ren and J. C. Zolper, *Wide Energy Bandgap Electronics Devices*: World Scientific Publishing, 2003.

[31] J. A. Cooper, "Advances in SiC MOS technology," *Physica Status Solidi a-Applied Research,* vol. 162, pp. 305-320, Jul 16 1997.

[32] T. Zheleva, A. Lelis, G. Duscher, F. Liu, I. Levin, and M. Das, "Transition layers at the SiO2/SiC interface," *Applied Physics Letters,* vol. 93, Jul 14 2008.

[33] P. Friedrichs, E. P. Burte, and R. Schomer, "Interface properties of metal-oxide-semiconductor structures on n-type 6H and 4H-SiC," *Journal of Applied Physics,* vol. 79, pp. 7814-7819, May 15 1996.

[34] R. Schorner, P. Friedrichs, D. Peters, and D. Stephani, "Significantly improved performance of MOSFET's on silicon carbide using the 15R-SiC polytype," *Ieee Electron Device Letters,* vol. 20, pp. 241-244, May 1999.

[35] P. Friedrichs, T. Kimoto, L. Ley, and G. Pensl, *Silicon Carbide*: Wiley-VCH, 2009.

[36] V. V. Afanas'ev and A. Stesmans, "Hydrogen-induced valence alternation state at SiO2 interfaces," *Physical Review Letters,* vol. 80, pp. 5176-5179, Jun 8 1998.

[37] V. V. Afanas'ev and A. Stesmans, "Positively charged bonded states of hydrogen at the (111)Si/SiO2 interface," *Journal of Physics-Condensed Matter,* vol. 10, pp. 89-93, Jan 12 1998.

[38] V. V. Afanas'ev and A. Stesmans, "H-complexed oxygen vacancy in SiO2: Energy level of a negatively charged state," *Applied Physics Letters,* vol. 71, pp. 3844-3846, Dec 29 1997.

[39] S. W. Wang, S. Dhar, S. R. Wang, A. C. Ahyi, A. Franceschetti, J. R. Williams, L. C. Feldman, and S. T. Pantelides, "Bonding at the SiC-SiO2 interface and the effects of nitrogen and hydrogen," *Physical Review Letters,* vol. 98, Jan 12 2007.

[40] J. Rozen, A. C. Ahyi, X. G. Zhu, J. R. Williams, and L. C. Feldman, "Scaling Between Channel Mobility and Interface State Density in SiC MOSFETs," *Ieee Transactions on Electron Devices,* vol. 58, pp. 3808-3811, Nov 2011.

[41] H. F. Li, S. Dimitrijev, H. B. Harrison, and D. Sweatman, "Interfacial characteristics of N2O and NO nitrided SiO2 grown on SiC by rapid thermal processing," *Applied Physics Letters,* vol. 70, pp. 2028-2030, Apr 14 1997.

[42] G. Y. Chung, C. C. Tin, J. R. Williams, K. McDonald, M. Di Ventra, S. T. Pantelides, L. C. Feldman, and R. A. Weller, "Effect of nitric oxide annealing on the interface trap densities near the band edges in the 4H polytype of silicon carbide," *Applied Physics Letters,* vol. 76, pp. 1713-1715, Mar 27 2000.

[43] G. Y. Chung, C. C. Tin, J. R. Williams, K. McDonald, R. K. Chanana, R. A. Weller, S. T. Pantelides, L. C. Feldman, O. W. Holland, M. K. Das, and J. W. Palmour, "Improved inversion channel mobility for 4H-SiC MOSFETs following

high temperature anneals in nitric oxide," *Ieee Electron Device Letters,* vol. 22, pp. 176-178, Apr 2001.

[44] G. Y. Chung, J. R. Williams, C. C. Tin, K. McDonald, D. Farmer, R. K. Chanana, S. T. Pantelides, O. W. Holland, and L. C. Feldman, "Interface state density and channel mobility for 4H-SiC MOSFETs with nitrogen passivation," *Applied Surface Science,* vol. 184, pp. 399-403, Dec 12 2001.

[45] G. Y. Chung, C. C. Tin, J. R. Williams, K. McDonald, M. D. Ventra, S. T. Pantelides, L. C. Feldman, and R. A. Weller, "The Effects of Post-Oxidation Anneal Conditions on Interface State Density Near the Conduction Band Edge and Inversion Channel Mobility for SiC MOSFETs," *MRS Online Proceedings Library,* vol. 622, pp. null-null, 2000.

[46] T. Shirasawa, K. Hayashi, S. Mizuno, S. Tanaka, K. Nakatsuji, F. Komori, and H. Tochihara, "Epitaxial silicon oxynitride layer on a 6H-SiC(0001) surface," *Physical Review Letters,* vol. 98, p. 136105, Mar 30 2007.

[47] P. Kruger, B. Baumeier, and J. Pollmann, "First-principles investigation of an epitaxial silicon oxynitride layer on a 6H-SiC(0001) surface," *Physical Review B,* vol. 77, p. 085329, Feb 2008.

[48] T. Shirasawa, K. Hayashi, H. Yoshida, S. Mizuno, S. Tanaka, T. Muro, Y. Tamenori, Y. Harada, T. Tokushima, Y. Horikawa, E. Kobayashi, T. Kinoshita, S. Shin, T. Takahashi, Y. Ando, K. Akagi, S. Tsuneyuki, and H. Tochihara, "Atomic-layer-resolved bandgap structure of an ultrathin oxynitride-silicon film epitaxially grown on 6H-SiC(0001)," *Physical Review B,* vol. 79, p. 241301(R), Jun 2009.

[49] D. Okamoto, H. Yano, T. Hatayama, and T. Fuyuki, "Removal of near-interface traps at SiO_2/4H-SiC (0001) interfaces by phosphorus incorporation," *Applied Physics Letters,* vol. 96, p. 203508, May 17 2010.

[50] D. Okamoto, H. Yano, K. Hirata, T. Hatayama, and T. Fuyuki, "Improved Inversion Channel Mobility in 4H-SiC MOSFETs on Si Face Utilizing Phosphorus-Doped Gate Oxide," *Ieee Electron Device Letters,* vol. 31, pp. 710-712, Jul 2010.

[51] Y. K. Sharma, A. C. Ahyi, T. Isaacs-Smith, A. Modic, M. Park, Y. Xu, E. L. Garfunkel, S. Dhar, L. C. Feldman, and J. R. Williams, "High-Mobility Stable 4H-SiC MOSFETs Using a Thin PSG Interfacial Passivation Layer," *Ieee Electron Device Letters,* vol. 34, pp. 175-177, Feb 2013.

[52] Y. K. Sharma, A. C. Ahyi, T. Issacs-Smith, X. Shen, S. T. Pantelides, X. Zhu, L. C. Feldman, and J. R. Williams, "Phosphorous Passivation of the SiO_2/4H-SiC Interface," *Solid-State Electronics,* vol. 68, pp. 103-107, 2012.

[53] J. Rozen, S. Dhar, S. K. Dixit, V. V. Afanas'ev, F. O. Roberts, H. L. Dang, S. Wang, S. T. Pantelides, J. R. Williams, and L. C. Feldman, "Increase in oxide hole trap density associated with nitrogen incorporation at the SiO_2/SiC interface," *Journal of Applied Physics,* vol. 103, Jun 15 2008.

Chapter 2. Characterization Techniques

2.1. General introduction

A range of surface and thin film characterization techniques, including X-ray photoelectron spectroscopy (XPS), Rutherford backscattering (RBS), nuclear reaction analysis (NRA), medium energy ion scattering (MEIS), and secondary ion mass spectrum (SIMS), have been used to study the physical properties of the SiO_2/SiC interface. Capacitance-voltage (CV) electrical measurements have also been used to determine the interface trap density. The principle of each technique is briefly introduced in this chapter.

2.2. X-ray photoemission spectroscopy (XPS)

X-ray photoelectron spectroscopy (XPS) is a spectroscopic technique based on the photoelectric effect to characterize the elemental composition, electronic and chemical states of solid-state materials in the near surface region (0 - 10nm). The precursor to modern day XPS was originally observed by Hertz[1] as part of the discovery of the photoelectric effect. It was then defined more precisely from the energetic point of view by Einstein.[2] The technique was further developed over the next decade for different metals by several others, including Robinson and Rawlinson.[3] Much later, Siegbahn et al[4, 5] developed XPS into a precise technique to determine the atomic binding energies; Siegbahn won the Nobel Prize in 1981 for the development. Today XPS has become one of the most powerful techniques for surface and thin film compositional analysis.

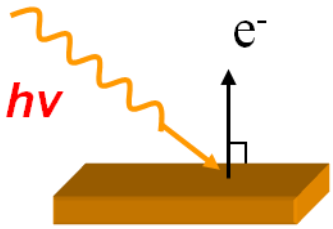

Fig. 2.1. Schematic of the photoelectron emission process in XPS.

2.2.1. X-ray photoemission spectroscopy basics

An XPS system uses monochromic X-rays to irradiate the sample and a spectrometer measures the kinetic energy and the number of electrons emitted from the test material. Ultra high-vacuum (UHV) instrumentation is essential for XPS. The pressures of XPS chambers are in the range of 10^{-8} to 10^{-10} Torr depending on the application.

The X-ray source used in most XPS studies emits photons typically in an energy range of 100-2000 eV. Photoelectrons are ejected from the surface of the samples via a photon absorption process.[6] Different X-ray sources provide different energy resolutions of the XPS system. A 0.9–1.0 eV range of energy resolution can be achieved using a non-monochromatic magnesium X-ray (1253.6 eV). With the use of a monochromatic aluminum K-alpha X-ray (1486.7 eV), the energy resolution can be improved to 0.2–0.4 eV. To obtain higher energy resolution, synchrotron radiation with a higher intensity and narrower energy width (obtained with a diffraction grating) can be used as the source.

A photoelectron can be generated by the interaction of an electron in the material under study with a photon of higher energy than the binding energy of that electron. As the mean free path of low energy electrons is rather short, only photoelectrons from the first few nanometers of the surface (<10 nm) can escape the material and reach the

spectrometer detector to contribute to the XPS spectra. The photoelectrons that fail to leave the material can contribute to the background in the spectra.

Fig. 2.1 illustrates the photoelectron emission process in XPS. In the process, an electron from one of the core electronic levels absorbed a photon emitted from the X-ray source. The kinetic energy *KE* of the ejected electron is measured by the electron energy analyzer and has the following relationship:

$$KE = h\nu - BE - \phi \qquad \text{(Eq. 2.1)}$$

where $h\nu$ is the photon energy of the X-ray source, *BE* is the binding energy of the atomic orbit from which the electron is ejected, and ϕ is the spectrometer work function.

Since each element has a unique set of binding energies, the XPS spectra can be used to identify the elements near the surface of the sample. The measured binding energy for a given element can vary by at least 5 eV due to different oxidation states of the atom and different local chemical environments. This variation in the atomic core-level binding energy is known as the chemical shift, which can be analyzed to determine the chemical states of the specimen.[7]

2.2.2. Atomic sensitivity factor

The peak areas in XPS spectra can be used to determine the chemical composition of the material. Each orbital of each element has a characteristic sensitivity for X-rays of a given energy. A higher relative concentration of one element with a low sensitivity can generate a peak with the same area as a lower concentration of another element with higher sensitivity. The sensitivity factors, S_i, have to be included for each element before converting the photoemission peak areas into a relative or absolute composition. For two

different elements A and B, the stoichiometric ratio of the two components can be calculated from the peak areas (I_A and I_B) with the sensitivity factors S_A and S_B, as follows,[8]

$$\frac{n_A}{n_B} = \frac{I_A/S_A}{I_B/S_B} \qquad \text{(Eq. 2.2)}$$

2.2.3. Depth profiling using angle resolve XPS

In XPS, before a photoelectron escapes to vacuum, it travels a distance inside the sample, during which elastic or inelastic collisions can occur with the lattice atoms. Those photoelectrons that are able to escape the sample without losing energy give rise to the XPS peaks. The kinetic energy of the photoelectrons decrease in inelastic collisions and form part of the lower energy background of the spectrum or do not escape from the solid. The probability for a photoelectron to escape from the depth d with its kinetic energy remaining essentially unchanged can be calculated as:

$$I \propto e^{-d/\lambda \cos\theta} \qquad \text{(Eq. 2.3)}$$

where λ stands for the photoelectron inelastic mean free path, and θ stands for the photoelectron emission angle relative to normal emission from the sample plane.

Fig. 2.2, the "universal curve", shows the electron mean free path as a function of electron kinetic energy for a range of materials.[9] The relatively short mean free path (nanometers) has enabled a non-destructive method to be developed that can be used to obtain depth profile of the sample in near surface regime. The method of depth profiling is called angular resolved photoelectron spectroscopy (ARPES),[10] in which the sample is analyzed using XPS at different emission angle. [Note that this method of employing ARPES to determine compositional profiles, should not be confused with ARPES to

determine electronic band structure.] By comparing intensities of the same peak acquired at different emission angles, the depth of the particular element can be estimated based on mathematical modeling.[10]

An accurate electron mean free path value is important for obtaining meaningful results. In this dissertation, the mean free path of Si 2p photoelectrons in SiC is determined in chapter 3.

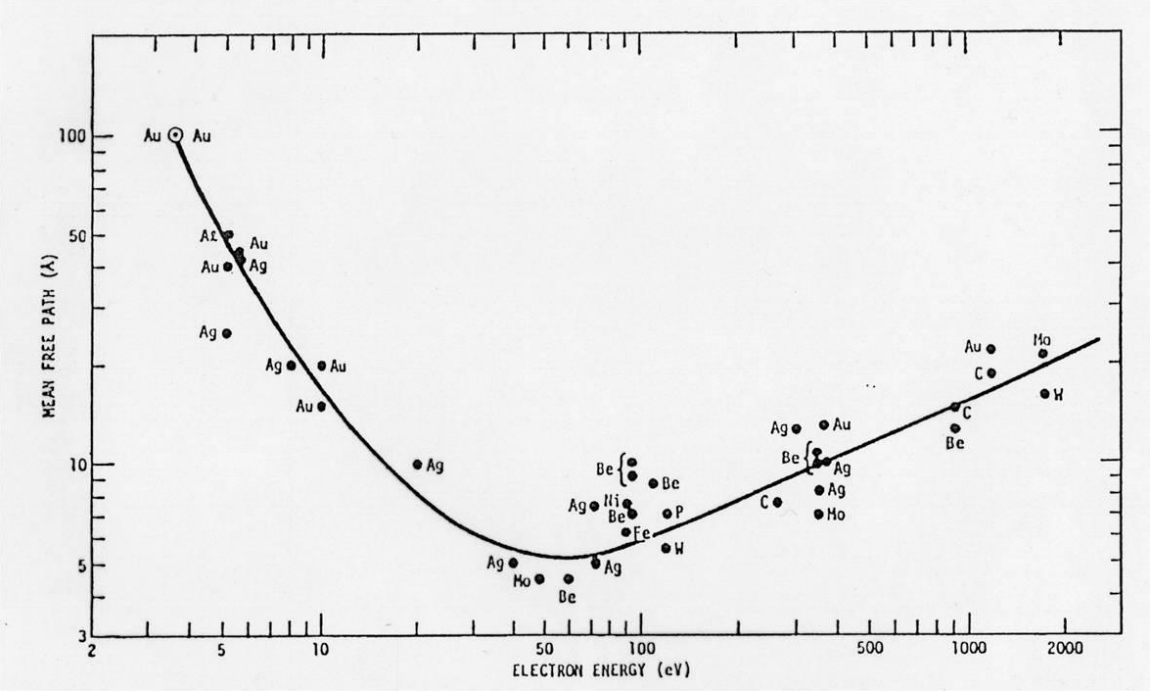

Fig. 2.2. Universal curve for electron mean free paths. Adapted from G. Somorjai, Chemistry in Two Dimensions: Surfaces.[9]

2.3. Rutherford backscattering (RBS)

Rutherford backscattering spectroscopy (RBS)[6, 11] is a widely used technique to determine the thin film composition, thickness and layer structure of a sample. In this method, the sample is bombarded with a high energy ion beam (incident beam) of a well-

defined energy. A fraction of the incident ions are backscattered by the sample. The backscattered ions are collected and energy analyzed, yielding a spectrum of intensity of backscattered ions as a function of energy (or energy loss). With appropriate information and modeling, the yield of the ions can be used to give information of the elemental composition (atomic mass), the concentration of the elements, and the position of each element in a sample.

In RBS measurements, monochromatic H^+ or He^{2+} ions are often used as incident beam. The incident beam, which usually falls within the energy range of 1~4 MeV, may undergoes elastic collisions and be backscattered with a scattering angle θ. The backscattering method is illustrated in Fig.2.3.

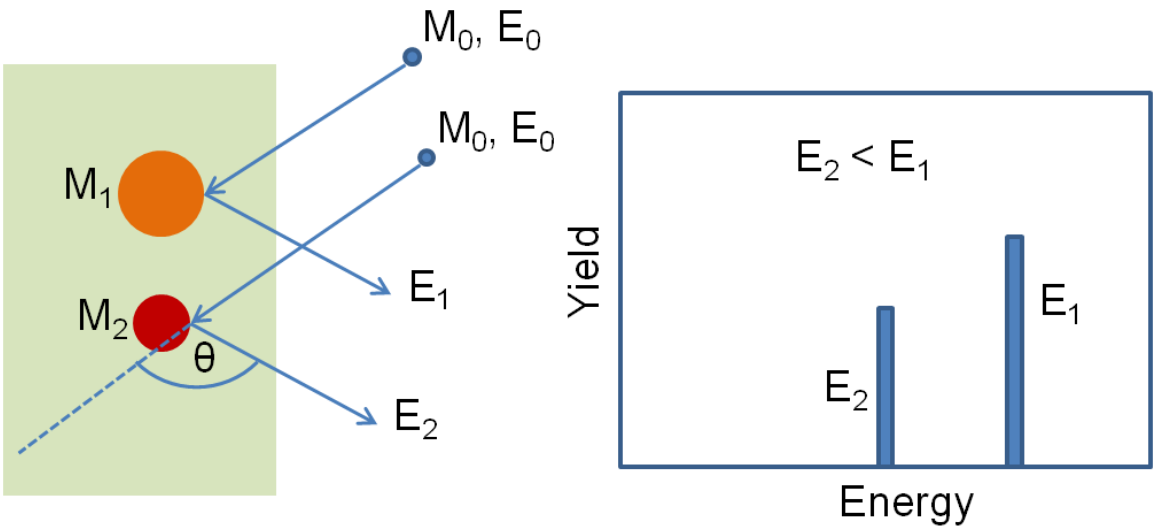

Fig. 2.3. Rutherford Back Scattering Spectroscopy (RBS) peaks reflects the mass difference of various target atoms in a sample. In this case, mass M_1 > mass M_2.

The energy of the scattered particles depends on the atomic mass of the target element, the initial energy of the incident beam, as shown in Fig. 2.3, and the scattering

angle. For an elastic collision, the energy (E) of the backscattered ions after the collision is directly proportional to the ion's initial energy E_0.

$$E = K E_0 \qquad \text{(Eq. 2.4)}$$

where K is referred as kinematic factor and can be calculated using the conservation of mass and momentum:

$$K_1 = \left(\frac{M_0 \cos\theta + \sqrt{{M_1}^2 - (M_0 \sin\theta)^2}}{M_0 + M_1} \right)^2 \qquad \text{(Eq. 2.5)}$$

From the equation, it is clear that K would be larger for heavier target atoms and smaller scattering angles. For the same scattering angle, the backscattered ions which collide with heavier elements would have higher energy than those collide with lighter element.

In ion scattering (both RBS and MEIS), the incident ions lose energy while penetrating the sample along the incident path as well as along the exit path after be backscattered by an atom in the sample. In addition to the loss that occurs during the nuclear collision, energy losses are caused interactions that occur between the incident ion, the target element's nuclei, other nuclei that the scattered particle may encounter along it's trajectory, and electrons that the scattered ion encounters on its way into or out of the material.[15] The energy of the detected ions is equal to the incident ion energy, minus the energy loss that occurs during the elastic scattering event, mius the energy loss that caused by the electrons of the solid, minus the sum of all other energy loss processes that occur along the ion's trajectory.[16] To a good approximation, the energy loss during the ion scattering process can be used to identify the distance traveled by the ion in the material, and thus provides a depth profile of target constituents, as shown in Fig. 2.4.

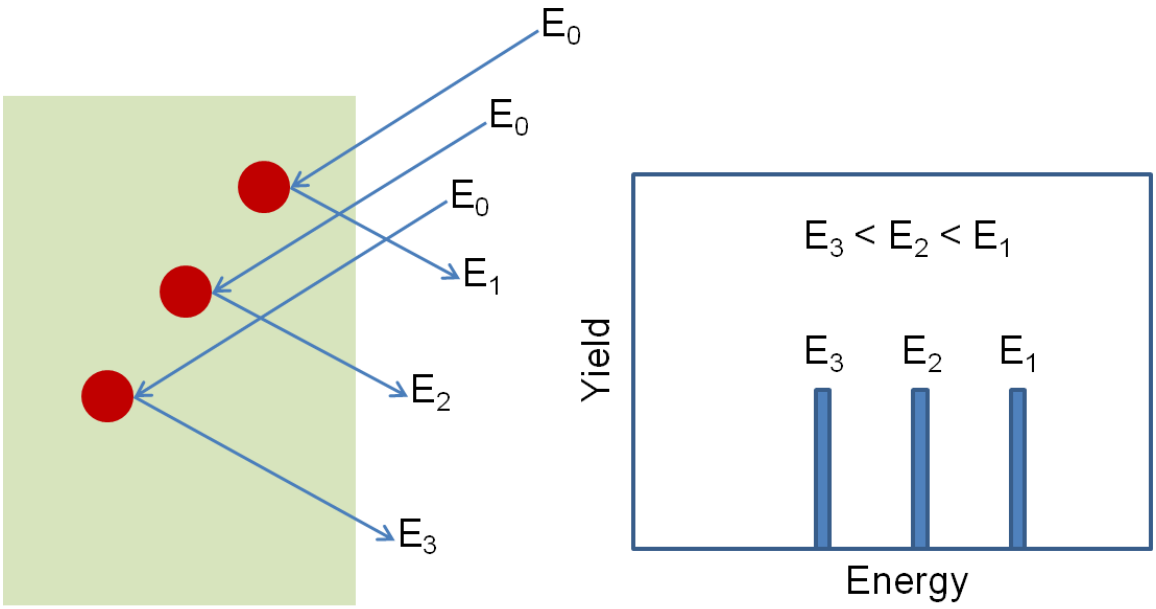

Fig. 2.4. The position of ion scattering peaks reflects the depth distribution of target atoms (or layers).

2.4. Nuclear Reaction Analysis (NRA)

The same ion accelerator that used in RBS can also be used to initiate simple nuclear reactions between two nuclei. When used to determine composition this method is referred to as *Nuclear Reaction Analysis* (NRA)[12], and can be a more sensitive probe of composition than conventional RBS particularly for light elements. In this work, the p-alpha reaction of ^{18}O is used. The reaction can be written as:

$$p + {}^{18}O \rightarrow {}^{15}N + {}^{4}He + Q \qquad \text{(Eq. 2.6)}$$

a proton beam with ~ 827 keV energy was used as incident beam to react with ^{18}O and generate high energy alpha particles. These alpha particles were collected and used to quantify ^{18}O in the film.

2.5. Medium energy ion scattering (MEIS)

For very thin films, a lower energy (20~200 keV), higher resolution variant of Rutherford backscattering can be employed that is called Medium Energy Ion Scattering (MEIS).[13, 14] A more sophisticated ion detection scheme is used in MEIS than is usually employed for RBS.

The amount of energy that the ion loses as a function of distance while travelling in a material is referred as the stopping power. The stopping power depends on the incident ion's energy, charge and mass, as well as the material of the sample. This stopping power is primarily due to electronic excitations (e-h creation) at in the 100 keV to 1MeV range, with nuclear stopping becoming dominant only at much lower energies. The energy loss caused by nuclear reactions between the incident ion nuclei and target nuclei is negligible.[17] Fig. 2.5 shows the electronic stopping power dependence of ions in pure Al films. The maximum of the electronic stopping power of both H^+ and He^+ beam occurs at around 100 keV, one key reason why MEIS uses ion of this energy range. Also, higher energy resolution detection systems are easier to employ for 100keV ions than 1MeV ones, and the higher energy resolution gives rise to a high depth resolution for MEIS.

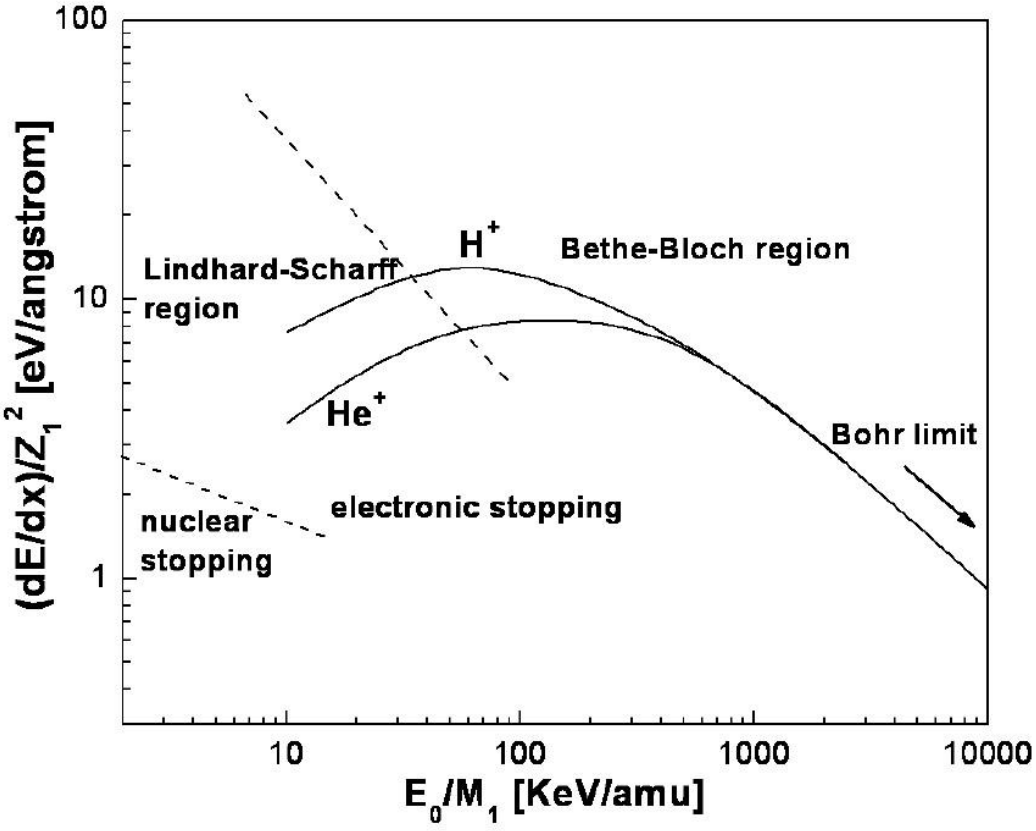

Fig. 2.5. Energy dependence of the electronic stopping power for different H^+ and He^+ incident energy, the target solid is Al film. The nuclear stopping dominated region is also indicated. Adopted from the PhD dissertation of Dr. T. Feng.[18]

The surface sensitivity of ion scattering can be enhanced by working in "channeling and blocking" methods,[19] widely used in determining the surface structure of samples with a crystalline substrate. When the ion beam is aligned parallel to a major crystallographic direction in a single crystal, the ions are deflected by the first atom in the row and lead to the formation of a shadow cone, which greatly reduces the backscattering yield of the first few atoms along the atomic string. As the beam penetrates deeper into the crystal most of the incident ions (~ 98%) acquire channeling trajectories. These

trajectories may be pictured as oscillatory and wave-like confined by the potential established by the atomic string. Channeled particles do not penetrate close enough to the atomic nuclei to undergo large angle scattering thus suppressing all close encounter events such as back scattering from deeper into the crystal. The spectrum generated is called a channeling spectrum. Channeling spectra can increase the sensitivity of all elements on a crystal surface or in an amorphous overlayer, as shown in Fig. 2.6, and are especially useful in quantifying light elements on/near the surface which would otherwise be hidden in the large background of bulk scattering. Channeling can also be used to investigate whether the sample and overlayer are crystalline and to determine precise structure in the bulk, or near a surface or interface.

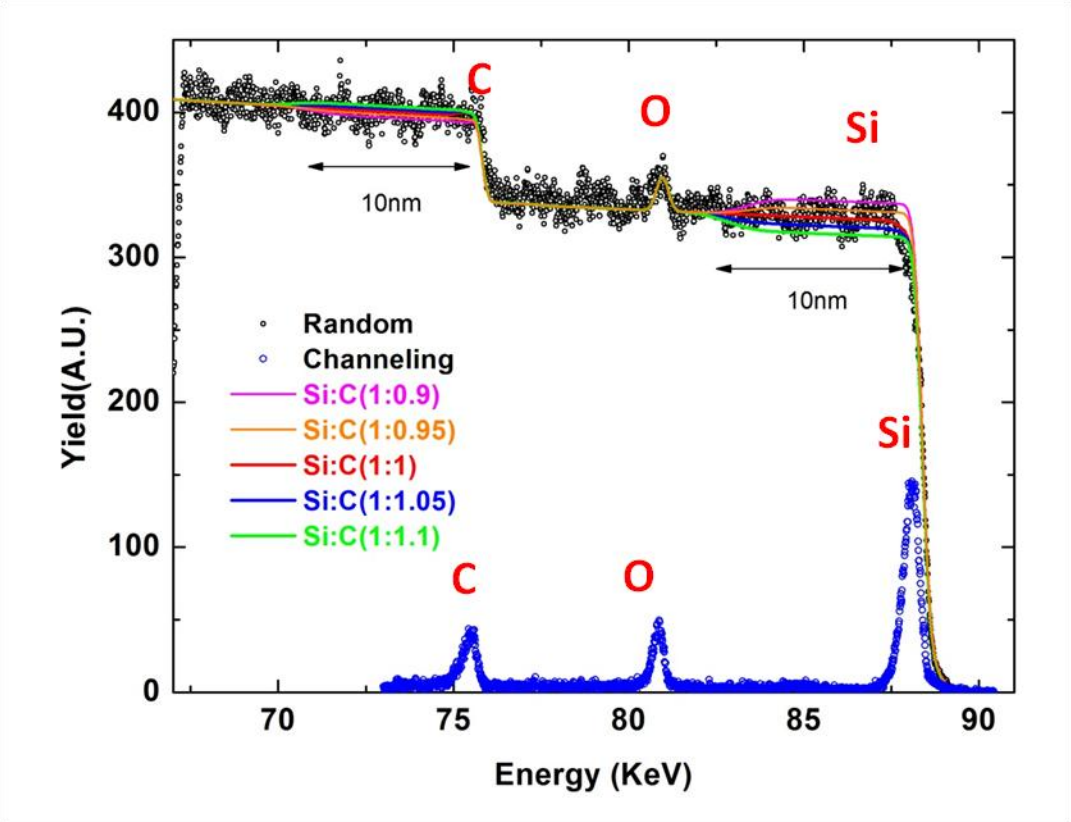

Fig. 2.6. Random and channeling spectrum of MEIS on SiC

2.6. Secondary ion mass spectrum (SIMS)

SIMS (secondary ion mass spectrometry) is a sensitive near-surface compositional method in which one uses a primary ion beam to bombard a sample surface, and then detects the emitted secondary ions by mass spectrometry.[6] The detection limits of SIMS can be as low as 1×10^{12} atoms/cm^3 ~ 1×10^{16} atoms/cm^3 depending on the element,[20] thus the technique is widely used for trace elemental analysis in solid materials.[20] The SIMS primary ion beam size can be reduced to less than 1 μm in diameter. The sample surface is slowly sputtered away during the SIMS analysis, and thus provides sample compositional information as a function of depth.

The primary ion beam sputters the sample surface and produces atomic and polyatomic particles from sample materials (secondary particles), along with electrons and photons. The secondary particles can be negative, positive or neutrally charged and carry zero to several hundred eV kinetic energies. The incident ion beam used in SIMS commonly includes Ar^+, Ga^+, O_2^+ or Cs^+ with energies ranging from 1 to 30 keV. The sputter rate depends on sample material, crystal orientation, primary beam species, energy and intensity, and usually ranges from 0.5 to 5 nm/s.[20]

Although the sputter rate can be controlled to a very slow rate, there are other factors limiting the depth resolution and sensitivity of SIMS. During the SIMS measurement, there are a series of binary collisions between the primary ions and target atoms. Some of the target atoms (recoil atoms) are energized by the primary ions and collide with more target atoms and continue to sputter the sample. Primary ions can be implanted and mixed with target atoms up to 10's of nm inside the sample (depending on the incident energy). Atoms from the surface can be driven deeper into the sample and

cause the material/interface mixing. Sputtering also leads to surface roughness and lattice damage in the sputtered region. On polycrystalline materials, SIMS measurement tends to cause more surface roughness than single crystal materials, mainly due to the different sputter rates of different crystallographic orientations. These effects and others limit the SIMS depth resolution. More problematic with SIMS is the problem of compositional accuracy in different matrices.

2.7. Capacitance-voltage (CV) electrical measurements

Numerous methods are used to measure the interface (electrical charge) trap density (D_{IT}), including conductance, low-temperature capacitance, charge pumping, sub-threshold current, low frequency (quasi-static), DC-IV and high-low frequency capacitance.[21, 22] The high-low frequency method is one of the most commonly applied methods in the SiC MOS field. D_{IT} is defined as

$$D_{IT} = \frac{(C_D+C_{IT})_{QS}-(C_D+C_{IT})_{HF}}{Se^2} \qquad \text{(Eq. 2.7)}$$

where $(C_D+C_{IT})_{QS}$ is the capacitance under quasi-static conditions, $(C_D+C_{IT})_{HF}$ is the capacitance with 100kHz probing frequency as an approximation of the theoretical semiconductor capacitance, and S represents the area of the gate electrode.

Given the quasi-static and oxide capacitances (C_{QS} and C_{OX}), the surface potential ψ_S can be represented as a function of the gate voltage VG as follows:

$$\psi_S(V_G) = \int \left(1 - \frac{C_{QS}}{C_{OX}}\right) dV_G + \psi_0 \qquad \text{(Eq. 2.8)}$$

where ψ_0 is the integration constant and is typically determined by the flat band capacitance measured under high frequency conditions.

References

[1] H. Hertz, "On an effect of ultraviolet light upon electric discharge," 1877.

[2] A. Einstein, "On a heuristic viewpoint concerning the production and transformation of light," *Annalen der Physik,* vol. 17, p. 132, 1905.

[3] H. Robinson and W. F. Rawlinson, *Phil. Mag.*, vol. 28, p. 177, 1914.

[4] K. Siegbahn, *Philosophical Transactions of the Royal Society of London Series A - Mathematical and Physical Sciences,* vol. 268, p. 33, 1970.

[5] K. Siegahn, C. Nordling, and A. Fahlman, *Nova Acta Regiae Soc. Sci Upsaliensis*, p. 20, 1967.

[6] L. C. Feldman and J. W. Mayer, *Fundamentals of Surface and Thin Film Analysis*. Elsevier Science Publishing Co., Inc: New York.: Elsevier Science Publishing Co., Inc: New York., 1986.

[7] K. Siegbahn, C. Nordling, and G. Johansson, *ESCA Applied to Free Molecules*. North-Holland Publishing Company: North-Holland Publishing Company, 1969.

[8] J. F. Moulder, W. F. Stickle, and P. E. Sobol, *Hand Book X-ray Photoelectron Spectroscopy. 2nd ed.* Eden Prairie, MN: Perkin-Elmer Corp., Physical Electronics Division.: Eden Prairie, MN: Perkin-Elmer Corp., Physical Electronics Division., 1992.

[9] G. Somerjai, *Chemistry in Two Dimensions: Surfaces* Cornell University Press, Ithaca, N.Y.: Cornell University Press, Ithaca, N.Y., 1981.

[10] S. H ̈ufner, *Photoelectron Spectroscopy*. Berlin: Springer-Verlag: Berlin: Springer-Verlag, 1996.

[11] J. R. Bird and J. S. Williams, *Ion Beams for Materials Analysis*. Academic Press: Academic Press, 1989.

[12] C. W. Magee, *Nucl. Instr. and Meth.*, vol. 191, p. 297, 1981.

[13] R. A. Weller, *Methods in Materials Research*. Wiley: Wiley, 2000.

[14] R. G. Smeenk, R. M. Tromp, and H. H. Kerson, *Nucl. Instr. and Meth.*, vol. 195, p. 581, 1982.

[15] J. A. Leavitt, L. C. McIntyre, and M. R. Weller, *Handbook of modern ion beam materials analysis*. Mater. Res. Soc.: Pittsburg: Mater. Res. Soc.: Pittsburg, 1995.

[16] W. K. Chu, J. W. Mayer, and M. A. NicoIet, *Backscattering Spectrometry*. New York: Academic Press: New York: Academic Press, 1978.

[17] J. F. Ziegler, "Stopping of energetic light ions in elemental matter," *Journal of Applied Physics*, vol. 85, pp. 1249-1272, Feb 1 1999.

[18] T. Feng, "Medium-energy ion scattering studies of interfaces in ultra-thin oxide films," Ph. D Ph. D dissertation, Physics, Rutgers University, 2011.

[19] L. C. Feldman, J. W. Mayer, and S. T. Picraux, *Materials analysis by ion channeling: submicron crystallography*. Academic Press: Academic Press, 1982.

[20] A. Benninghoven, F. G. Rüdenauer, and H. W. Werner, *Secondary Ion Mass Spectrometry: Basic Concepts, Instrumental Aspects, Applications, and Trends*. Wiley, New York: Wiley, New York, 1987.

[21] D. K. Schroder, *Semiconductor Material and Device Characterization, Third Edition,*. A JOHN WILEY & SONS, INC., PUBLICATION: A JOHN WILEY & SONS, INC., PUBLICATION, 2006.

[22] H. Yoshioka, T. Nakamura, and T. Kimoto, "Accurate evaluation of interface state density in SiC metal-oxide-semiconductor structures using surface potential based on depletion capacitance," *Journal of Applied Physics,* vol. 111, Jan 1 2012.

Chapter 3. Atomic State and Characterization of Nitrogen at the SiC/SiO_2 Interface

3.1. Introduction

The performance of SiC MOSFETs in high power or other applications is limited by interface defects formed during high temperature oxidation.[1] Interface defect concentrations for SiO_2/4H-SiC following dry oxidation (dry O_2) are 1-2 orders of magnitude larger than those that form during SiO_2 growth on Si using similar procedures and are not significantly lowered by forming gas (H_2) anneals.

Introducing nitrogen (N) into SiO_2/SiC structures using a nitric oxide (NO) anneal[2,3] reduces the large interface state density[4] and improves the channel mobility, and thus device performance. Earlier measurements by our group and others have shown that the N accumulates in a very narrow layer (<1.5nm) at the oxide/semiconductor interface[5] with a coverage in the sub-monolayer range.

Tochihara, et al.[6] and Kosugi, et al.[7] performed x-ray photoemission studies on NO annealed SiC/dielectric structures. They found a strong N 1s signal after the oxide was mostly etched away indicating that N incorporates very near the SiO_2/SiC interface. The nitrogen areal density was estimated to be ~ $10^{14}/cm^2$. They confirmed that N incorporation results in a reduction in the density of interface traps by about an order of magnitude. Although elemental depth profiles across the interface for these systems have been reported by our group and others,[5, 8] the atomic level bonding and chemistry of nitrogen incorporation is not well-understood. In addition to the use of NO, successful nitrogen incorporation and passivation using a nitrogen (N_2) plasma[9] has been reported.

In this chapter, we examine the chemistry of nitrogen at the SiO_2/SiC interface. As noted above, nitrogen is incorporated into SiC-based MOSFETs because it improves the electrical properties of devices. As discussed in this chapter, we find that it locates predominantly at the SiO_2/SiC interface independent of how it is introduced into the system. We study the chemical environment and quantify the areal density of nitrogen in this system formed by NO anneals, by N_2 plasma nitridation, and by direct nitridation in a very high temperature N_2 (g) anneal. In Section 3.1 we present a brief overview of the motivation of the chapter. In section 3.2, the different nitridation processes are described. In section 3.3, the differences between the etching behavior of interfacial N on Si and SiC surfaces are studied. In section 3.4, The interfacial N content is measured by X-ray photoelectron spectroscopy (XPS), medium energy ion scattering (MEIS), and dynamic secondary ion mass spectrometry (SIMS). The results from these three techniques are in reasonable agreement. The photoelectron mean free path in SiC is also extracted. The quantification of buried layers (via SIMS) and etched surfaces (via XPS and MEIS) demonstrate that, within the error of different techniques, all of the interfacial nitrogen present prior to etching remains after a BOE etch (buffered oxide etchant, mixture of HF and NH_4F). In section 3.5, the source of un-etchable N and O on NO-annealed SiC are identified through isotope experiments and nuclear reaction analysis (NRA). In section 3.6 and 3.7, we investigated the interfacial N and O bonding and interface structure on NO annealed SiC using both experimental and theoretical methods. Different possible structural models are calculated (in collaborative work) and discussed in section 3.7. In section 3.8, accurate N depth profiles at the SiO_2/SiC interface are studied using MEIS and angle resolved XPS, and finally we are able to determine the depth profile of most of

the N at interface. In section 3.9, we also described preliminary results of nitridation by plasma and high temperature N_2 (g) anneals, both of which result in similar bonding configurations to NO-annealed samples (although with different total N content).

3.2. Description of sample fabrication and apparatus

We discuss a range of nitrogen incorporation chemistries. However NO annealing remains the dominant process currently used in SiC MOSFET research and production and receives the most attention in this chapter. Wafers of 4H-SiC obtained from Cree, Inc. (miscut by ~4 deg.) were used. Nitrogen was introduced via three different processes:

1) Clean SiC was first dry oxidized at 1150^{o}C to grow a 50-60 nm oxide and then annealed in an NO gas flow (1 atm, 500 sccm) at 1175^{o}C for 2 hrs. For comparison purposes silicon carbide and pure silicon with oxides of the same thickness were processed in parallel using NO (g).

2) SiC with a 50-60 nm dry oxide was exposed to N_2 (g) in a 5000W remote plasma at 1160^{o}C. The flow rate of N_2 was kept at 200 sccm while the other side of the furnace was simultaneously pumped to achieve a dynamic equilibrium with a constant gas pressure of 2.75 Torr. After the N_2 plasma step, a post-plasma anneal was added in which the sample was kept in the furnace under N_2 at 1160^{o}C, 1 atm, for 30 minutes with the plasma turned off. The purpose of this step is to help anneal out the electron and ion bombardment damage caused by the plasma and the microwave, and thus to improve the oxide properties and reliability while retaining the benefit of the N_2 plasma treatment.[10]

3) Clean SiC exposed to N_2 (g) at temperatures from 1250 to 1600^{o}C.

Details of the various sample exposures are listed in Table 1.

XPS studies were performed in a Thermo K-Alpha system with a monochromatic Al Kα x-ray source. The Au $4f_{7/2}$ peak, as well as C and Si substrate peaks were used for energy referencing. Additional compositional analysis employed secondary ion mass spectroscopy (SIMS) and medium energy ion scattering (MEIS).[8] NO (g) annealed SiC samples measured by SIMS showed no detectable N within the "bulk" region of the oxide (within the sensitivity limit of SIMS ~$10^{17}/cm^3$) and an accumulation of N at the interface, consistent with earlier reports by TEM, SIMS and MEIS.[5, 8]

3.3. Comparison of N etching behavior on SiC and Si interface

Fig. 3.1 shows a wide energy range XPS spectrum of NO-annealed SiO_2/SiC sample, etched to leave ~1.5 nm of oxide, and the wide spectra from the same sample etched to completely remove all the oxide. In the case of "full" oxide removal, the intensity of the N 1s peak increases relative to the Si (and O) peaks since the overlayer SiO_2 no longer attenuates the outgoing N 1s photoelectrons. All such etches were performed in a 7:1 buffered HF solution (BOE) unless otherwise stated. Note the presence of Si 2p photoemission intensity close to 104 eV, which indicates substantial remaining oxide in the partially etched sample. The same experiment and XPS measurement were also performed on the pure Si NO (g) annealed sample, the N 1s spectrum were shown in the Fig. 3.2(b).

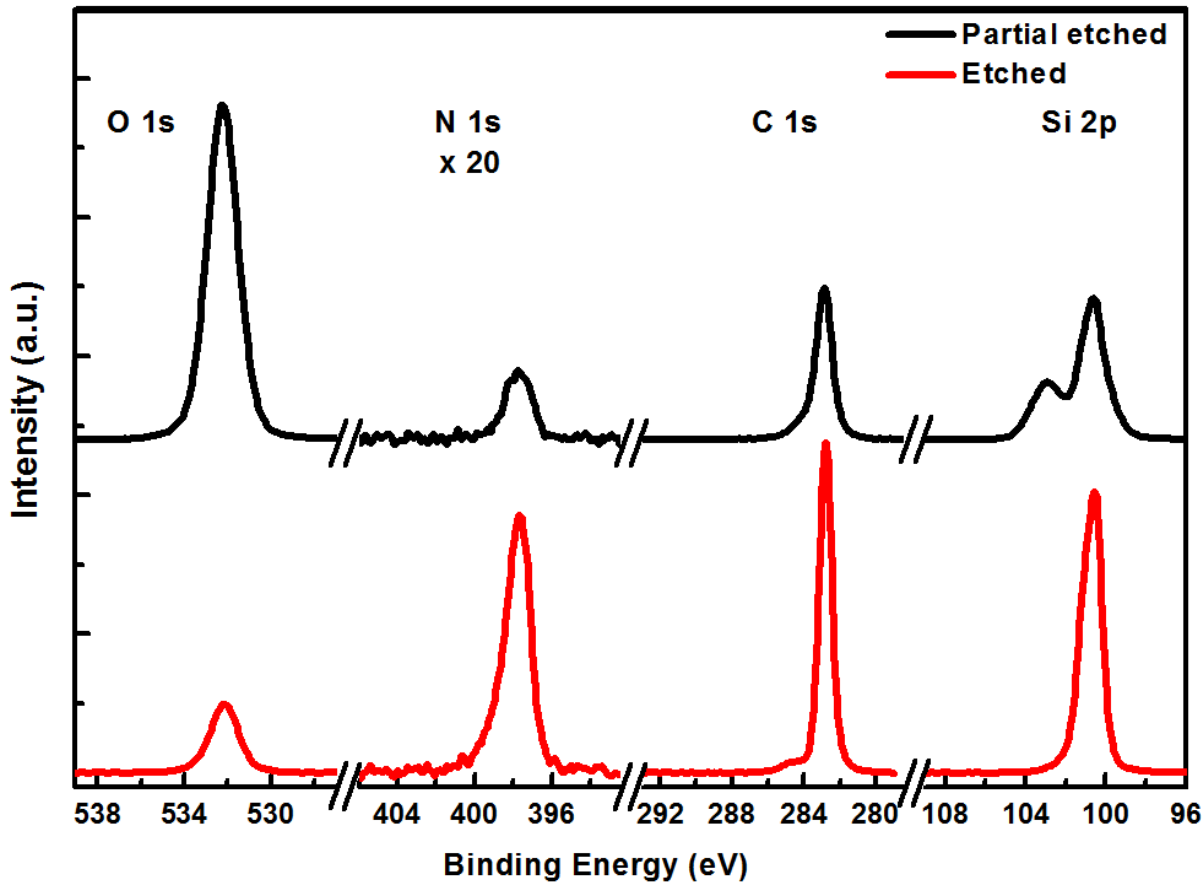

Fig. 3.1. Wide energy range XPS spectra of a NO annealed SiO_2/SiC sample partially etched (black) to ~1.5 nm of oxide on SiC and completely etched (red), with the N 1s intensity magnified 20 times.

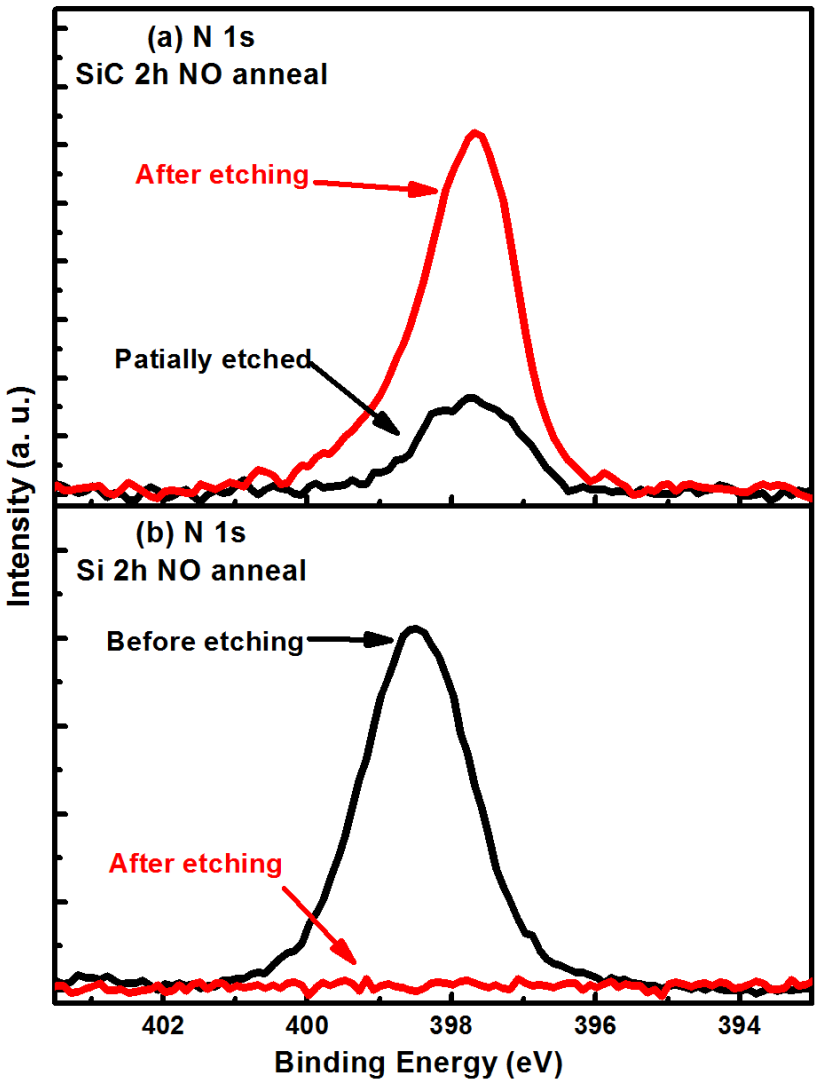

Fig. 3.2. XPS spectrum of before and after 5 minute BOE etching from NO annealed (a) SiC and (b) Si. The increase in the signal strength in (a) is due to the elimination of attenuation by the overlayer.

To understand the N bonding differences between Si and SiC MOS, Fig. 3.2 reports XPS data for samples that are etched in BOE. Fig. 3.2(a) compares the N 1s XPS spectra for NO annealed SiO_2/SiC samples partially and completely etched. The spectra are

normalized to the same incident x-ray flux. A quantitative analysis using 2.2nm as the Si 2p electron escape length in the SiC (calculated from XPS and MEIS data) indicates that there is no detectable N removal in the case of the "completely" etched SiO_2 overlayer on SiC. Fig. 3.2(b) shows the same sequence for the silicon system (SiO_2/Si) indicating complete removal of the N (within the XPS sensitivity limit) after the SiO_2 layer is etched by BOE. In the NO annealed SiO_2/Si system it was shown that N accumulates primary at the interface.[11, 12] The figure focuses on the N 1s signal in both cases, indicating that the binding energy of the N 1s for SiO_2/SiC does not change upon etching, while the N signal in the SiO_2/Si system (prior to its removal during etching) is indeed shifted in energy relative to N bound at the SiC interface.

We conclude that N is bound to SiC in a manner which minimizes removal during an HF etch of the oxide, quite unlike the behavior observed on Si. Furthermore, the data show that the NO anneal introduces more nitrogen at the interface when grown on a Si sample (for the same NO exposure, the N content in the Si sample is about twice that observed at the SiO_2/SiC interface), although no nitrogen is detected after the BOE etch of the Si sample. The different chemical behavior of N at Si and SiC interfaces under the same etching conditions and the different N binding energies that we observe by XPS indicates that N has a different chemical environment in the two systems.

We note that a BOE process etches Si_3N_4 at a rate of ~2 nm/s (under conditions similar to our SiO_2/SiC etching), and thus a thin pure nitride should easily be etched if present in our films, ruling out the possibility that N atoms are incorporated into a stable bulk-like nitride on SiC. Our results are consistent with experimental results[6, 7,13,14] and a theoretical model[15,16] which implies that instead of pure Si_3N_4 or a simple SiNO layer, the

N is directly involved in bonding to the SiC substrate at the interface, or possibly embedded within first layer or two of the substrate, forming a stable, BOE-etch-resistant interfacial region.

In an earlier report, Dhar et al.[17] measured the residual oxygen following etching of thermal oxides on both Si and SiC using isotopically labeled O_2 analyzed by nuclear reaction analysis (NRA).[17] The results confirm earlier findings for Si which show that BOE etching of oxide on Si leaves a hydrogen terminated surface. Surprisingly, etching of the oxide on SiC leaves a residual oxide monolayer on SiC, to be precise, an oxygen terminated surface on Si-face and an –OH terminated surface on C-face.[17] As a possible explanation, the authors noted that etching at the SiO_2/Si interface requires the insertion of F into the Si-Si bond,[18] and (ii) that this insertion mechanism may not be operative in the SiO_2/SiC case due to the higher stability of the Si-C bond relative to Si-Si.[17] Analogously, we suggest that this last layer of N-Si at the SiC interface is also resistant to etching due to the stability (and resulting lower reactivity toward HF) of the Si-C bond relative to the Si-Si bond.

Other possible explanations for the enhanced stability of N at the SiC interface include: (i) differences in the formation energy, and hence the etching kinetics, of etchable intermediates on Si and SiC, or (ii) the formation of a stable interface phase such as a carbon nitride or oxy-nitride.[19,20] However, the surface excess carbon reported by Zhu et al[8] using MEIS is ~1.8×10^{14} cm^{-2}, sets a limit to this type of C_xN_y phase. An additional possibility is that some of the N might be incorporated into the near surface of the substrate (but within the escape depth of XPS) such that oxide etching does not apply.

It has been reported that an N-doped near surface layer in SiC may result in "counter doping" and improved electrical properties.[21,22]

3.4. Quantification and photoelectron mean free path

The N coverage can be quantified with XPS peak intensities, but the accuracy is limited by the uncertainty in the attenuation length of the relevant photoelectrons. Assuming that the thin SiO_2 layer on the surface would attenuate the N 1s and Si $2p_{2/3}$ peak intensity in the same way, and knowing that N amount is sub-monolayer, thus assuming N layer thickness to be 1.3 Å, same as the N atom's diameter, N coverage can be quantified with XPS peaks intensities by following equation:

$$\frac{I_N / \sigma_N}{I_{Si/SiC} / \sigma_{Si/SiC}} = \frac{N_N}{N_{Si/SiC}\lambda_{Si/SiC}(1-\frac{t_N}{\lambda_{Si/SiC}})} \qquad \text{(Eq 1)}$$

Where I_N and $I_{Si/SiC}$ are N 1s and Si $2p_{3/2}$ (from SiC substrate) peak intensity, σ_N and $\sigma_{Si/SiC}$ stand for the cross section of the two photoemission process, N_N and $N_{Si/SiC}$ represent the number of atoms per cm^2, t_N is the thickness of nitrogen layer, $\lambda_{Si/SiC}$ is the Si $2p_{3/2}$ photoelectron effective attenuation length in SiC. In this equation, N_N is unknown and $\lambda_{Si/SiC}$ is not well known. We have used medium energy ion scattering (MEIS), further supported by secondary ion mass spectrometry (SIMS) and earlier reports using NRA[23] for quantification. SIMS provides a measure of the total nitrogen content in the films (without a BOE removal of the oxide layer), and MEIS gives an independent and more accurate measure of the nitrogen content on etched (or thin un-

etched) samples. The available evidence implies that after BOE etching the nitrogen is retained, which is also consistent with the result reported by Kosugi et al.[7]

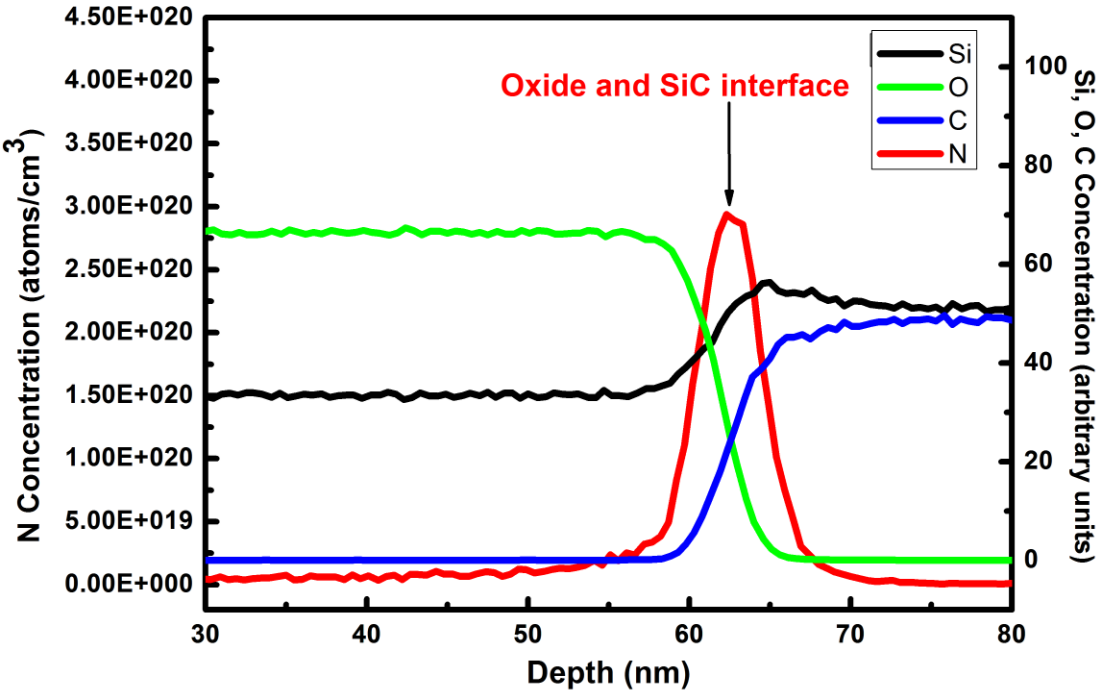

Fig. 3.3. One set of SIMS profiles of silicon, oxygen, carbon, and nitrogen near the Si-face SiO_2/SiC interface. Silicon, oxygen, and carbon intensities are in arbitrary units (right), and the nitrogen concentration is in atoms/cm^3 (left). The depth profile is limited by the SIMS depth resolution.

SIMS (Fig. 3.3) indicates that N accumulates at or close to the Si-face SiO_2/SiC interface, with an interface profile (based on the FWHM) of less than 10 nm. The interface 'width' based on this metric is limited by the depth resolution of SIMS; the true width is very likely less than 10 nm.

Accurate quantification of the N content on the fully etched sample was achieved with medium energy ion scattering (MEIS) using a 100 keV proton beam in a channeling direction (the <0001> axis)[8]. Fig. 3.4 shows (a) the MEIS spectra of a 2 hour NO annealed SiC sample followed by 5 min of HF etching and (b) the nitrogen part of the MEIS spectrum. The MEIS measurement yielded an interfacial N areal density of $4.0(\pm 0.6)\times 10^{14}$ cm^{-2}, which agrees (within experimental error) with the SIMS result of $6.0(\pm 2.0) \times 10^{14}$ cm^{-2}.[24] A surface N density of 4.0×10^{14} cm^{-2} corresponds to ~ one third of a monolayer of surface Si atoms on SiC.

Using the MEIS and XPS results from the same sample, the Si $2p_{3/2}$ photoelectron attenuation length in SiC ($\lambda_{Si/SiC}$) is calculated to be ~2.1 (±0.3) nm, assuming all the nitrogen is at the interface. Comparing MEIS and XPS results from multiple samples yields an average $\lambda_{Si/SiC}$ as ~2.2 nm. The combination of results, both absolute values of the N coverage, and the extraction of the mean free path (mfp), indicates that the NO process is well controlled and reproducible. Our calculated mfp for Si $2p_{3/2}$ photoelectron attenuation Si is somewhat smaller that the literature value of 2.9 nm,[25] which is estimated using the average of the mfp of Si and C listed in the NIST database.[26] Our result however is quite reasonable given that SiC has a significantly higher density than Si and C. Using our value of the mean free path, $\lambda_{Si/SiC}$, the oxygen areal density on the freshly etched sample is estimated to be 1.4×10^{15} cm^{-2}, close to one monolayer of oxygen (1.2×10^{15} cm^{-2}). The majority of the oxygen signal comes from the non-etchable portion of the initial oxide described in the work of Dhar et al[17], with some adventitious oxygen due to exposure to the ambient atmosphere.

The comparison of the N content via SIMS, done without pre-chemical etching, and MEIS and XPS performed after complete etching indicates that all of the interfacial nitrogen content is preserved in the wet etching process, at least within the sensitivity of these techniques (~10%).

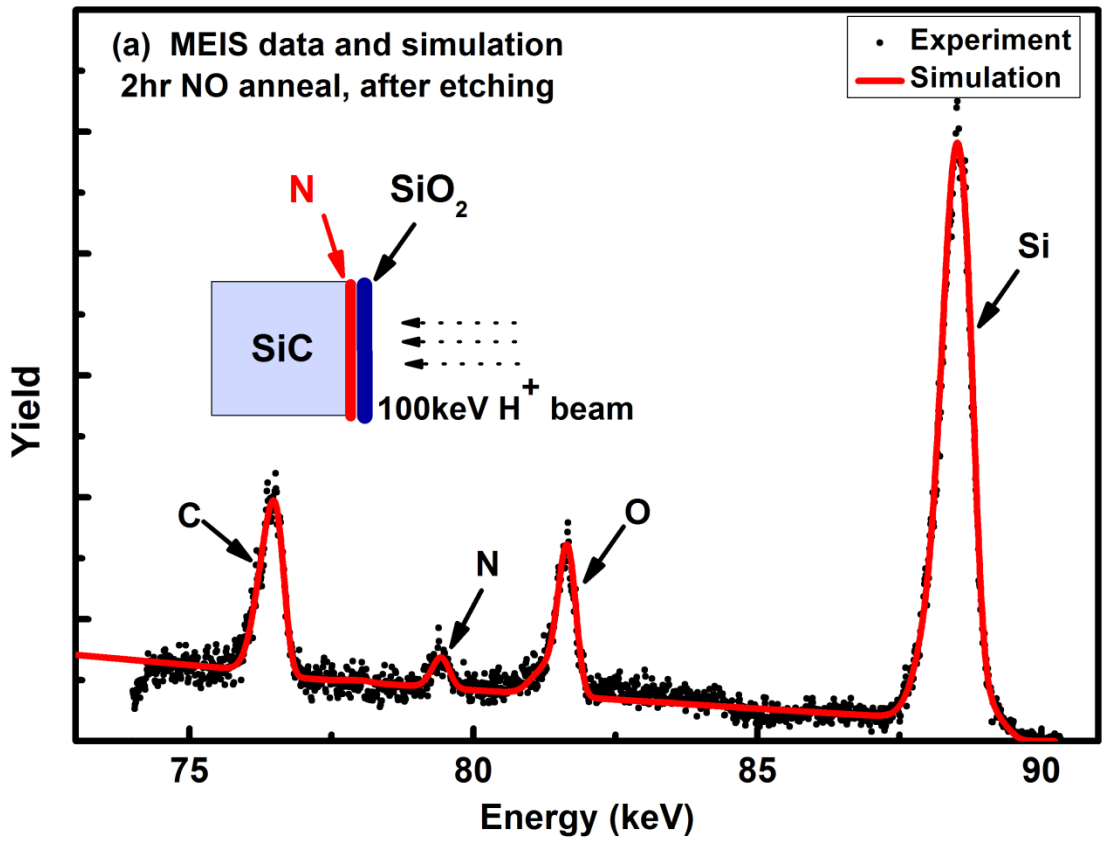

Fig. 3.4.(a) MEIS full spectrum of 4H-SiC annealed in NO for 2 hours, followed by 5 minute BOE etching.

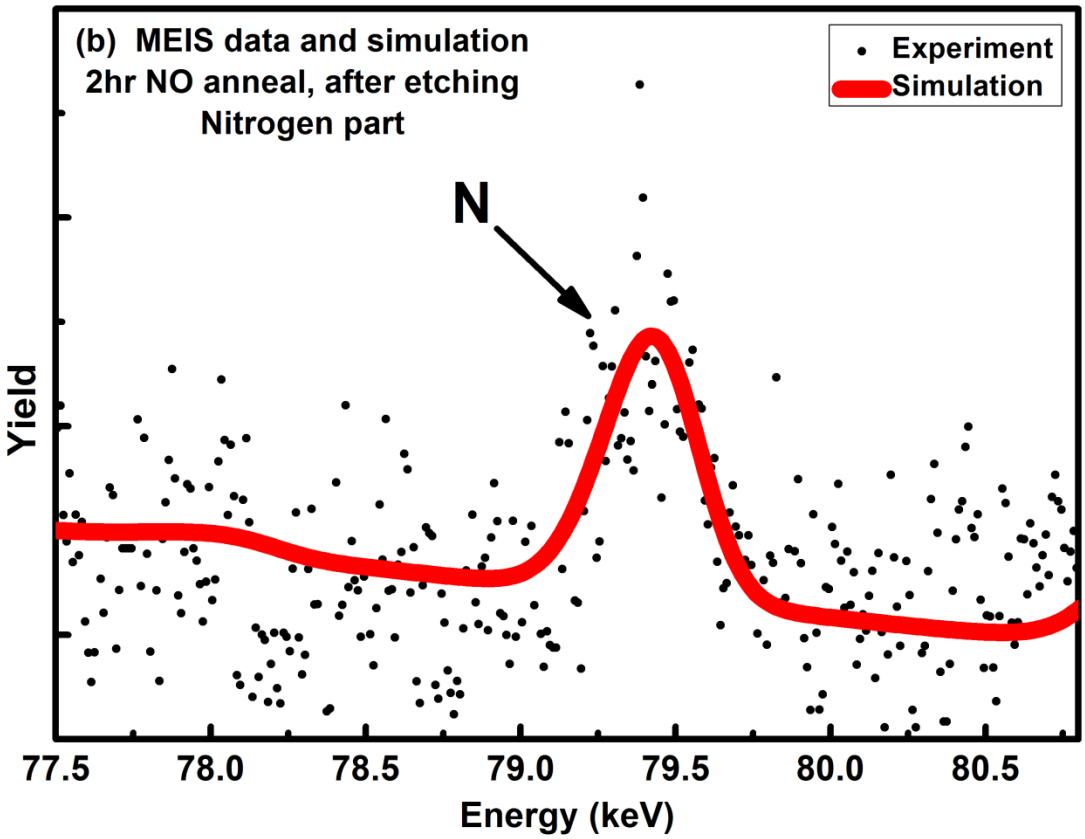

Fig. 3.4.(b) Nitrogen part of the MEIS spectrum of 4H-SiC annealed in NO for 2 hours, followed by 5 minute BOE etching.

3.5. Isotope Experiment

In an earlier report, Dhar et al.[17] measured the residual oxygen following etching of thermal oxides on both Si and SiC using isotopically labeled O_2 analyzed by nuclear reaction analysis (NRA).[17] The results confirm earlier findings for Si which show that BOE etching of oxide on Si leaves a hydrogen terminated surface. Surprisingly, etching of the oxide on SiC leaves a residual oxide monolayer on SiC.[17]

As shown in Fig. 3.1, on the completely etched NO(g)-annealed SiC surface (red line), an oxygen signal can still be detected by XPS. There are 2 possible sources of the

oxygen on the HF-etched NO-annealed SiC: (i) from the unetchable oxide that were studied by Dhar, et al;[17] and (ii) from hydrocarbons in ambient air which is chemically or physically adsorbed when the sample was transferred in the air. To further investigate the source of the oxygen and the chemical state of nitrogen at the SiO_2/SiC interface, an isotope experiment was performed.

Two pieces of clean SiC sample were annealed in isotope enriched $^{15}N^{18}O$ (g, 98% ^{14}N and 98% ^{18}O, Sigma Aldrich, Inc) at 1175^{o}C for 1 hr. The NO annealed process was slightly different than a standard NO (g) anneal process in a few aspects:

(i) At high temperature, NO (g) can decompose into N_2 and O_2, so the standard NO (g) anneal is done with 500 sccm NO (g) flow, to refresh the NO gas. In this experiment, due to the high cost of $^{15}N^{18}O$ (g), the anneal was performed in a static mode, with both ends of the furnace being sealed.

(ii) In the standard NO (g) anneal, the pressure in the furnace is 1 atm, while in this experiment, the pressure was kept to be about 5 psi higher than 1 atm to reduce the air leaking into the furnace.

(iii) The annealing time was 2 hrs in the standard NO (g) anneal, while in this experiment, the time is reduced to 1 hr. It was shown by McDonald, et al,[27] that in a static mode NO (g) anneal, after a certain time period, the interfacial N coverage decreases due to the NO (g) decomposition generates O_2 and then re-oxidizes the N sites.[27] At 1175^{o}C, in a static mode, the N coverage reaches a maximum at 1 hr.[27]

(iv) This isotope experiment is done using a clean SiC sample, without any pre-oxidation, since we are more interested in the new interface created by the NO anneal step.

After the $^{15}N^{18}O$ (g) anneal, one sample was analyzed by RBS (with channeling), NRA and ellipsometry. RBS channeling was done using a 2 MeV $^{4}He^{+}$ incident beam and collected for 50 μC total beam dose. The RBS channeling result is shown in Fig. 3.5. The total oxygen from silicon dioxide is estimated to be about $44.6 \times 10^{15}/cm^2$, and agrees with the ellipsometry result of 9 nm oxide thickness. The interfacial nitrogen amount is too low to be seen in the RBS channeling spectrum. The RBS result shows that in the oxide layer, the oxygen contains about 87% ^{18}O and 13% ^{16}O. The ^{18}O ratio is lower than the $^{15}N^{18}O$ gas (98% ^{18}O) that was used in the annealing, which we assume is predominantly caused by oxygen exchange between the gas inside and outside the furnace during the annealing. Based on the RBS results, ^{18}O and ^{16}O distributed evenly in the oxide layer, indicating that the oxide is grown primarily with $^{15}N^{18}O$.

The sample is then analyzed using NRA. The measurement is performed using a 824 keV proton beam and collected for 1 μC total beam dose. The nuclear reaction used here can be described as:

$$p + {}^{18}O \rightarrow {}^{15}N + \alpha + Q$$

The data points between 500 keV and 1250 keV are shown in Fig. 3.6(a) are the collected α particles from the nuclear reaction. This NRA result confirms the presence and amount of ^{18}O, and is also used to calibrate and quantify the ^{18}O content after etching.

The other sample that was prepared simultaneously was etched in 7:1 BOE for 5 min to remove all the oxide, and then analyzed by NRA, XPS and MEIS channeling. Fig.

3.6(b) shows the NRA result of the etched $^{15}N^{18}O$-annealed SiC sample. The measurement is also carried on using a 824 keV proton beam and collected for 20 μC total beam dose (to obtain a better signal to noise ratio for the unetchable oxygen). In this measurement, the ^{18}O areal density is estimated to be $1.1 \times 10^{15}/cm^2$, and based on the data below 500 keV, the ^{15}N amount is estimated to be $0.12 \times 10^{15}/cm^2$.

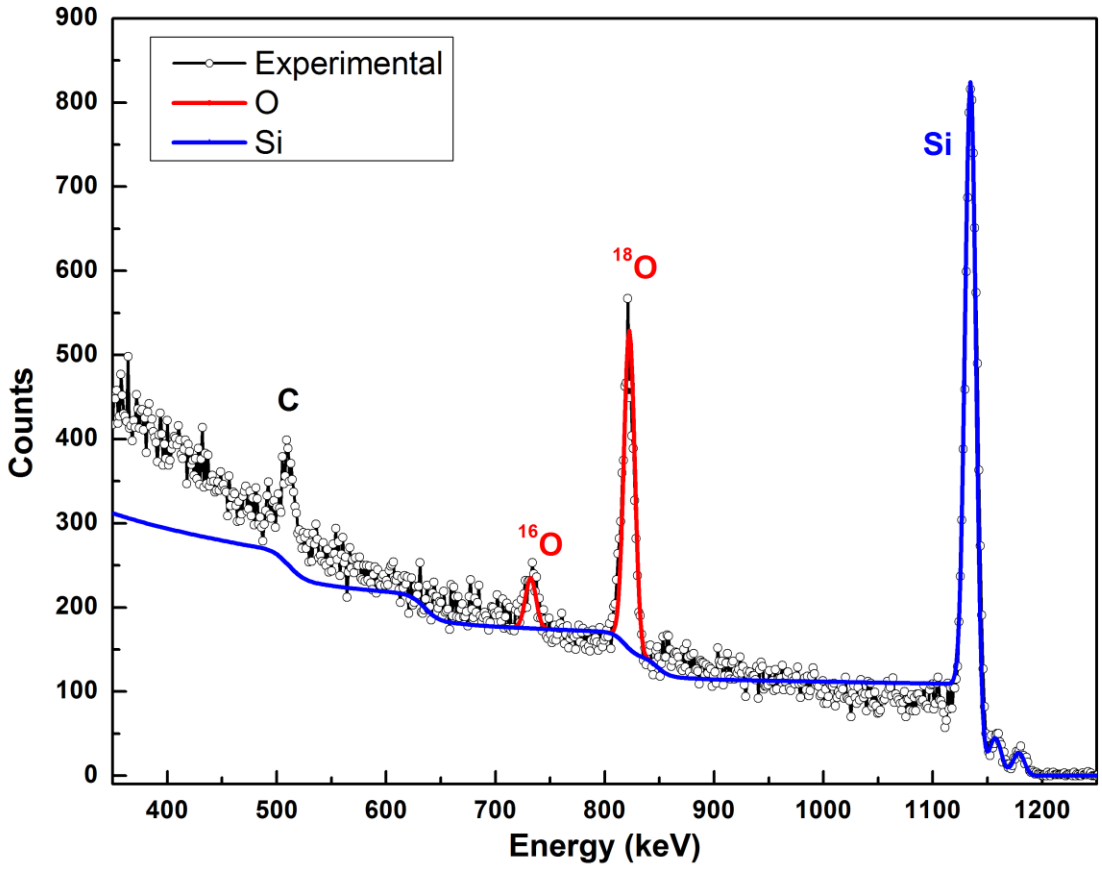

Fig. 3.5. Channeling RBS spectrum of un-etched $^{15}N^{18}O$ annealed SiC

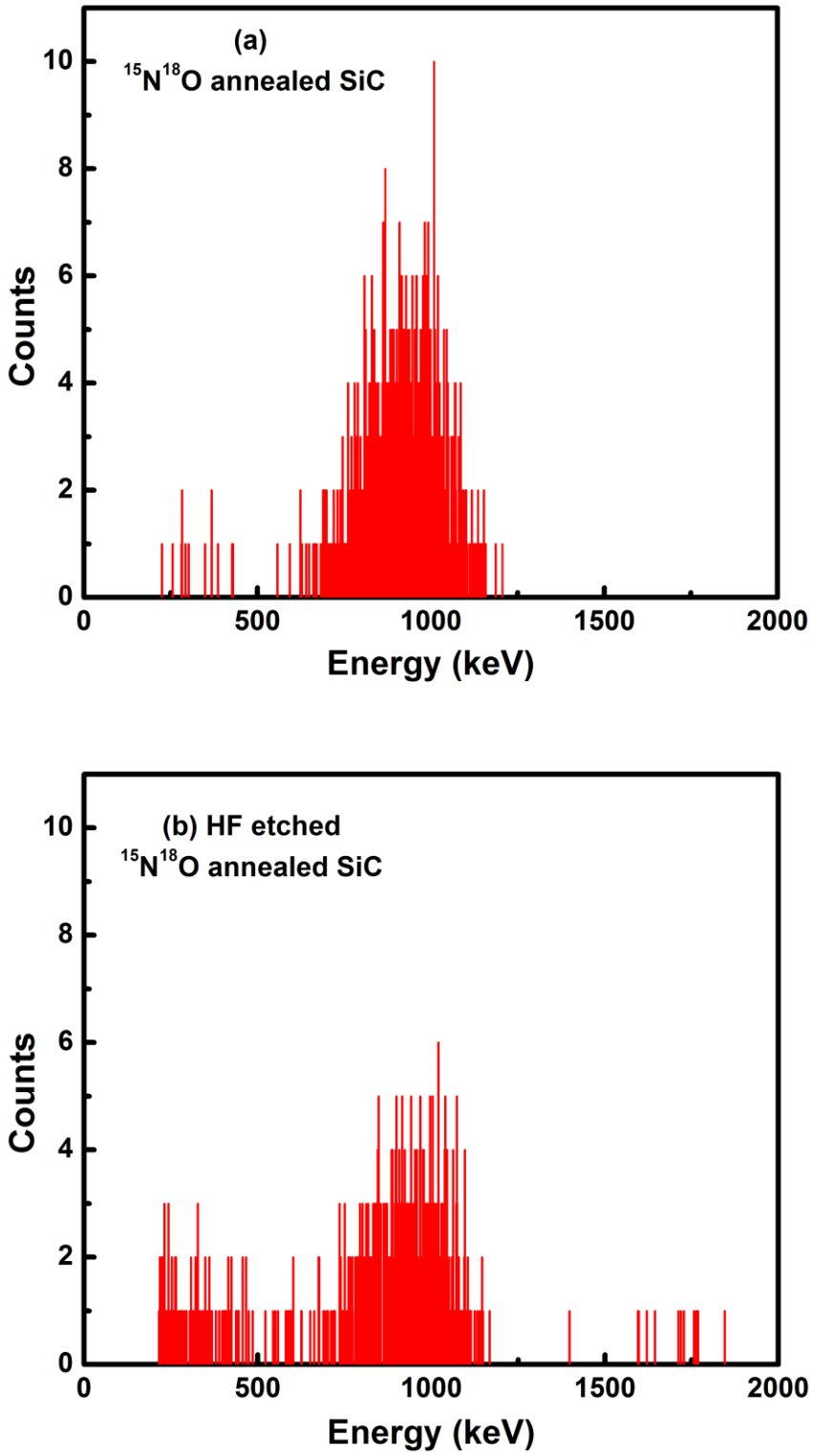

Fig. 3.6. NRA spectrum of (a) un-etched $^{15}N^{18}O$ annealed SiC and (b) etched $^{15}N^{18}O$ annealed SiC.

Fig. 3.7 shows the MEIS spectrum of the etched $^{15}N^{18}O$ annealed SiC. The measurement is done using a 100 keV proton beam in the channeling direction. MEIS results indicates that all the oxygen, including both ^{18}O and ^{16}O, are on top of the SiC surface. ^{18}O and ^{16}O amounts are estimated to be $1.1 \times 10^{15}/cm^2$ and $0.84 \times 10^{15}/cm^2$, respectively. Using the ^{18}O and ^{16}O ratios in the bulk oxide that formed during the $^{15}N^{18}O$ anneal, it can be calculated that of the $0.84 \times 10^{15}/cm^2$ ^{16}O fraction, approximately $0.17 \times 10^{15}/cm^2$ are from the un-etchable oxide and $0.67 \times 10^{15}/cm^2$ are from the adventitious oxygen. Adding up the ^{15}N and un-etchable O, including ^{18}O and ^{16}O, gives a number of about $1.4 \times 10^{15}/cm^2$, which is close to the number of $1.25 \times 10^{15}/cm^2$ Si atoms (or C atoms) in one monolayer of a SiC crystal on the Si-face or C-face. The experiment process and results are summarized in Fig. 3.8 and Table 3.1.

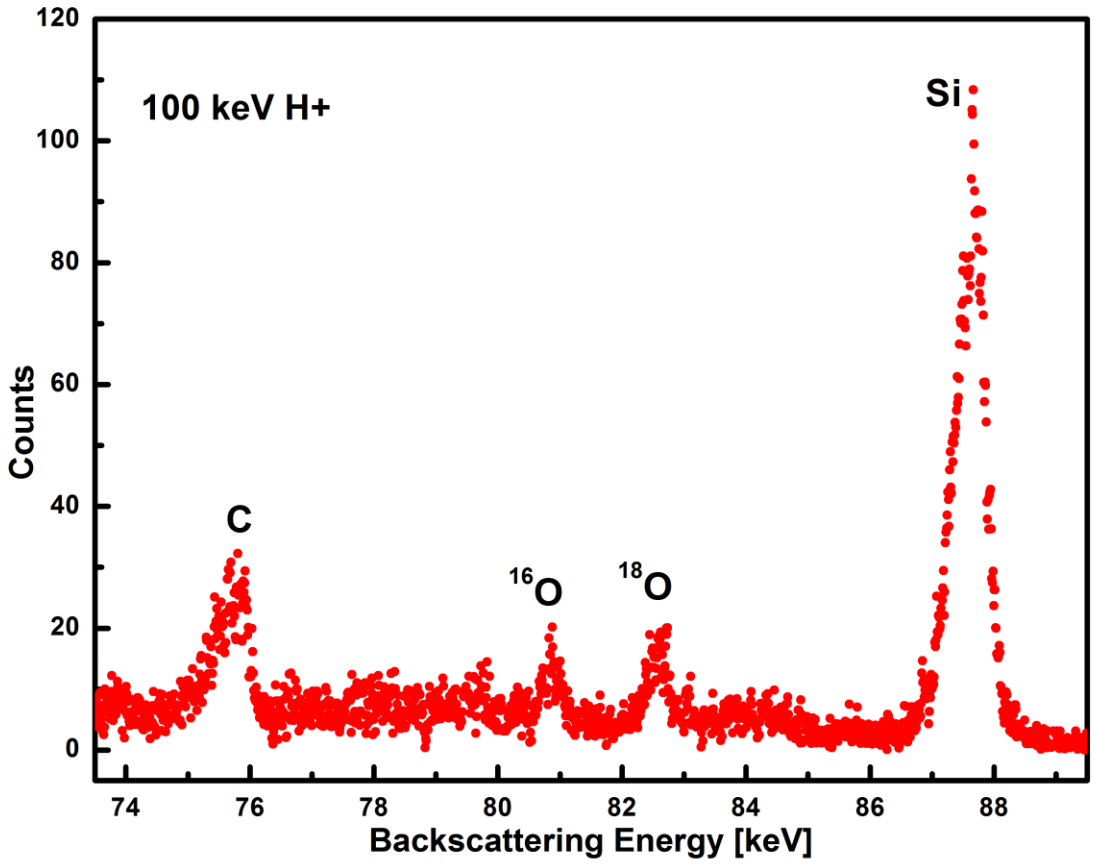

Fig. 3.7. MEIS spectrum on etched $^{15}N^{18}O$ annealed SiC

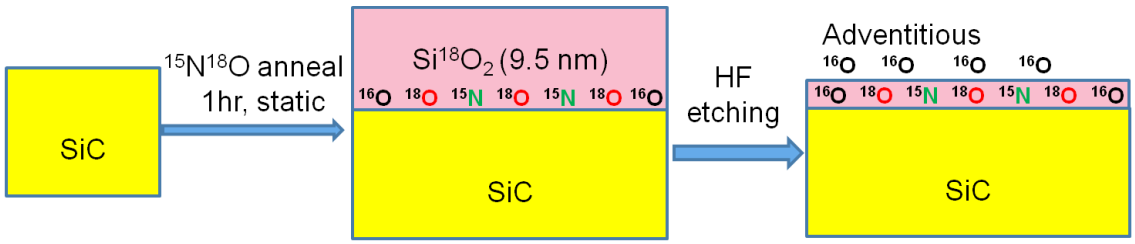

Fig. 3.8. Summary of the experiment

Table 3.1. MEIS, RBS, NRA, XPS result

Sample		RBS & NRA	MEIS	XPS
With oxide	Oxide thickness (nm)	9.5		
	^{18}O coverage (cm^{-2})	38.4×10^{15}		
	^{16}O coverage (cm^{-2})	6.2×10^{15}		
	^{18}O percentage	87%		
Etched	^{15}N coverage (cm^{-2})	0.12×10^{15}		0.15×10^{15}
	^{18}O coverage (cm^{-2})	1.1×10^{15}	1.1×10^{15}	
	^{16}O coverage (cm^{-2})		0.84×10^{15}	
	^{16}O from unetched oxide		0.17×10^{15}	
	^{16}O from adventitious sources		0.67×10^{15}	
	O total coverage (cm^{-2})		1.9×10^{15}	1.6×10^{15}

3.6. Bonding state at the interface: Experimental

To provide further insight into the chemical state of nitrogen at the SiO_2/SiC interface, the N 1s spectrum is fit with a set of three Gaussians representing three

different bonding configurations (Fig. 3.9). The fit includes a main peak centered at a binding energy of 397.5 eV and secondary peaks centered at ~ 398.4 eV and ~ 399.5 eV. Comparing these N 1s peaks to previously reported values indicates possible nitrogen bonding environments.[28] However, surface/interface dipoles and calibration methods together can result in significant variations of binding energy values between experiments.[29] Therefore, caution must be exercised when comparing experiments that do not use a common reference.

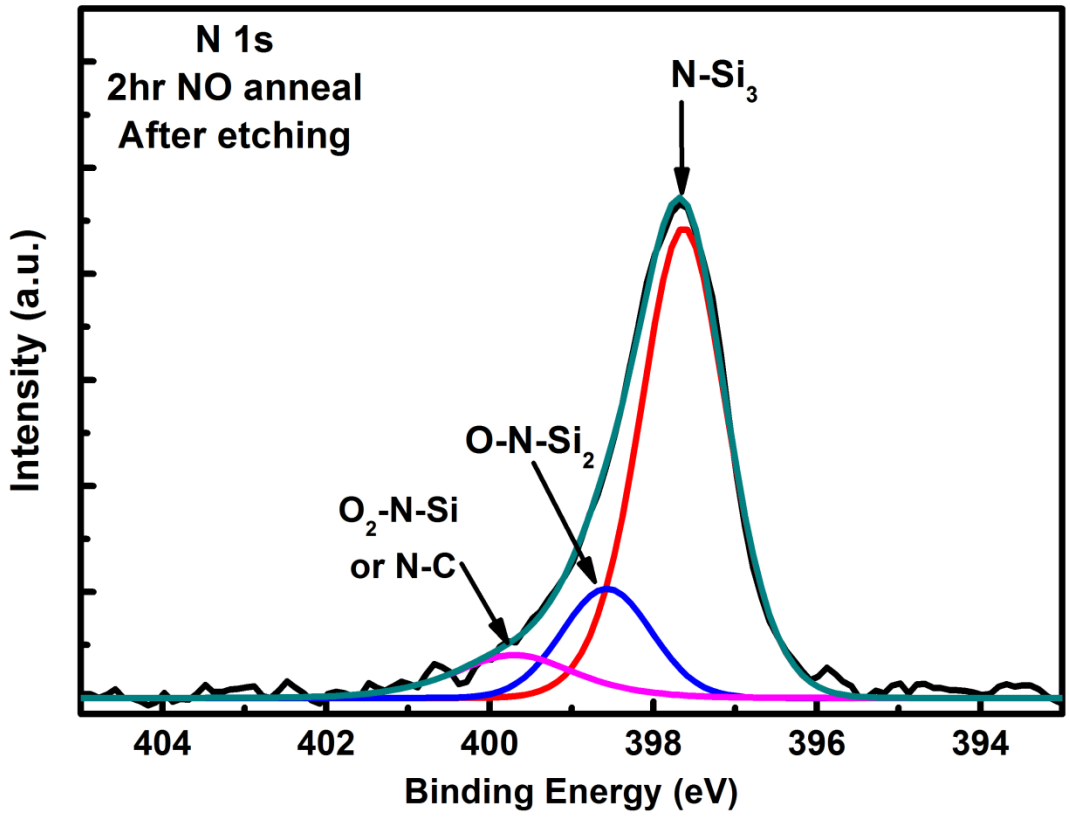

Fig. 3.9. N 1s XPS spectrum with possible peak assignments of 4H-SiC annealed in NO for 2 hours, followed by 5 minute BOE etching.

We can benefit from the extensive work published concerning the N 1s signals of oxy-nitride thin films on silicon.[30] The dominant N 1s peak binding energy for oxynitrides of varying nitrogen content range from 397.0 to 398.0 eV, and are attributed to nitrogen bound to three silicon nearest neighbors. The lower binding energy value observed is associated with N within a Si_3N_4-like near interfacial environment whereas the higher value is associated with N still bound to three Si atoms but within a SiO_2 environment, with the number of second nearest neighbor oxygen atoms being an important determining factor.

Higher binding energy N 1s peaks are less well understood, with peaks at ~ 399 eV attributed to nitrogen bound to one oxygen and two silicon atoms, and peaks at ~ 400 eV attributed to nitrogen bound to one silicon and two oxygen. A recent study of complex nitrogen molecules on silicon surfaces[31] corroborates these assignments. In addition, N bound to two silicon and one carbon was found to produce an N 1s peak at 398.4 eV suggesting an alternative bonding possibility for XPS peaks in this range. While the above results provide a starting point for understanding our N 1s peaks, calibration and interface issues prevents a definitive comparison to our XPS results. Below we describe the calibration method used here to carefully compare various nitrogen bonding configurations with respect to theoretical estimates.

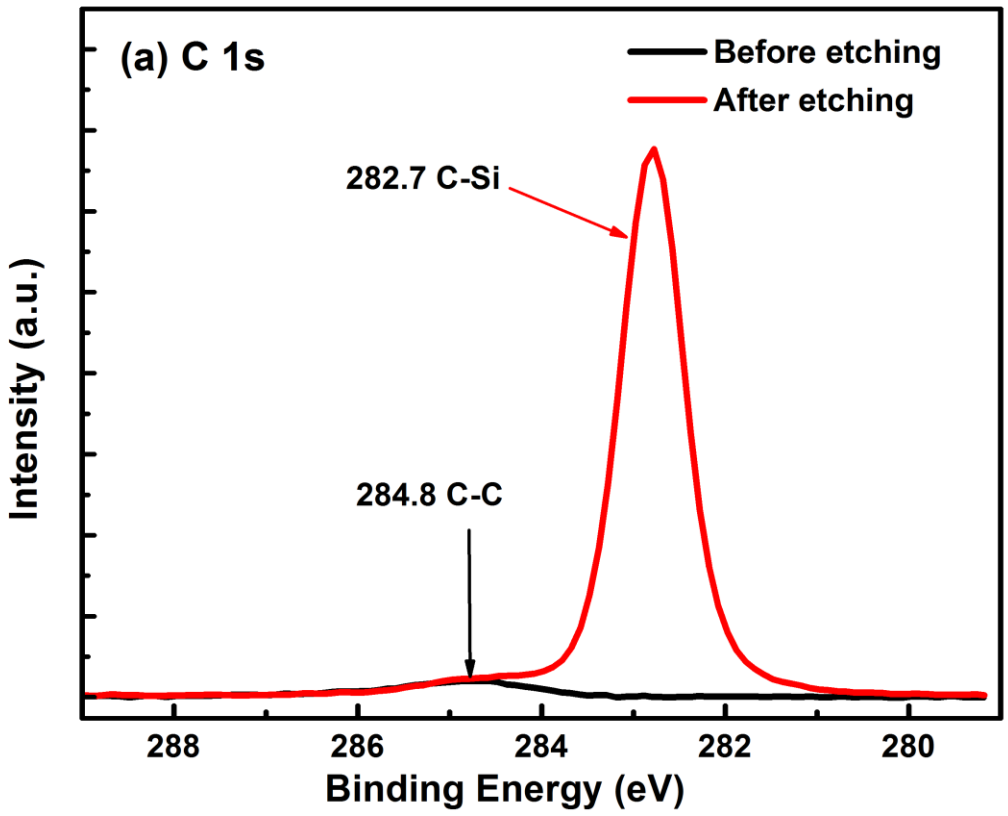

Fig. 3.10(a). XPS of C 1s on NO annealed SiC surface – before and after a 5 min. BOE etch.

In Fig. 3.10(a) we plot the XPS spectra of C 1s on an NO annealed SiC surface, before (black) and after (red) etching in BOE for 5 min. The sample has around a 50-60 nm oxide prior to etching. The peak around 284.8 eV binding energy in the before etching curve (black) in Fig. 3.10(a) represents the adventitious carbon that attached to the surface while the sample is transferred ex-situ. In the C 1s after etching curve (red), the major peak that around 282.7 eV binding energy represents the carbon atoms from SiC substrate. As for the smaller peak at around 285.0 eV, judging from the peak intensity and binding energy it likely comes from the adventitious carbon on the samples

surface. The consistency of the adventitious carbon peak on the before and after etching curves also validates our energy reference method.

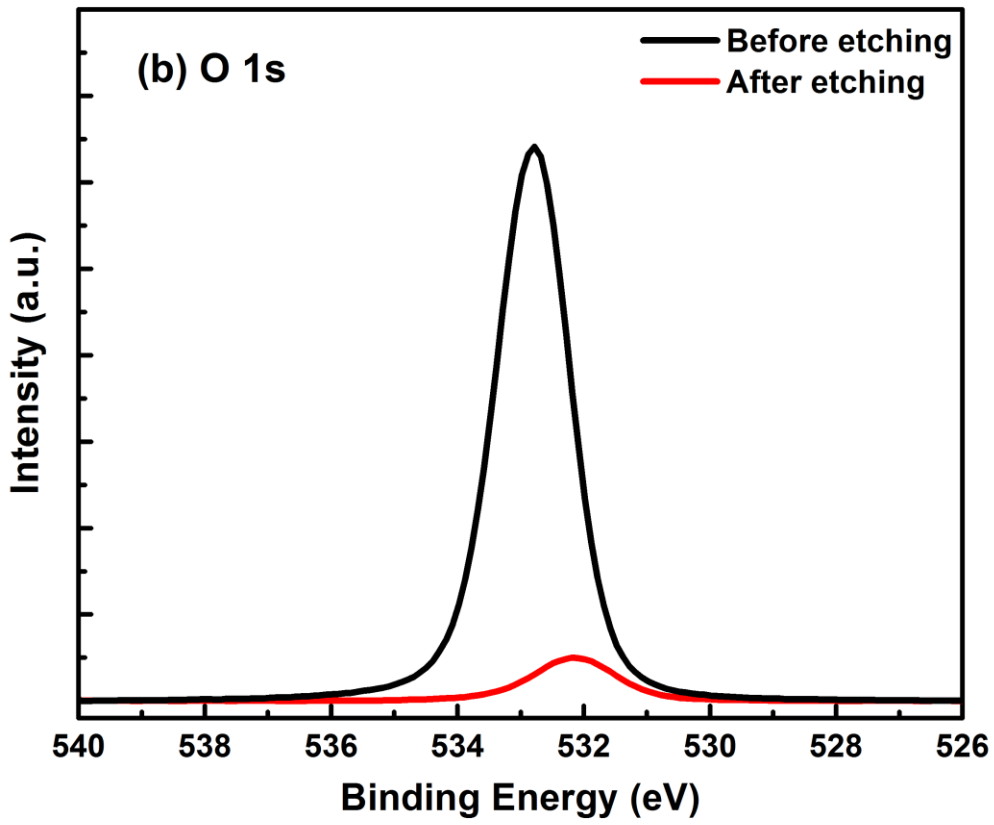

Fig. 3.10(b). XPS of O 1s on NO annealed SiC surface – before and after 5 min BOE etching.

As shown in Fig. 3.1 and section 3.4, there is less than one monolayer of un-etchable oxygen on the completely etched NO annealed SiC surface. Fig. 3.10(b) shows the XPS spectra of O 1s on the NO annealed SiC surface, before (with an approximately 60 nm oxide overlayer, black) and after (red) a 5 min. BOE etch. The O 1s peak from the before etch curve is from the SiO_2. After etching, the O 1s peak shifted to the lower

binding energy side for about 0.7 eV, which is consistent with the fact that the un-etchable oxygen atoms are closer to the semiconductor compared to the oxygen in the bulk oxide.

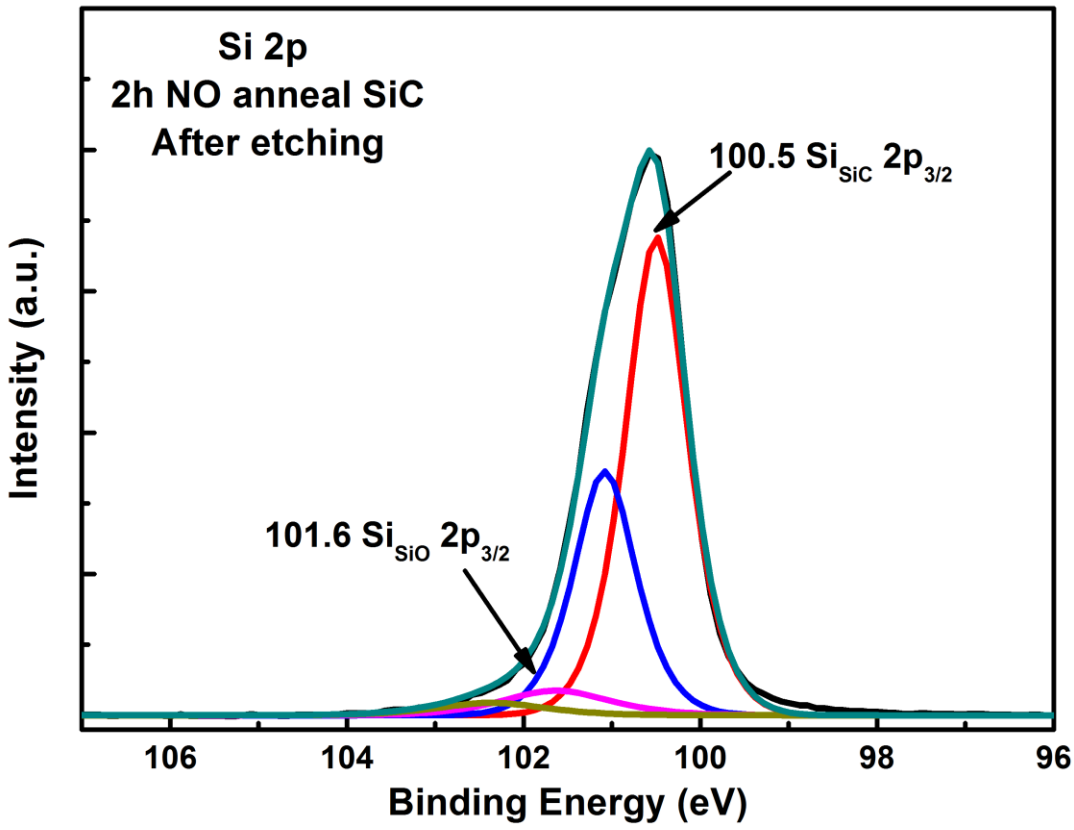

Fig. 3.11. XPS Si 2p peak deconvolution and peak assignment of 4H-SiC annealed in NO for 2 hours, followed by a 5 minute BOE etch.

To further understand oxygen bonding at the SiO_2/SiC interface, we can look into the Si XPS spectrum. Fig. 3.11 shows the Si 2p XPS peak deconvolution and assignment of completely etched NO annealed SiC. The Si 2p spectrum is fitted with 2 sets of doublets, one has a $2p_{3/2}$ peak at 100.5 eV binding energy and is identified as the SiC

substrate peak. The other has a $2p_{3/2}$ peak at a higher binding energy, 101.6 eV, and is consistent with partially oxidized Si, which in our case, is most likely bound with the un-etchable oxygen and nitrogen. Using the photoelectron mean free path calculated in section 3.4, the partially oxidized Si is estimated to be around one monolayer.

3.7. Bonding State of N: Theoretical Calculations

To further elucidate the nature of nitrogen bonding at the SiO_2/SiC interface, we have performed first principles electronic structure calculations on realistic interface models (this work was done in collaboration with Dr. B. Tuttles and Dr. S. T. Pantelides[32]). Our theoretical calculations employ the VASP electronic structure package[33] to calculate core level energies[34] within the frozen valence approximation. We have studied numerous interface structures with typical super-cell sizes ~ 1.0 × 1.0 × 2.0 nm with between 100 – 300 atoms, including 5 layers of a SiC(0001) substrate with an oxygen-nitrogen cap. For each model, atomic positions are initially relaxed to their lowest energy positions with T = 0 K. In all cases we use periodic boundary conditions, hence we are usually working with crystalline models of the interface, not truly amorphous ones. In reality, the overlayers are thought to become amorphous rather quickly as one moves into the oxide. We compute the relative difference between the N 1s core level and the bulk C 1s level, which provides a common reference when comparing to experiments as absolute core level energies are not accurate. In order to calibrate the method, we use a system where both the microstructure and the N 1s core level binding energies are known. Shirasawa et al.[13,14,15,16] have proposed a crystalline oxygen-nitrogen overlayer on the Si face of SiC(0001). Experimentally, the XPS core

level of the N 1s level is 398.7 eV with a core level difference between C 1s and N 1s being 114.8 eV.[6] This latter difference is also found in the present samples and is used to calibrate our theoretical calculations. In Fig. 3.12, Model 1 is a reproduction of the structure reported by Shirasawa et al. that we used in our calibrations. We estimate a numerical uncertainty of 0.2 eV for our reported N 1s core levels. The structures in Fig. 3.12 and Fig. 3.13 represent the oxide and SiC interface structure prior to the HF etching.

3.7.1. Unstrained layers

Our experiments on NO processed samples suggest an inter-layer with about 1/3 monolayer coverage of nitrogen, consistent with the previously determined range of 0.1 – 0.4 monolayers.[7] Coincidentally, a 1/3 monolayer of N could, in principle, perfectly passivate all the silicon dangling bonds on the SiC(0001) surface (if each N atom were bound to three Si atoms below it).[35] However, this surface would preclude any oxide from growing, would be highly strained, and is not really a relevant or practical model for nitrogen at the SiO_2/SiC interface. We have investigated the properties of more realistic models with nitrogen coverages similar to those observed experimentally. In Fig. 3.12, Model 2 shows an interlayer with a 1/2 monolayer coverage of nitrogen. The interlayer forms a two dimensional crystal with a primitive unit cell of 0.45 nm by 1.03 nm including 3 nitrogen atoms. Using the calibration mentioned above we can compare our calculations directly to our experiments. Theoretically, the average N 1s XPS level is 397.0 eV for Model 2, close to our experimental result for the main XPS peak of 397.5 eV. In Model 2, the nitrogen interlayer involves rows of nitrogen atoms, each with three silicon nearest neighbors, bonding directly on top of SiC(0001). The average N-Si

distance is 0.176 nm, close to the 0.174 nm value in bulk silicon nitride. The second nearest neighbors of the nitrogen atoms include nitrogen, carbon and oxygen atoms. Because of the agreement with XPS and the low strain of the Si-N bonds, Model 2 is an attractive model for the Si-N-O interlayer. However, the 0.5 monolayer of N is slightly larger than the observed coverage indicating that the actual interlayer is more complex than the crystal structure presented in Model 2.

3.7.2. Strained layers

To investigate the properties of nitrogen in a strained interlayer, we constructed Model 3 which is shown in Fig. 3.12. There is 5/12 of a monolayer of nitrogen atoms bonded directly to the SiC surface in this model. For Model 3, we calculated the N 1s core level energy for each N atom in the model. For 4 of the 5 nitrogen atoms, the N 1s core level is 397.4±0.2 eV, while for the remaining one it is 397.7 eV. In this latter case, the nitrogen is under considerable tensile strain, with a Si-N bond elongated by 5 %, to 0.182 nm. As in Model 2, the second nearest neighbors include nitrogen, carbon and oxygen atoms. With only nitrogen second nearest neighbors, bulk silicon-nitride (Si_3N_4) does not capture the nitrogen bonding environment at the SiO_2/SiC interface.

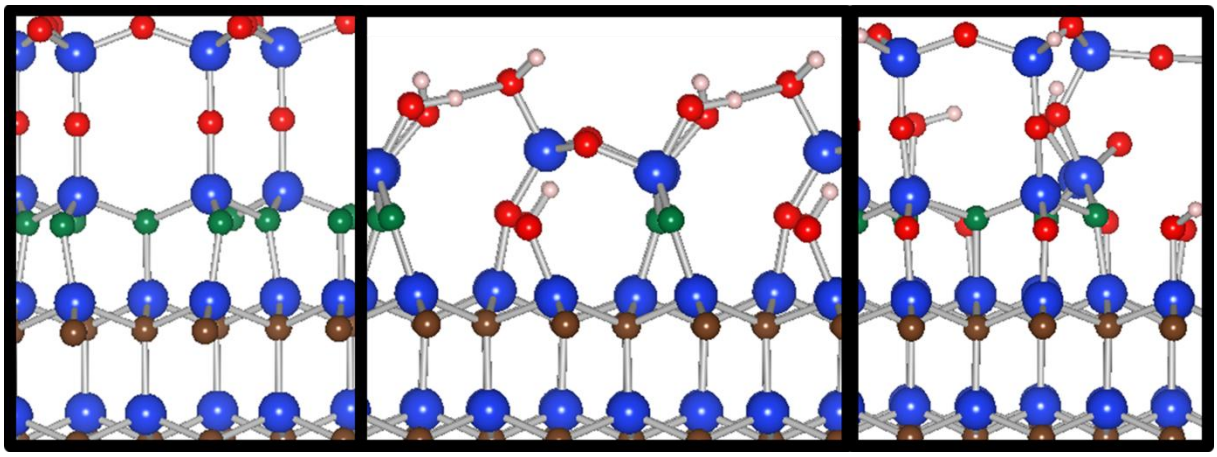

Fig. 3.12. Model 1 Model 2 Model 3

Ball and stick figures of the SiC/oxynitride interfaces (before etching) with Si (blue), C (brown), N (green), O (red) and hydrogen (white).

3.7.3. Nitrogen containing secondary peaks

Our proposed nitrogen bonding environments from Models 2 and 3 are consistent with the main N 1s peak that we report in Fig. 3.9. However, the secondary peaks reported in Fig. 3.9 are likely due to different local chemical environments. Nitrogen bound to oxygen at the interface may explain the observed secondary XPS peaks. Therefore, we have created Si-N-O molecular structures on a SiC(0001) surface in order to test the influence of nearest neighboring oxygen on the N 1s binding energy. In Fig. 3.13, ball and stick structures of the models are shown for nitrogen on top of SiC with silicon nearest neighbors including (a) zero oxygen, (b) one oxygen, and (c) two oxygen nearest neighbors. Other surface silicon atoms are passivated with OH bonds. The theoretical N 1s binding energies are found to be 397.1 eV, 398.5 eV and 400.3 eV for the structures of Fig. 3.13 (a), (b) and (c), respectively. These results are systematically lower than the corresponding N 1s peak values reported.[31] The different results may be

due to calibrations used N XPS on Si substrate versus SiC substrate. Also, Si and SiC surfaces will have different interface dipoles which would affect the XPS values.

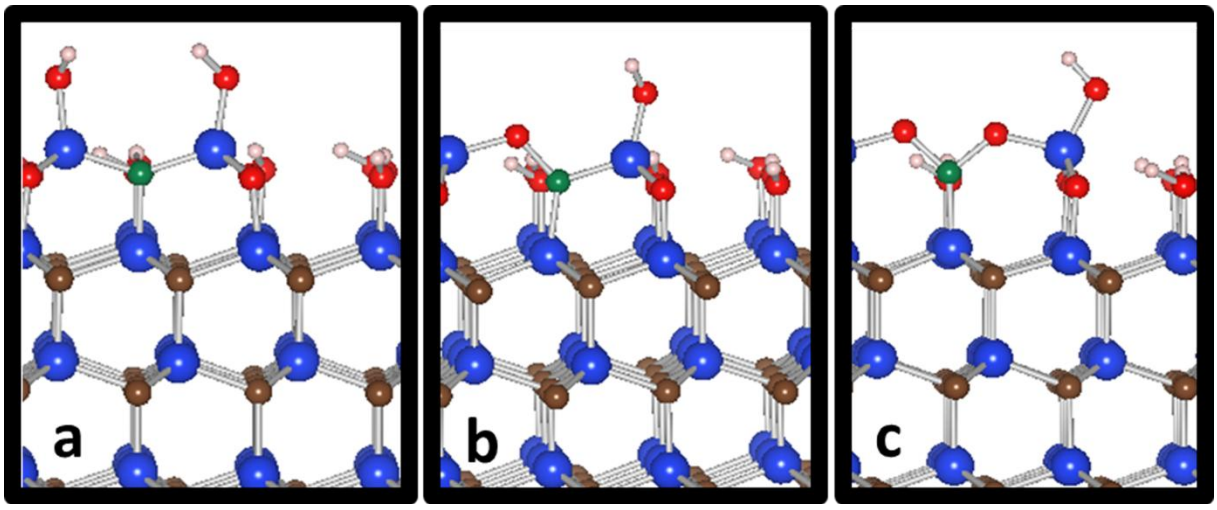

Fig. 3.13. Ball and stick figures of the SiC surface with a single nitrogen adsorbed with three different oxidation states. Si (blue), C (brown), N (green), O (red) and hydrogen (white).

In case (a) where nitrogen has only three silicon neighbors, the N 1s binding energy is 397.1 eV, within the range 397.0 – 397.4 eV found for relaxed nitrogen in Models 2 and 3 above. These surface results agree with the previous results that include an oxide cap, indicating that the N 1s binding energy is mainly sensitive to nearest neighbor effects. In case (b), the N 1s binding energy 398.5 eV is close to the observed secondary peak at 398.4 (see Fig. 3.9). In Fig. 3.9, the XPS N 1s binding energy data are fit with three Gaussians. The highest energy peak is reported at 399.5 eV. This tertiary Gaussian is much broader than the other two with a relatively small maximum, suggesting one or more low probability configurations are involved. In Fig. 3.13 (c), we present nitrogen

bound to two oxygen atoms. In this case, the N 1s binding energy is calculated to be 400.3 eV, which is 0.8 eV higher than the value of the experimentally determined tertiary peak. Overall, nitrogen bound to some oxygen atoms are close to the experimental secondary peaks. However, the concentration of N-O bonds after an anneal to > 1000^{o}C is likely to be very low, thus other candidate structures need to be considered.

3.7.4. Substitutional nitrogen

As the interfacial layer grows, EPR experiments indicate that nitrogen atoms can replace carbon[36] or fill silicon vacancies[37] below the interface, i.e. occupy either Si or C sites, substitutional, in SiC. Estimates from low temperature magnetic resonance studies place the concentrations of ionized nitrogen substituting for C within SiC at ~ 5×10^{12} cm^{-2} or about 1% of the total interfacial N. Near interface substitutional nitrogen has also been invoked to explain threshold voltage shifts in NO annealed devices.[11, 36] Starting with Model 2, we have considered two distinct cases, both involve nitrogen substituting for carbon in the first layer below the SiO_2/SiC interface. In our calculations, we find such neutral and ionized nitrogen atoms have N 1s binding energies of 398.4 eV and 399.3 eV, respectively. These configurations are likely to contribute to the higher energy, secondary peaks observed in the XPS peak fitting (Fig. 3.9).

3.7.5. Modeling summary

While interlayer Model 1 in Fig. 3.12 has been proposed and discussed by Shirasawa, et al., we believe that Models 2 and 3 in Fig. 3.12 are more likely models for nitrogen incorporation at actual SiO_2/SiC interfaces. To be clear, the models in Fig. 3.12

represent possible structures just before an HF etch of the last oxide layer. Examining the chemical reactions involved in HF etching is beyond the scope of the present study. However, for Models 1 – 3, molecular dynamics simulations were performed at elevated temperatures (between 300 K and 2000 K) to explore the stability of each model. For each simulation, we equilibrated the models at the given temperature and then recorded position data. In all simulations, there is no observation of Si-N bond dissociation. For the T = 1000 K simulations, the average Si-N bond lengths and standard deviations are reported in Table 3.2, along with XPS core level results discussed above. In all three models, each nitrogen forms three strong bonds with bond lengths and angles close to those observed in crystalline silicon nitride. The Si-N bonds in Models 2 & 3 may be in a more stable configuration than those in Model 1, based on the lower average bond lengths and lower bond length deviations. Each oxygen atom forms a bridging bond between two silicon with bond lengths and angles similar to those found in crystalline and amorphous silicon dioxide. These simulation results encourage confidence in the quality of interface Models 2 and 3, as representative of actual interfaces. Our N 1s XPS calculations indicate the main observed peak is from a configuration of N bound to three Si atoms. The effect of second nearest neighbors appears to be minimal. The observed secondary XPS peaks may be due to N-Si bonds under tensile strain and/or substitutional nitrogen below the SiO_2/SiC interface.

Table 3.2: Summary of theoretical simulation data for three interface models for N incorporation. See text for more details.

Model Number	Nitrogen Coverage	N 1s core level XPS (eV)	T= 0 K Si-N distance (nm)	Average Si-N distance (nm) 1000 K	Si-N stand. dev. (nm) 1000 K
1	1.0	398.7	0.177	0.178	0.0017
2	0.5	397.0	0.176	0.174	0.0013
3	5 / 12	397.4	0.176	0.177	0.0006
experiment	1/3	397.5			

3.8. N depth profile

The mechanism of how N appears to lower interface trap density, increase mobility, and generally improve device electrical performance is not fully understood. It was argued in early works by Jamet *et al.*,[38] Shirasawa *et al.*,[13] and Chung *et al.*[2] that N can be a passivating agent for the C-related interface states and oxide traps, which in turn gives rise to a lower D_{it} value for devices. Earlier work by McDonald et al, also suggests that N might be dissolving the C clusters near the interface, a type of interface defects, further reducing D_{it} and increasing mobility.[39] Another possible mechanism to explain the improvements in performance is "counter doping", proposed by Liu *et al.*,[40] which suggest that some N atoms can move into substitutional sites in SiC (near the interface) forming a counter-doped layer, which in turn gives rise to a higher conductivity. This counter doping mechanism will be discussed in detail in chapter 5. It is important to note

that the passivation and counter doping concepts are not contradictory to each other, and that nitrogen incorporation can actually function in both ways at the same time (with nitrogen atoms on both sides of the interface).

Having more information about the N profile across the interface would help us to better understand the role that nitrogen plays at the interface of SiC device. SIMS analysis is limited in accurate depth profiling due to ion bombardment induced roughness. In this case, MEIS channeling and angle resolve XPS studies can help produce higher depth resolution results.

The MEIS result not only provides accurate quantification but also indicates that the nitrogen is confined to within ~ 1nm of the surface, consistent with earlier reports of a sharp interfacial N profile. Fig. 3.14 (a) shows the MEIS spectrum and 2 different fittings for NO annealed SiC with the oxide completely etched off. The analysis is done using a 100 keV proton beam directed towards the sample at 58 ° off-normal, and then detected normal to the sample (122 ° backscattering). The red curve fitting represents a model with all of the N atoms sitting on top of the SiC, in other words, in the layer of silicon oxide closest to the SiC substrate, while the blue curve fitting represents the model that all of the N atoms located in the SiC, 5 Å below the SiO_2/SiC interface, approximately equivalent to 2 layers of the SiC crystal. Fig. 3.14 (b) shows the same data and fitting of Fig. 3.14 (a) but zoomed in the nitrogen energy range. It is clear from the MEIS data fitting that the model that N exist in the last layer of oxide is a better fit, which is also an agreement with the isotope experiment discussed in section 3.5, and theoretical calculations in section 3.7.

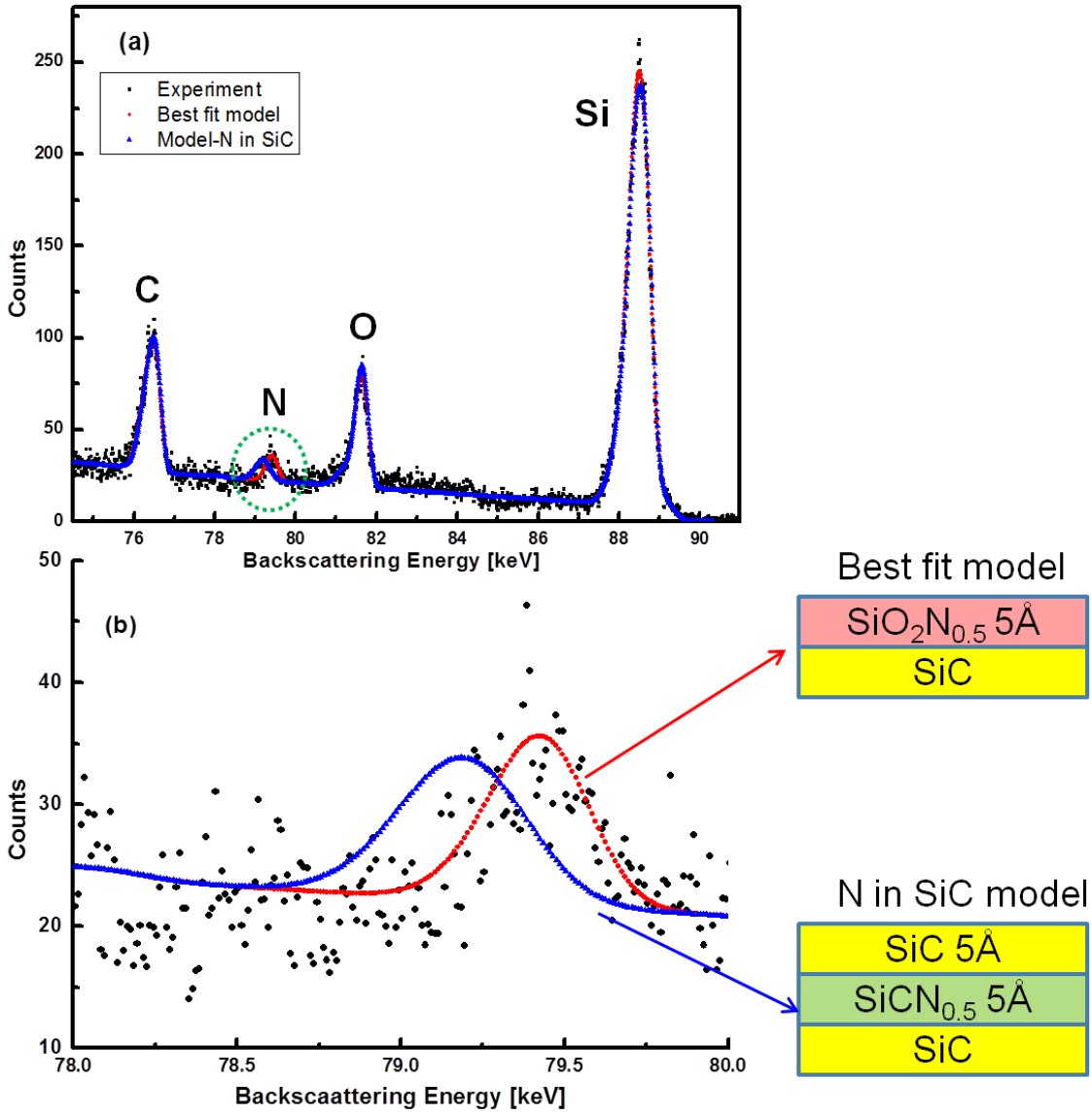

Fig. 3.14. MEIS modelling of N near the SiO_2/SiC interface.

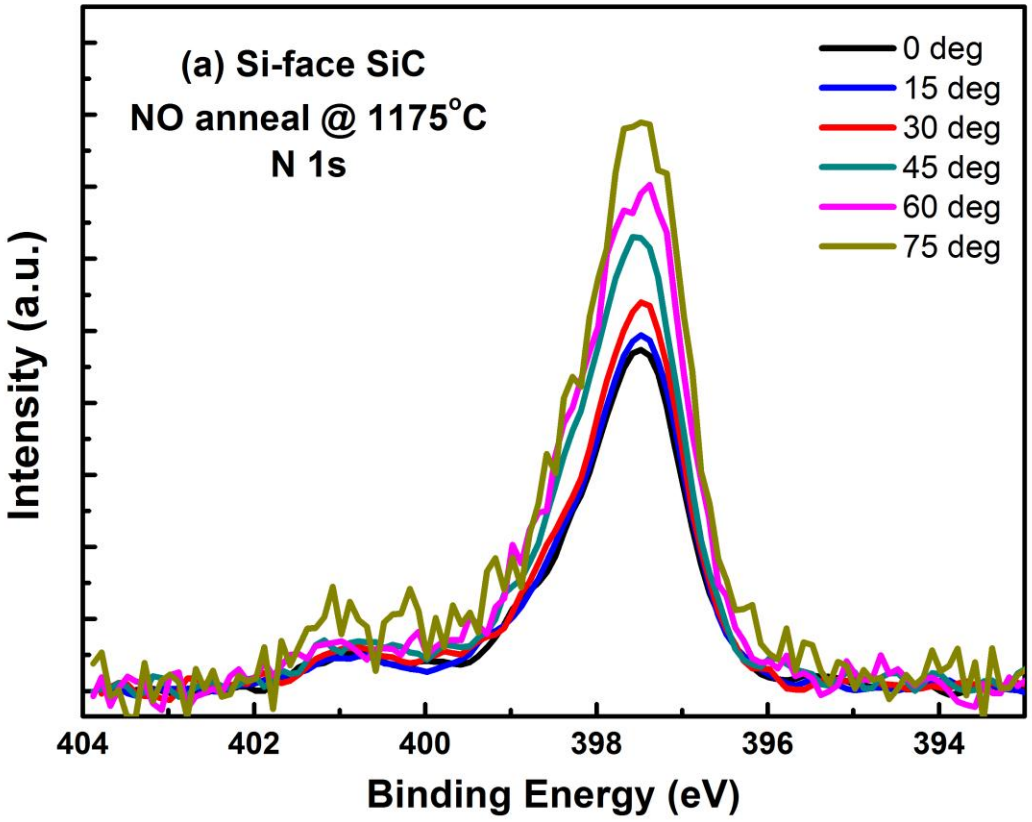

Fig. 3.15 (a) XPS angle resolve measurement of N 1s on etched NO annealed SiC. To aid in comparing different spectra, this sample set were all normalized to a constant Si 2p peak intensity.

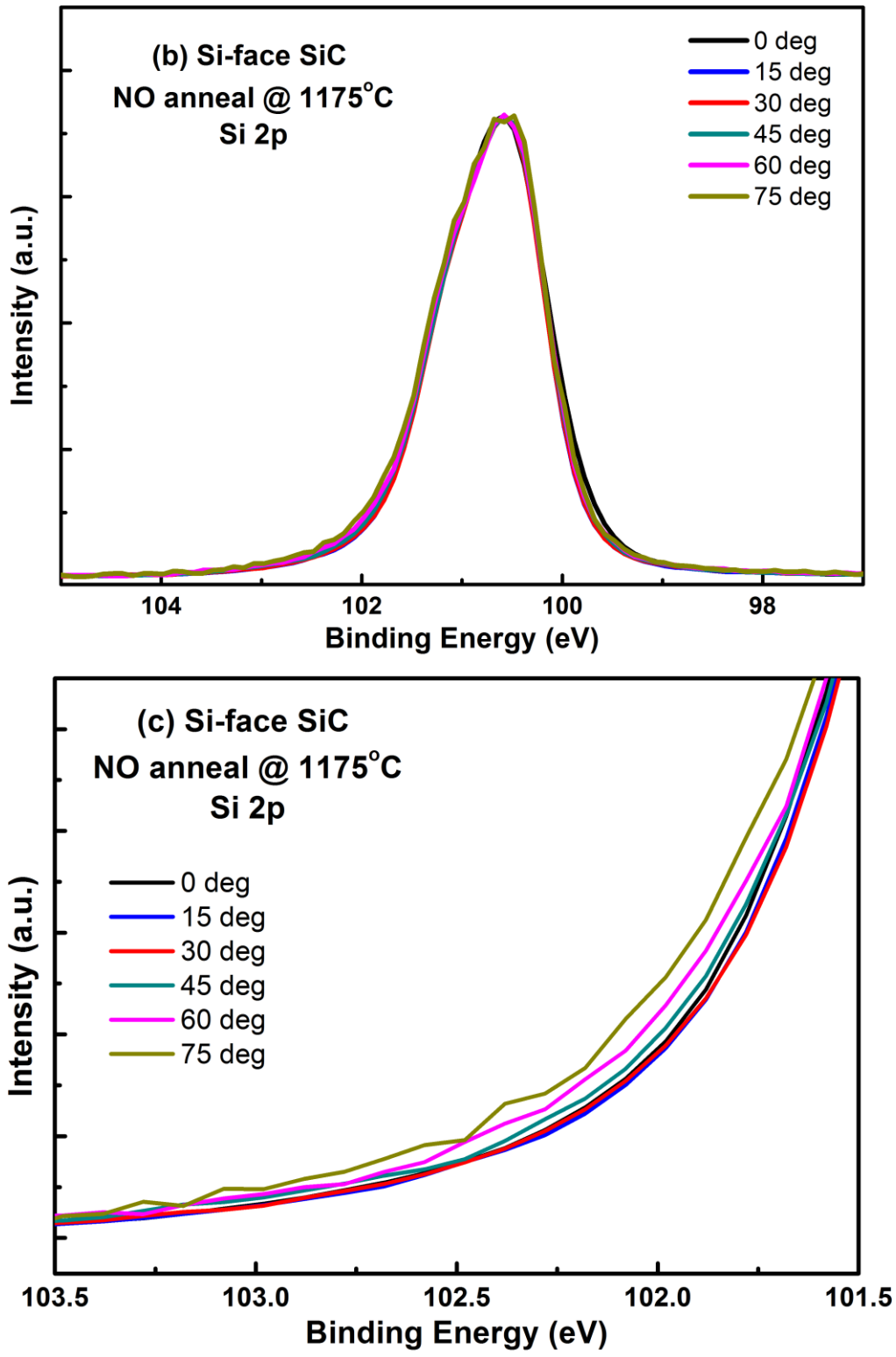

Fig. 3.15 (b) Si 2p spectrum (normalized intensities) and (c) zoomed Si 2p spectrum of angle resolve XPS measurement on etched NO annealed SiC.

Although the MEIS result rules out the possibility that all N atoms are buried within the SiC substrate, it is still unclear that if all N atoms sit in the last layer of oxide or the first layer of SiC. The fit for a model in which N atoms sit in the first layer of SiC would be somewhere between the blue curve and red curve in the MEIS modeling, thus is hard to confirm from the model if all of the N atoms sit in the last layer of oxide. In order to obtain more information about the N position and chemistry, angle resolve XPS measurements were performed.

The experiment is realized by taking a series of XPS spectra at different exit angles (the angle between the sample normal and the analyzer). Data were collected with angles from 0^o to 75^o. As the angle between sample normal and analyzer is increased, the photo-electrons collected become increasingly surface sensitive. Fig. 3.15 (a) shows the N 1s XPS spectrum of the angle resolve measurement with N peak intensities adjusted with normalized Si 2p peak intensities. If the N atoms sit in the same layer as the first SiC layer does, after normalizing to the Si 2p peak intensity the N 1s peak intensities should increase slightly with the increasing emission angle. Data in Fig. 3.15 (a) shows that with respect to the same Si 2p intensity, the N 1s peak intensity increases with increasing angle, in other word, the photo electrons from SiC substrate are attenuated more than that of N, which indicates that N atoms are slightly above/on top of SiC substrate.

Fig. 3.15 (b) shows that the normalized Si 2p XPS spectrum from the angle resolve measurement, and Fig. 3.15 (c) zooms in on the peak tail region at higher binding energy. The peak tail is identified in Fig. 3.11 as partially oxidized Si. There is a hint in Fig. 3.15 (c) that the peak tail is increased with respect to the main substrate peak, indicating that

these species sit on top of the SiC substrate, similar to the N atoms. This also supports our peak assignment in section 3.6.

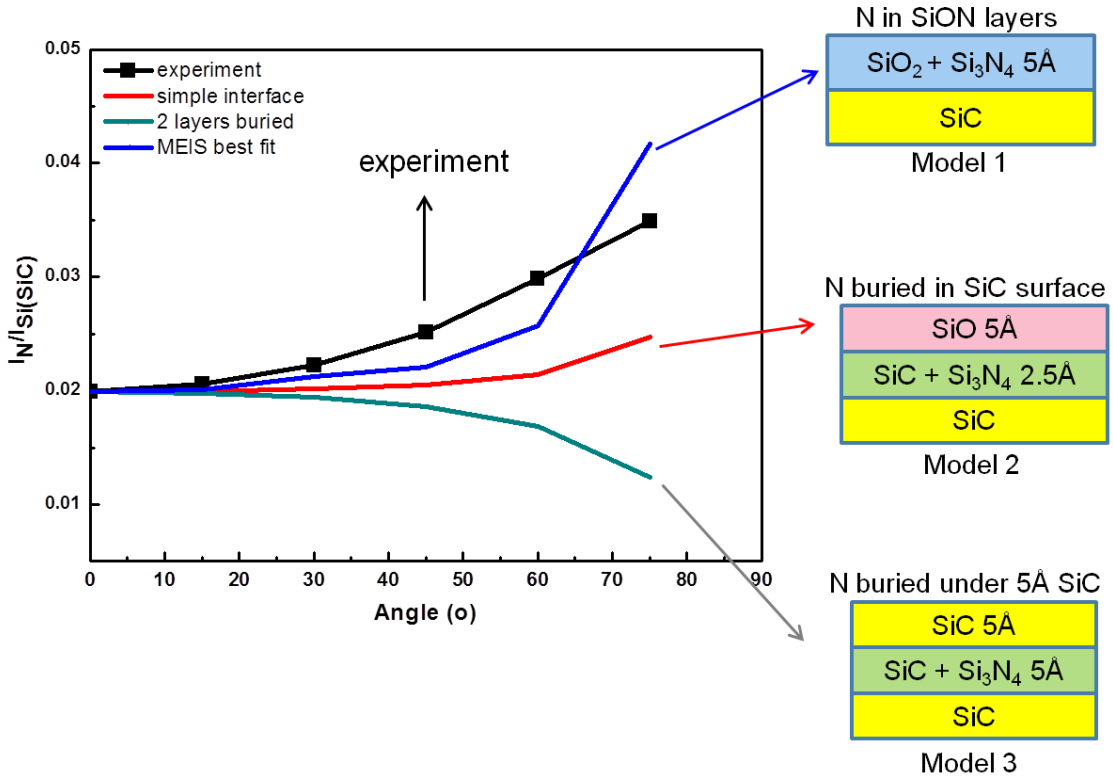

Fig. 3.16. XPS and MEIS simulations of depth profile. Model 1 is both the best MEIS fit and the best XPS fit.

To compare the angle resolve XPS and MEIS results, the intensity ratio of the N 1s peak relative to the Si 2p one at different photo-emission angles are calculated for different MEIS models and plotted in Fig. 3.16. The black curve is the experimental result. The blue curve represent the model that all the N atoms sit in the last layer of oxide on top of SiC (model 1), and N peak intensity increases with increasing angle. The red curve represent a model in which all the N atoms sit in the first layer of SiC (model 2),

and the ratio of N and Si peak intensities stays constant at different angles, with a slightly increase at high angles. The green curve represent a model in which all the N atoms are buried 5 Å into the SiC substrate (model 3), and the relative N 1s peak intensity decreases with increasing angle. Note that model 1 is the best fit to the angle resolve XPS result and also the best fit model for MEIS.

The N depth profile study in this section suggests that the majority of the sub-monolayer of N atoms, together with the un-etchable O atoms, sit on top of the SiC substrate, lowering the density of dangling bonds on the SiC surface, which also agrees with the computational results presented in section 3.7. This interface structure supports the model in which N passivates the interface defects.

3.9. Alternative methods of N incorporation

Above we have reported detailed experimental and theoretical analyses of the N 1s XPS results for samples grown using standard NO processing.[2,9,41] We also examined nitrogen introduced by two "new" processes: i) non-oxidized SiC exposed to pure N_2 at high temperature (1250~1600 ^{o}C) and ii) oxidized SiC exposed to a nitrogen plasma.[9] Fig. 3.17 shows the N 1s XPS spectral region of SiC prepared by (i) a high temperature N_2 anneal, (ii) an 8 hour N_2 plasma, (iii) a 4 hour N_2 plasma, (iv) a standard NO anneal (as in Fig. 3.9), and (v) a bare 4H-SiC sample. All the samples were etched in BOE for 5 minutes to remove the oxide layer and retained the N species with similar N 1s peak shapes and similar binding energies (although the total nitrogen peak areas differed). This implies that N atoms occupy essentially the same local chemical environment at the interface regardless of the nitridation method (close to one monolayer). Both the N_2

plasma method and the high temperature N_2 anneal resulted in approximately three times as much N at the interface relative to that obtained in the standard NO anneal, as reported in Table 1.

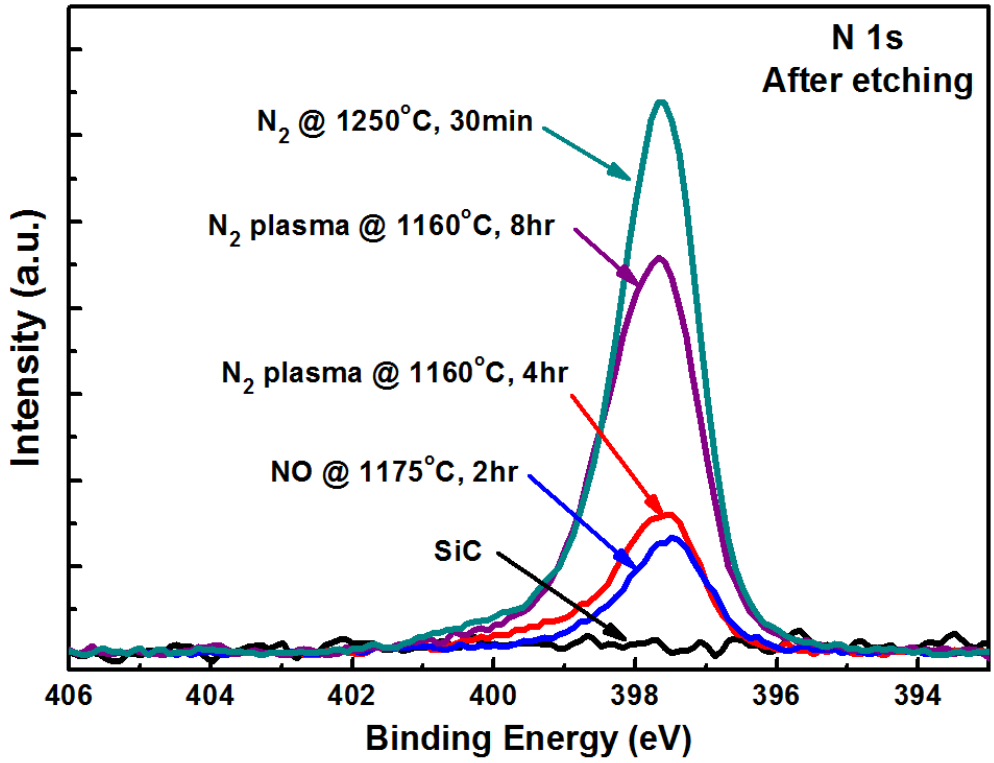

Fig. 3.17. N 1s XPS spectrum of SiC with different nitridation treatments, followed by a 5 minute BOE etch to remove all the oxide.

Table 3.3: Sample preparation, and N and O areal densities at the SiO_2/SiC interface prepared by different methods. All the samples were etched in BOE for 5 minutes before examination by XPS:

	Substrate	N Process	Oxide thickness(nm)	Mobility ($cm^2/V\ s$)	N amount ($10^{14}/cm^2$)	O amount ($10^{14}/cm^2$)
Fig. 3.2a	4H-SiC(0001)	NO, 1175 ℃, 1 atm, 2 hrs	50-60	~ 40[2,3]	4.0	14.0
Fig. 3.2b	Silicon (100)	NO, 1175 ℃, 1 atm, 2 hrs	50-60			
Fig. 3.17	4H-SiC(0001)	N_2 plasma, 1160 ℃, 4 hrs	50-60	~ 55[9]	4.1	10.4
Fig. 3.17	4H-SiC(0001)	N_2 plasma, 1160 ℃, 8 hrs	50-60		10.0	9.9
Fig. 3.17	6H-SiC(0001)	N_2, 1600 ℃, 5 min	50-60		11.1	12.4
Fig. 3.17	6H-SiC(0001)	N_2, 1350 ℃, 30 min			10.3	5.4
Fig. 3.17	6H-SiC(0001)	N_2, 1250 ℃, 30 min			12.4	7.6

*The N processes on 4H-SiC involved starting with a ~50 nm thermal oxide (SiO_2) grown on SiC(0001) at 1150 ℃. For 6H-SiC, a bare (no oxide) sample was used for the N_2 exposure. The Si substrates also have a 50nm thermal oxide prior to NO exposure.

Note that there is relatively little oxygen present before the HF etch on both the plasma and N_2 anneal samples. After the HF etch, the NO sample continues to show a significant oxygen signal, much greater than the plasma and N_2 samples after etch. This indicates that this "unetchable" oxide layer associated with NO processing, first reported by Dhar et al.[17], is intrinsic to the NO process and may play a role in the electrical characteristics of devices fabricated via the different processing conditions studied here.

The continuous growth of the NO oxide might limit the efficiency of this nitridation process as a passivating agent. It is well-known that pure oxidation without any N creates a poor electrical interface. Our data indicate that these two alternative nitridation methods might be superior to the traditional NO anneal because they result in a higher N to O ratio at the SiO_2/SiC interface.

3.10. Summary and discussion

In conclusion, SiO_2/SiC(4H-Si face) structures with nitrogen added by an NO anneal, a N_2 plasma, and high temperature anneals in N_2 were examined by XPS following BOE etching. In all cases a significant fraction of the N added, varying from 1/3 to 1 monolayer (where 1 monolayer is defined as the density of Si atoms in a single SiC (1000) atomic plane), was bonded to the substrate at the interface and was not susceptible to etching. This is in sharp contrast to the behavior of N on silicon surfaces, where complete etching of N occurs in similarly prepared samples. All nitridation methods resulted in similar photoemission spectra in the N 1s XPS region, indicating similar nitrogen bonding at the interface. Both N 1s peak fitting and a bonding model are suggested to describe the N bonding at the interface.

The analysis by angle resolve XPS and MEIS suggest that the majority of N atoms sit at the interface, passivating more dangling bonds at the SiO_2/SiC interface than than that of only oxygen. N passivation reduces the interfacial traps, while a small portion of the N atoms may counter-dope the N type SiC semiconductor[40] (the counter-doping mechanism will be discussed in chapter 5). A recent study shows that in addition to interface passivation, N at the interface may also reduce the width of the transition layer[42] between SiC and SiO_2.

References:

[1] J. A. Cooper, M. R. Melloch, R. Singh, A. Agarwal, and J. W. Palmour, "Status and prospects for SiC power MOSFETs," *Ieee Transactions on Electron Devices,* vol. 49, pp. 658-664, Apr 2002.

[2] G. Y. Chung, C. C. Tin, J. R. Williams, K. McDonald, R. K. Chanana, R. A. Weller, S. T. Pantelides, L. C. Feldman, O. W. Holland, M. K. Das, and J. W. Palmour, "Improved inversion channel mobility for 4H-SiC MOSFETs following high temperature anneals in nitric oxide," *Ieee Electron Device Letters,* vol. 22, pp. 176-178, Apr 2001.

[3] S. Dimitrijev, P. Jamet, and P. Tanner, "Effects of nitridation in gate oxides grown on 4H-SiC," *Journal of Applied Physics,* vol. 90, pp. 5058-5063, Nov 15 2001.

[4] J. Rozen, A. C. Ahyi, X. G. Zhu, J. R. Williams, and L. C. Feldman, "Scaling Between Channel Mobility and Interface State Density in SiC MOSFETs," *Ieee Transactions on Electron Devices,* vol. 58, pp. 3808-3811, Nov 2011.

[5] K. C. Chang, Y. Cao, L. M. Porter, J. Bentley, S. Dhar, L. C. Feldman, and J. R. Williams, "High-resolution elemental profiles of the silicon dioxide/4H-silicon carbide interface," *Journal of Applied Physics,* vol. 97, p. 104920, May 15 2005.

[6] H. Tochihara and T. Shirasawa, "The epitaxial crystalline silicon-oxynitride layer on SiC(0001): Formation of an ideal SiC-insulator interface," *Progress in Surface Science,* vol. 86, pp. 295-327, Nov-Dec 2011.

[7] R. Kosugi, T. Umeda, and Y. Sakuma, "Fixed nitrogen atoms in the SiO_2/SiC interface region and their direct relationship to interface trap density," *Applied Physics Letters,* vol. 99, p. 182111, Oct 31 2011.

[8] X. Zhu, H. D. Lee, T. Feng, A. C. Ahyi, D. Mastrogiovanni, A. Wan, E. Garfunkel, J. R. Williams, T. Gustafsson, and L. C. Feldman, "Structure and stoichiometry of (0001) 4H-SiC/oxide interface," *Applied Physics Letters,* vol. 97, p. 071908, Aug 16 2010.

[9] X. Zhu, A. C. Ahyi, M. Y. Li, Z. J. Chen, J. Rozen, L. C. Feldman, and J. R. Williams, "The effect of nitrogen plasma anneals on interface trap density and channel mobility for 4H-SiC MOS devices," *Solid-State Electronics,* vol. 57, pp. 76-79, Mar 2011.

[10] X. Zhu, "Alternative Growth and Interface Passivation Techniques for SiO_2 on 4H-SiC," Ph.D dissertation, Department of Physics, Auburn University, 2008.

[11] H. C. Lu, E. P. Gusev, E. Garfunkel, B. W. Busch, T. Gustafsson, T. W. Sorsch, and M. L. Green, "Isotopic labeling studies of interactions of nitric oxide and nitrous oxide with ultrathin oxynitride layers on silicon," *Journal of Applied Physics,* vol. 87, pp. 1550-1555, Feb 1 2000.

[12] M. L. Green, E. P. Gusev, R. Degraeve, and E. L. Garfunkel, "Ultrathin (< 4 nm) SiO_2 and Si-O-N gate dielectric layers for silicon microelectronics: Understanding the processing, structure, and physical and electrical limits," *Journal of Applied Physics,* vol. 90, pp. 2057-2121, Sep 1 2001.

[13] T. Shirasawa, K. Hayashi, S. Mizuno, S. Tanaka, K. Nakatsuji, F. Komori, and H. Tochihara, "Epitaxial silicon oxynitride layer on a 6H-SiC(0001) surface," *Physical Review Letters,* vol. 98, p. 136105, Mar 30 2007.

[14] T. Shirasawa, K. Hayashi, H. Yoshida, S. Mizuno, S. Tanaka, T. Muro, Y. Tamenori, Y. Harada, T. Tokushima, Y. Horikawa, E. Kobayashi, T. Kinoshita, S. Shin, T. Takahashi, Y. Ando, K. Akagi, S. Tsuneyuki, and H. Tochihara, "Atomic-layer-resolved bandgap structure of an ultrathin oxynitride-silicon film epitaxially grown on 6H-SiC(0001)," *Physical Review B,* vol. 79, p. 241301(R), Jun 2009.

[15] F. Devynck, Z. Sljivancanin, and A. Pasquarello, "Electronic properties of an epitaxial silicon oxynitride layer on a 6H-SiC(0001) surface: A first-principles investigation," *Applied Physics Letters,* vol. 91, p. 061930, Aug 6 2007.

[16] P. Kruger, B. Baumeier, and J. Pollmann, "First-principles investigation of an epitaxial silicon oxynitride layer on a 6H-SiC(0001) surface," *Physical Review B,* vol. 77, p. 085329, Feb 2008.

[17] S. Dhar, O. Seitz, M. D. Halls, S. Choi, Y. J. Chabal, and L. C. Feldman, "Chemical Properties of Oxidized Silicon Carbide Surfaces upon Etching in Hydrofluoric Acid," *Journal of the American Chemical Society,* vol. 131, pp. 16808-16813, Nov 25 2009.

[18] P. Jakob, Y. J. Chabal, K. Raghavachari, R. S. Becker, and A. J. Becker, "Kinetic-Model of the Chemical Etching of Si(111) Surfaces by Buffered Hf Solutions," *Surface Science,* vol. 275, pp. 407-413, Sep 15 1992.

[19] A. E. T. Kuiper, H. G. Pomp, P. M. Asveld, W. A. Bik, and F. H. P. M. Habraken, "Nitrogen and Oxygen Incorporation during Rapid Thermal-Processing of Si in N_2O," *Applied Physics Letters,* vol. 61, pp. 1031-1033, Aug 31 1992.

[20] S. A. Correa, C. Radtke, G. V. Soares, I. J. R. Baumvol, C. Krug, and F. C. Stedile, "Presence and resistance to wet etching of silicon oxycarbides at the SiO_2/SiC interface," *Electrochemical and Solid State Letters,* vol. 11, pp. H258-H261, 2008.

[21] S. Dhar, S. H. Ryu, and A. K. Agarwal, "A Study on Pre-Oxidation Nitrogen Implantation for the Improvement of Channel Mobility in 4H-SiC MOSFETs," *Ieee Transactions on Electron Devices,* vol. 57, pp. 1195-1200, Jun 2010.

[22] G. Liu, A. C. Ahyi, Y. Xu, T. Isaacs-Smith, Y. K. Sharma, J. R. Williams, L. C. Feldman, and S. Dhar, "Enhanced Inversion Mobility on 4H-SiC (11(2)over-bar0) Using Phosphorus and Nitrogen Interface Passivation," *Ieee Electron Device Letters,* vol. 34, pp. 181-183, Feb 2013.

[23] K. McDonald, L. C. Feldman, R. A. Weller, G. Y. Chung, C. C. Tin, and J. R. Williams, "Kinetics of NO nitridation in SiO_2/4H-SiC," *Journal of Applied Physics,* vol. 93, pp. 2257-2261, Feb 15 2003.

[24] R. Arora, J. Rozen, D. M. Fleetwood, K. F. Galloway, C. X. Zhang, J. S. Han, S. Dimitrijev, F. Kong, L. C. Feldman, S. T. Pantelides, and R. D. Schrimpf, "Charge Trapping Properties of 3C-and 4H-SiC MOS Capacitors With Nitrided Gate Oxides," *Ieee Transactions on Nuclear Science,* vol. 56, pp. 3185-3191, Dec 2009.

[25] S. Tanuma, C. J. Powell, and D. R. Penn, "Calculations of electorn inelastic mean free paths. II. Data for 27 elements over the 50-2000 eV range," *Surface and Interface Analysis*, vol. 17, pp. 911-926, Dec 1991.

[26] NIST-Database, *http://www.nist.gov/srd/nist82.cfm*.

[27] K. McDonald, "Nitrogen incorporation and interface trap reduction in silicon dioxide/4H-silicon carbide," Ph.D Dissertation, Department of Physics, Vanderbilt University, 2001.

[28] F. Y. Tian, D. F. Taber, and A. V. Teplyakov, "-NH- Termination of the Si(111) Surface by Wet Chemistry," *Journal of the American Chemical Society*, vol. 133, pp. 20769-20777, Dec 28 2011.

[29] J. R. Shallenberger, D. A. Cole, and S. W. Novak, "Characterization of silicon oxynitride thin films by x-ray photoelectron spectroscopy," *Journal of Vacuum Science & Technology a-Vacuum Surfaces and Films*, vol. 17, pp. 1086-1090, Jul-Aug 1999.

[30] G. M. Rignanese, A. Pasquarello, J. C. Charlier, X. Gonze, and R. Car, "Nitrogen incorporation at Si(001)-SiO_2 interfaces: Relation between N 1s core-level shifts and microscopic structure," *Physical Review Letters*, vol. 79, pp. 5174-5177, Dec 22 1997.

[31] T. R. Leftwich and A. V. Teplyakov, "Calibration of computationally predicted N 1s binding energies by comparison with X-ray photoelectron spectroscopy measurements," *Journal of Electron Spectroscopy and Related Phenomena*, vol. 175, pp. 31-40, Dec 2009.

[32] Y. Xu, X. Zhu, H. D. Lee, C. Xu, S. M. Shubeita, A. C. Ahyi, Y. Sharma, J. R. Williams, W. Lu, S. Ceesay, B. R. Tuttle, A. Wan, S. T. Pantelides, T. Gustafsson, E. L. Garfunkel, and L. C. Feldman, "Atomic state and characterization of nitrogen at the SiC/SiO_2 interface," *Journal of Applied Physics,* vol. 115, pp. -, 2014.

[33] G. Kresse and J. Furthmuller, "Efficient iterative schemes for ab initio total-energy calculations using a plane-wave basis set," *Physical Review B,* vol. 54, pp. 11169-11186, Oct 15 1996.

[34] L. Kohler and G. Kresse, "Density functional study of CO on Rh(111)," *Physical Review B,* vol. 70, p. 165405, Oct 2004.

[35] G. Pennington and C. R. Ashman, "Nitrogen passivation of (0001) 4H-SiC silicon-face dangling bonds," *Applied Physics Letters,* vol. 91, p. 072106, Aug 13 2007.

[36] T. Umeda, K. Esaki, R. Kosugi, K. Fukuda, T. Ohshima, N. Morishita, and J. Isoya, "Behavior of nitrogen atoms in $SiC-SiO_2$ interfaces studied by electrically detected magnetic resonance," *Applied Physics Letters,* vol. 99, p. 142105, Oct 3 2011.

[37] C. J. Cochrane, P. M. Lenahan, and A. J. Lelis, "The effect of nitric oxide anneals on silicon vacancies at and very near the interface of 4H SiC metal oxide semiconducting field effect transistors using electrically detected magnetic resonance," *Applied Physics Letters,* vol. 102, p. 193507, May 13 2013.

[38] P. Jamet, S. Dimitrijev, and P. Tanner, "Effects of nitridation in gate oxides grown on 4H-SiC," *Journal of Applied Physics,* vol. 90, pp. 5058-5063, Nov 15 2001.

[39] K. McDonald, R. A. Weller, S. T. Pantelides, L. C. Feldman, G. Y. Chung, C. C. Tin, and J. R. Williams, "Characterization and modeling of the nitrogen passivation of interface traps in SiO_2/4H-SiC," *Journal of Applied Physics,* vol. 93, pp. 2719-2722, Mar 1 2003.

[40] G. Liu, A. C. Ahyi, Y. Xu, T. Isaacs-Smith, Y. K. Sharma, J. R. Williams, L. C. Feldman, and S. Dhar, "Enhanced Inversion Mobility on 4H-SiC (1120) Using Phosphorus and Nitrogen Interface Passivation," *Ieee Electron Device Letters,* vol. 34, pp. 181-183, Feb 2013.

[41] H. Yoshioka, T. Nakamura, and T. Kimoto, "Generation of very fast states by nitridation of the SiO_2/SiC interface," *Journal of Applied Physics,* vol. 112, p. 024520, Jul 15 2012.

[42] J. A. Taillon, J. H. Yang, C. A. Ahyi, J. Rozen, J. R. Williams, L. C. Feldman, T. S. Zheleva, A. J. Lelis, and L. G. Salamanca-Riba, "Systematic structural and chemical characterization of the transition layer at the interface of NO-annealed 4H-SiC/SiO_2 metal-oxide-semiconductor field-effect transistors," *Journal of Applied Physics,* vol. 113, Jan 28 2013.

Chapter 4. Kinetics of nitrogen incorporation at the SiO_2/4H-SiC interface during NO passivation

4.1. Introduction

As noted above, nitridation of the SiO_2/SiC interface using a nitric oxide (NO, g) post oxidation anneal is the most established process for achieving quality SiC MOS interfaces, and hence a higher mobility MOSFET device.[1-6] Explanations of the nitrogen passivation mechanism had been offered proposed on computer simulations,[7] but a complete understanding of the kinetics of nitridation process is still missing. In this chapter, the kinetics of N incorporation at the SiO_2/SiC interface has been investigated for C-face, Si-face and a-face 4H-SiC. In section 4.2, the experimental details are described, including sample preparation, and physical and electrical analysis. In section 4.3, the results of nitrogen uptake using the standard NO process on the C-, Si-, and a-faces of 4H-SiC are shown. In section 4.4, we investigate the saturation nitrogen coverage on different crystal faces, and present several possible explanations. In section 4.5, we describe results of NO annealing at different temperatures and times, obtain the N uptake curves on all three different crystal faces at various of temperatures, and propose a first-order kinetics model. In section 4.6, we present and discuss the correlation between N coverage and the interface trap density on the C-face.

4.2. Sample preparation

Following organic and RCA cleaning, 8^o miscut $(000\bar{1})$ C-face, 4^o miscut (0001) Si-face and on-axis $(11\bar{2}0)$ a-face 4H-SiC samples (5 × 5mm piece) were oxidized in a

500 sccm O_2 flow at 1150°C in a quartz-glass tube for 15 hrs, 1hr and 15 hrs, respectively, to obtain oxides that are approximately 65 nm thick on all the samples. The oxidation times were chosen based on the anisotropic oxidation rates of the various SiC faces.[8-10] All samples were then annealed in a 577 sccm NO flow at different temperatures. The NO (g) annealing process parameters are shown in Table 4.1.

The nitrogen coverage on the surface was characterized by secondary ion mass spectroscopy (SIMS), Medium Energy Ion Scattering (MEIS), and X-ray photoelectron spectroscopy (XPS), as discussed above. XPS measurements were performed using a monochromatic Al Kα x-ray source (K-Alpha, Thermo Scientific Inc.). Medium Energy Ion Scattering (MEIS) measurements were performed using a 100 keV proton beam at the direction 58 ° off-normal into the sample and normal out (122 °) backscattering.[11] The oxides were etched in 7% HF for 5 min prior to measurements for the XPS and MEIS studies, while for SIMS, the profiling was accomplished on the un-etched as grown oxide.

In addition to the physical analysis, electrical measurements were carried out on C-face MOS capacitors which had been fabricated with the standard NO passivation at 1175^{o}C for various times after thermally growing a 65 nm oxide. Sputter deposited Mo was used as gate metal. Simultaneous high-low frequency capacitance-voltage (C-V) measurements were performed at room temperature, and the interface trap density (D_{it}) near the conduction band-edge of 4H-SiC was extracted as a function of annealing time.

Table 4.1. NO (g) annealing process parameters. “C-” stands for C-face samples, “Si-” stands for Si-face samples and “a-” stands for a-face samples.

T (^{o}C) / Anneal time	1175	1100	1050	1000
7.5 min	C-, a-			
15 min	C-, Si-, a-	C-	C-	C-
30 min	C-, Si-, a-	C-, Si-	C-, Si-	C-
1 hr	C-, Si-	C-, Si-	C-, Si-	C-
1.5 hr	a-			
2 hr	C-, Si-	C-, Si-	C-, Si-	C-
4 hr	Si-			
6 hr		Si-	Si-	

4.3. Nitrogen update kinetics

Fig. 4.1a and Fig. 4.1b show SIMS results for silicon, oxygen, carbon, (left) and nitrogen (right) near the C-face and a-face SiO_2/SiC interface The data indicates that N accumulates at or close to the SiO_2/SiC interface, with a sharp profile of a FWHM of 5 nm or less, limited by SIMS depth resolution. This result is very similar to that observed on the Si-face.[12, 13] While SIMS has low detection limits, quantification of the interfacial N coverage involves the complexities of SIMS yields and sputtering rate at interfaces. To overcome this uncertainty, MEIS and XPS were used to quantifying the total nitrogen coverage. Both MEIS and XPS were performed on samples that had been fully etched in

7% HF solution. It is shown that on a Si-face, NO-annealed SiO_2/SiC sample, more than 90% of the interfacial N remains on the surface after HF fully removed the oxide.[14, 15] Here we assume it is the same case for the C-face and a-face. The MEIS measurement (Fig. 4.2) was only done on the C-face sample annealed at 1175^{o}C for 136 min, give the N coverage of 6.6 $\times 10^{14}$/cm^2. Using the extracted photoelectron mean free path from chapter 3, XPS measurement on the same sample result a N coverage of 6.5 $\times 10^{14}$/cm^2. The SIMS integral of N profile give a total N coverage of 2.3 $\times 10^{14}$/cm^2. From the result of 3 different techniques, the XPS result is proven to be reliable. Thus the nitrogen coverage of samples prepared under other temperatures and time periods were only quantified using XPS.

Fig. 4.3 and Fig. 4.4 show the nitrogen uptake on the C-face and a-face of SiC during an NO anneal at 1175^{o}C. The results were plotted based on (a) SIMS and (b) XPS results. On each crystal face, although the absolute nitrogen coverage differs (based on different characterization techniques), it is clear that the nitrogen incorporation process has the same trend on each particular crystal face.

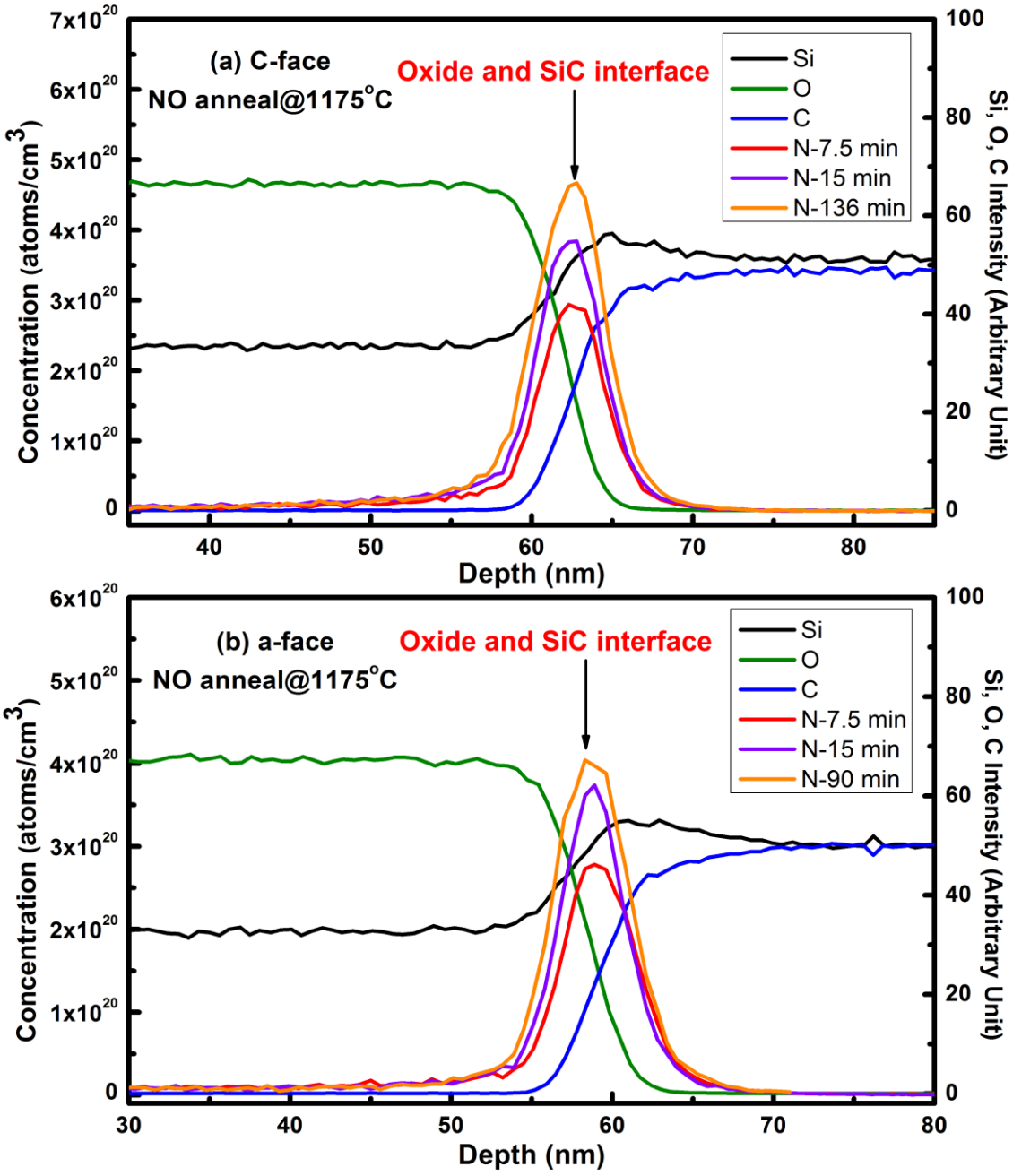

Fig. 4.1. SIMS profiles of silicon, oxygen, carbon, (right) and nitrogen (left) near the C-face of a SiO_2/SiC interface. Silicon, oxygen, and carbon profiles are in arbitrary units, while the nitrogen is in atoms/cm^3. The 3 nitrogen profiles, from low to high, corresponding to different NO passivation times.

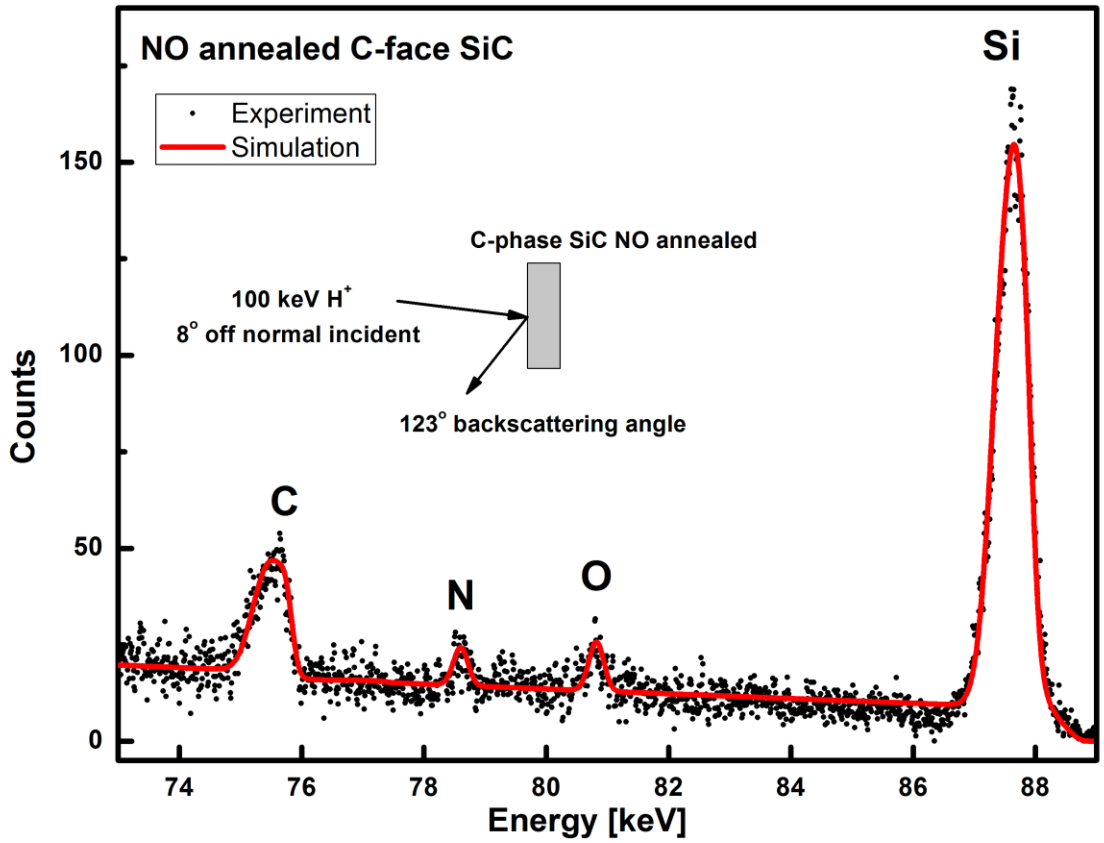

Fig. 4.2. MEIS spectrum of an NO-annealed (1175^{o}C, 136 min) C-face SiC sample.

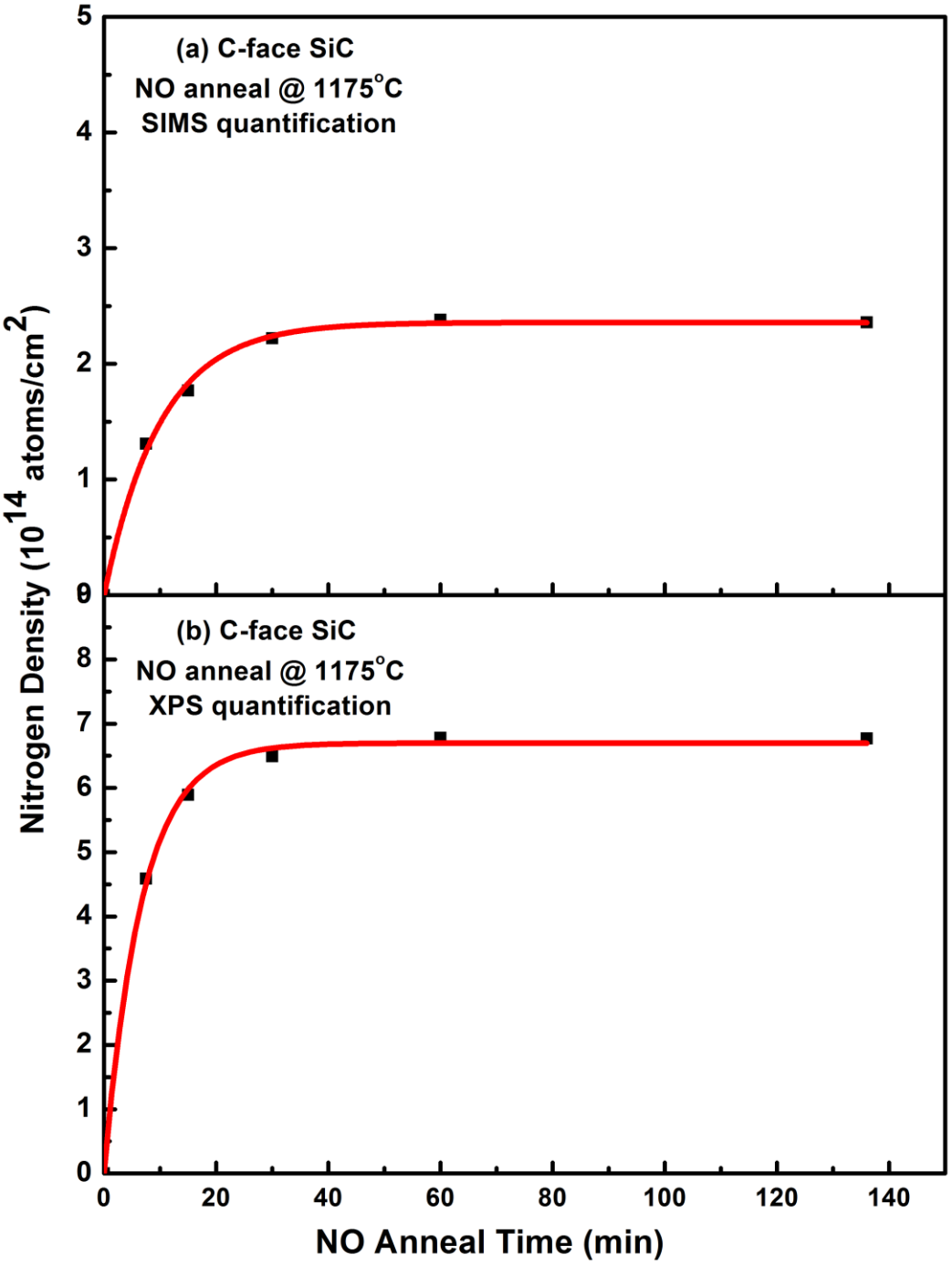

Fig. 4.3. Nitrogen uptake on the C-face of SiC during an NO anneal under 1175°C; the results were plotted for both (a) SIMS and (b) XPS results.

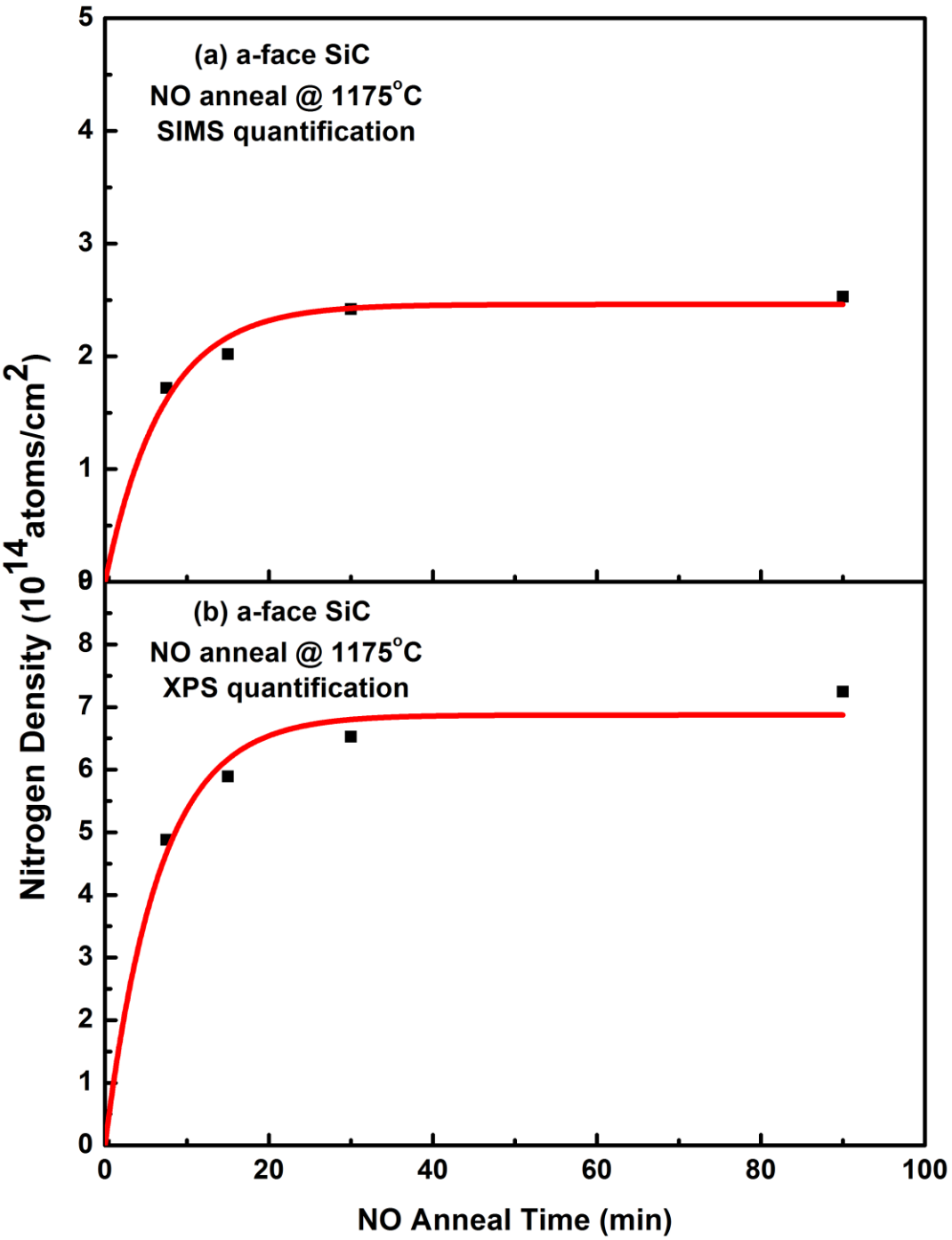

Fig. 4.4. Nitrogen uptake on the a-face of SiC during an NO anneal under 1175^{o}C, the results were plotted for both (a) SIMS and (b) XPS results.

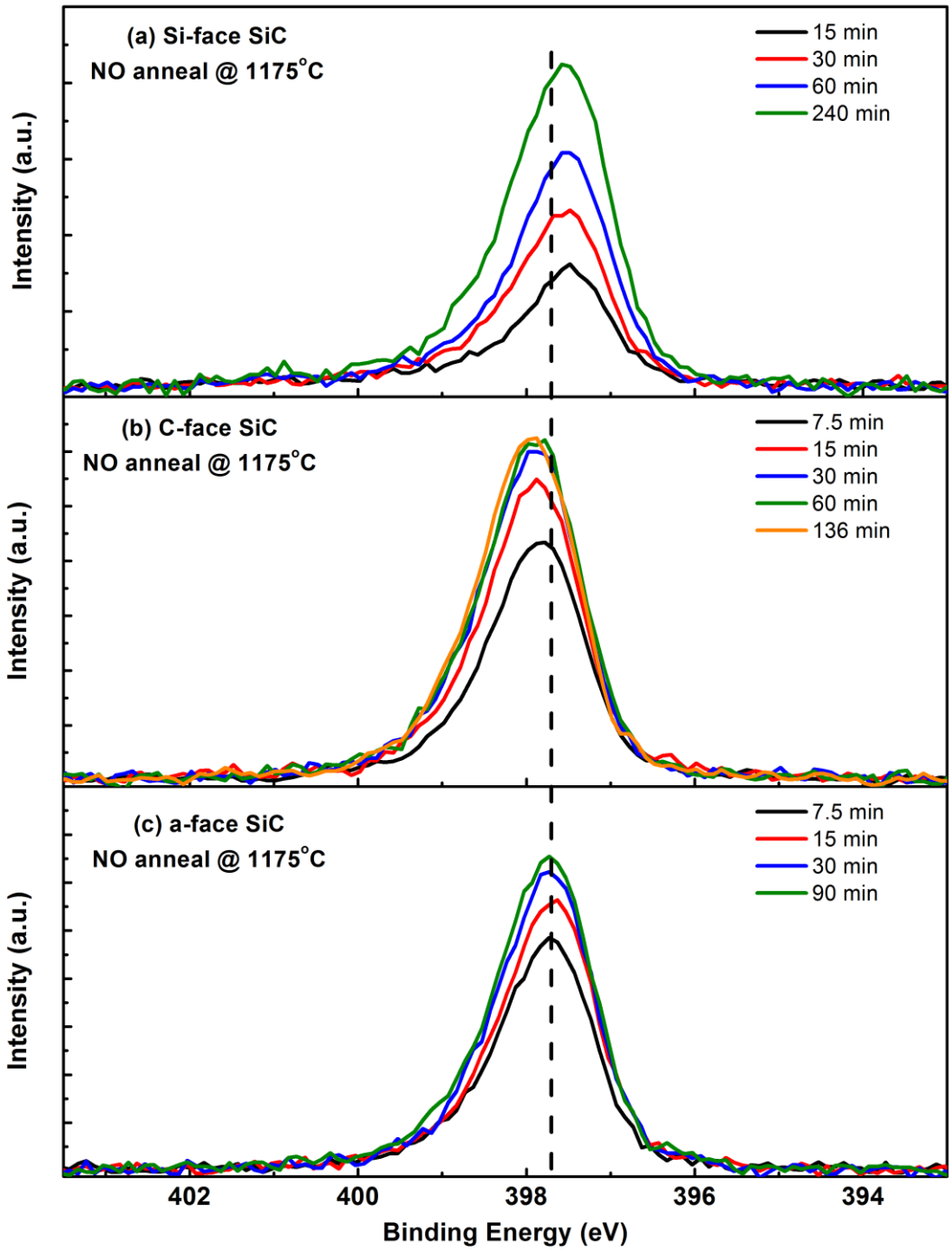

Fig. 4.5. N 1s XPS spectra of NO annealed SiO_2/SiC at 1175°C on the (a) Si-face, (b) C-face and (c) a-face. Samples were annealed in NO (g) at 1175°C for various periods of time.

N 1s XPS spectrum from all three crystal faces are shown in Fig. 4.5. The C-, Si- and a-faces display the similar N 1s peak shape, and the peak binding energies all fall in the range 397.5 eV ~ 397.9 eV, suggesting that N atoms reside in very similar local chemical environments regardless of the external crystal face. The detailed bonding and structures of N at the Si-face SiO_2/SiC interface was investigated in chapter 3 and also in a separate paper.[15] The current results show that N atoms are also primarily bound to Si atoms on the C- and a-faces of SiC. The N 1s peak binding energy is 397.5 eV on the Si-face, 397.9 eV on the C-face, and 397.7 eV on the a-face. The small differences of the N 1s binding energies between the different crystal faces is not well understood; one possible reason is the different Si structure and symmetry on the different crystal faces. Shirasawa *et al.* proposed a structure in which each N atom at the interface is bound to three Si atoms passivating all the dangling bonds at the interface.[15, 16] On the Si-face, each N atom bonds to one Si atom from the SiC substrate and two Si atoms from the oxide,[15, 16] while on the C-face, N atoms have a much higher chance to bond with Si atoms or even C atoms from SiC substrate, and thus slightly shift the N 1s binding energy. As of a-face, there are 50% Si atoms and 50% C atoms on the surface, and the binding energy is between that of Si-face and C-face, as expected.

4.4. Saturation on different faces and N coverage vs. miscut angle

Fig. 4.6 shows the comparison of Si-face, C-face and a-face N incorporation uptake following a 1175^{o}C NO anneal. The N coverage data points are measured with XPS and fit with a first order Langmuir kinetics model to extract the saturation coverage value. The interfacial nitrogen coverage appears to saturate on all three crystallographic

faces explored at all temperatures examined. In addition, the nitridation process is quite anisotropic on 4H-SiC.[17] The nitrogen areal densities on the C-face and a-face were observed to saturate faster (in less than 1 hr) than that on the Si-face, and they also reach a higher saturation value than that of the Si-face. The saturation values are predicted to be below one full monolayer by a previous theoretical investigation.[18]

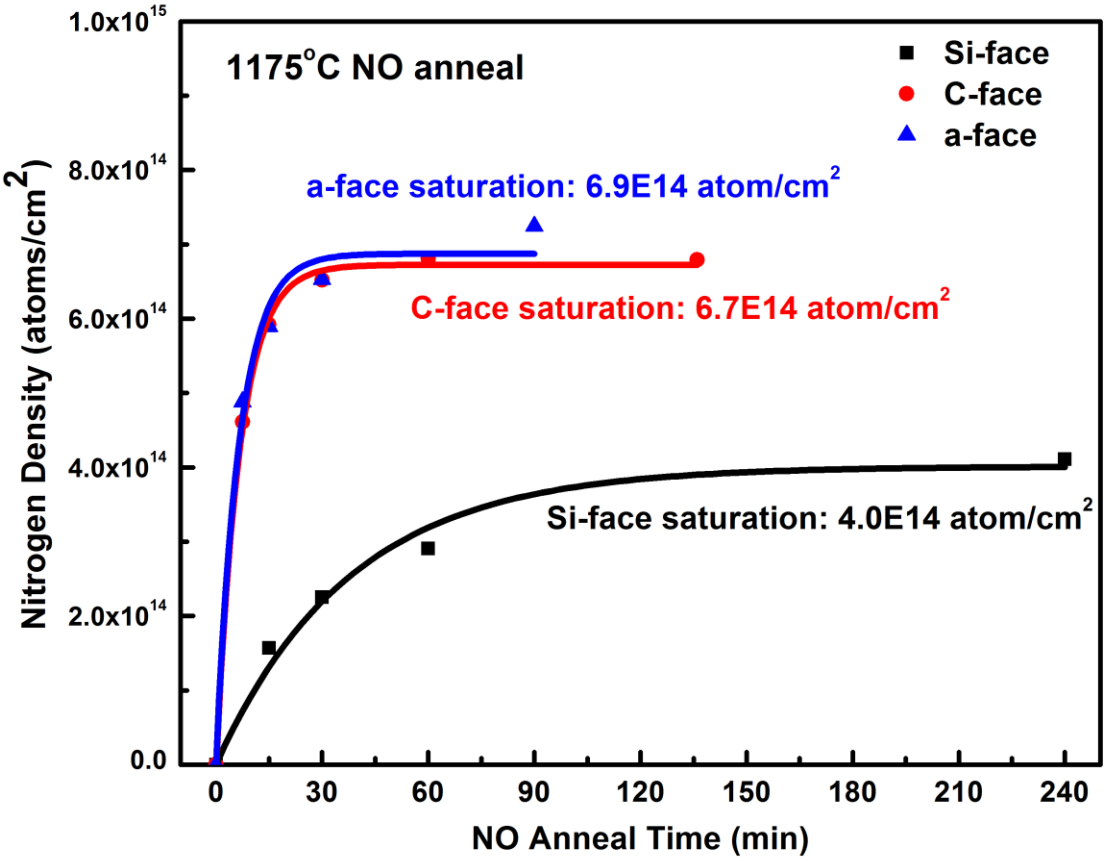

Fig. 4.6. Comparison of the Si-face, C-face and a-face N uptake for an 1175°C NO anneal. The N coverage data points are measured with XPS and fit with a first order Langmuir kinetics to extract the saturation coverage value.

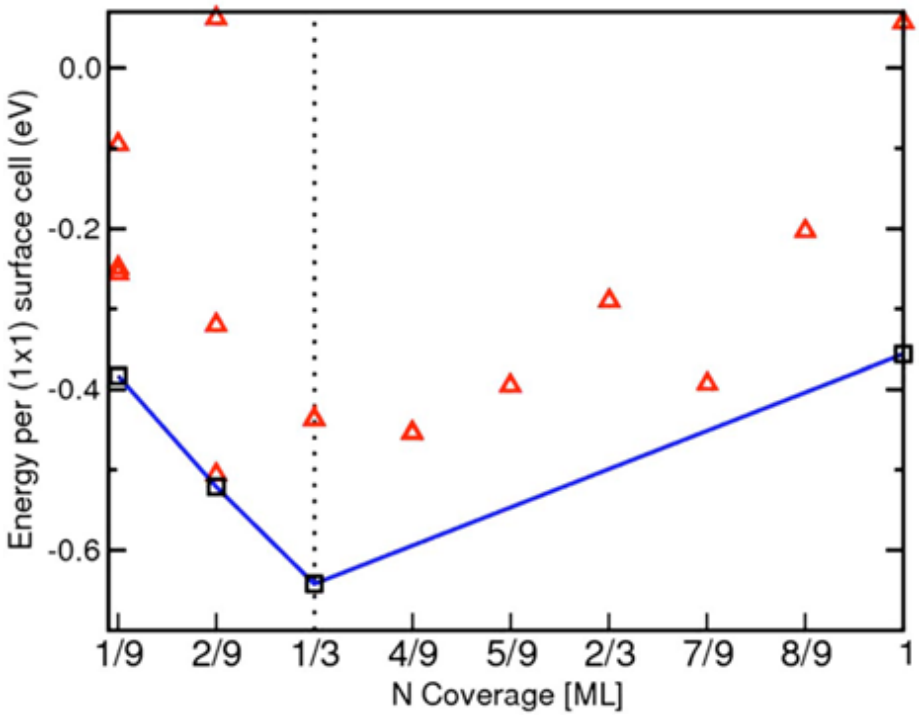

Fig. 4.7. (Adopted from ref. 18) Symbols indicate N adsorption energy per 1×1 surface cell (on the Si-face). Stable structure at each coverage was represented by black squares. Higher energy (less favorable) structures were represented by red triangles. The most stable phase of the structures probed occurs at 1/3 ML coverage.[18]

The N saturation coverage on the Si-face has been investigated using DFT calculations by Pennington, et al.[18] The result is shown in Fig. 4.7.[18] The study found stable structures at N coverage at or below 1/3 monolayer. For coverages greater than 1/3 of a monolayer of N, the relative N stability decreased for most structures explored, although at full monolayer coverage, the system appeared relatively stable.[18] This result is in agreement with our observation in chapter 3 (perhaps by coincidence), that on the Si-face, the N coverage is either 1/3 monolayer (using NO anneal or N_2 plasma) or 1 monolayer (using N_2 plasma or N_2 thermal anneal).

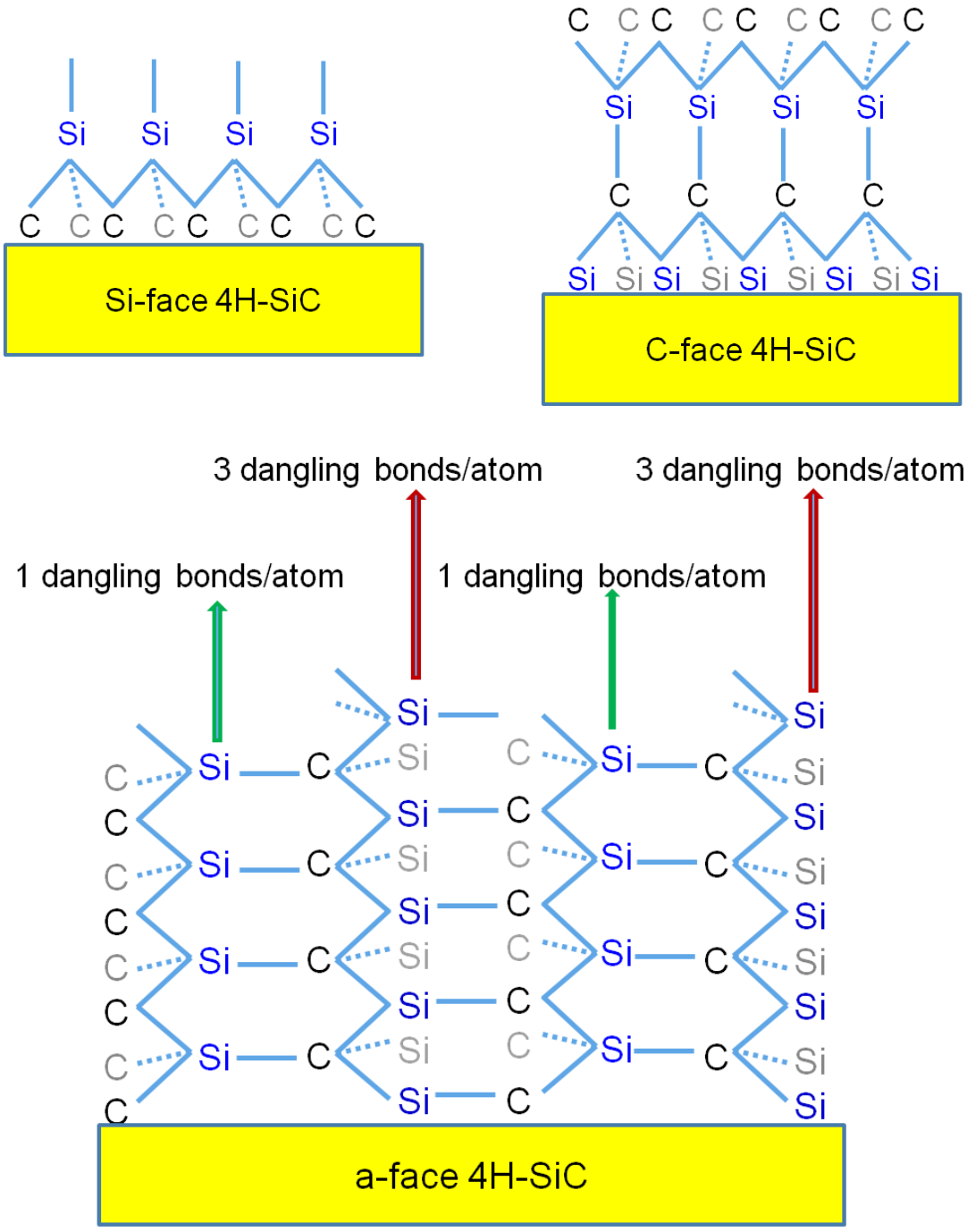

Fig. 4.8. Sketches of different dangling bond configurations and symmetry of different crystal faces on 4H-SiC.

The reason for the anisotropic nitrogen saturation values is not fully understood, but there are different possible explanations. One is that the different dangling bond configurations and symmetries of different crystal faces result in different stable N structures. As shown in Fig. 4.8, the dangling bond density and configuration is quite different on the different faces, as the C-face and a-face have more available dangling bonds with which N atoms can be bound with.

To further support this explanation, we performed an experiment on the Si-face of SiC at different miscut angles. If we consider a miscut Si-face as a combination of Si- and a-faces, while an on-axis Si-face sample is 100% Si-face. The N coverage densities (cm^{-2}) on miscut samples following a 2hr NO anneal are shown in Fig. 4.9. From Fig. 4.6 we find that the a-face has an N saturation value about 1.65 times of that of the Si-face. If we consider the miscut surface as steps, with the long side Si-face and short side a-face, and the N coverage density (N) can be approximately calculated as,

$$N_{miscut} = 1.65 \times \sin\theta \times N_{Si-face} + \cos\theta \times N_{Si-face} \quad (1)$$

The result of this step model is shown in Fig. 4.9 in red. We see that this model is still not close enough to the experimental results (black). In this step model, the surface area is different for different miscut angles. We next create another surface combination model, which keeps the a-face and Si-face ratio same as the step model, and also keeps the same total surface area. In this model, the N coverage can be calculated as,

$$N_{miscut} = \frac{1.65\times\sin\theta\times N_{Si-face}+\cos\theta\times N_{Si-face}}{\sin\theta+\cos\theta} \quad (2)$$

The result of this surface combination model is shown in Fig. 4.9 in blue, and it agrees much better with the experimental results.

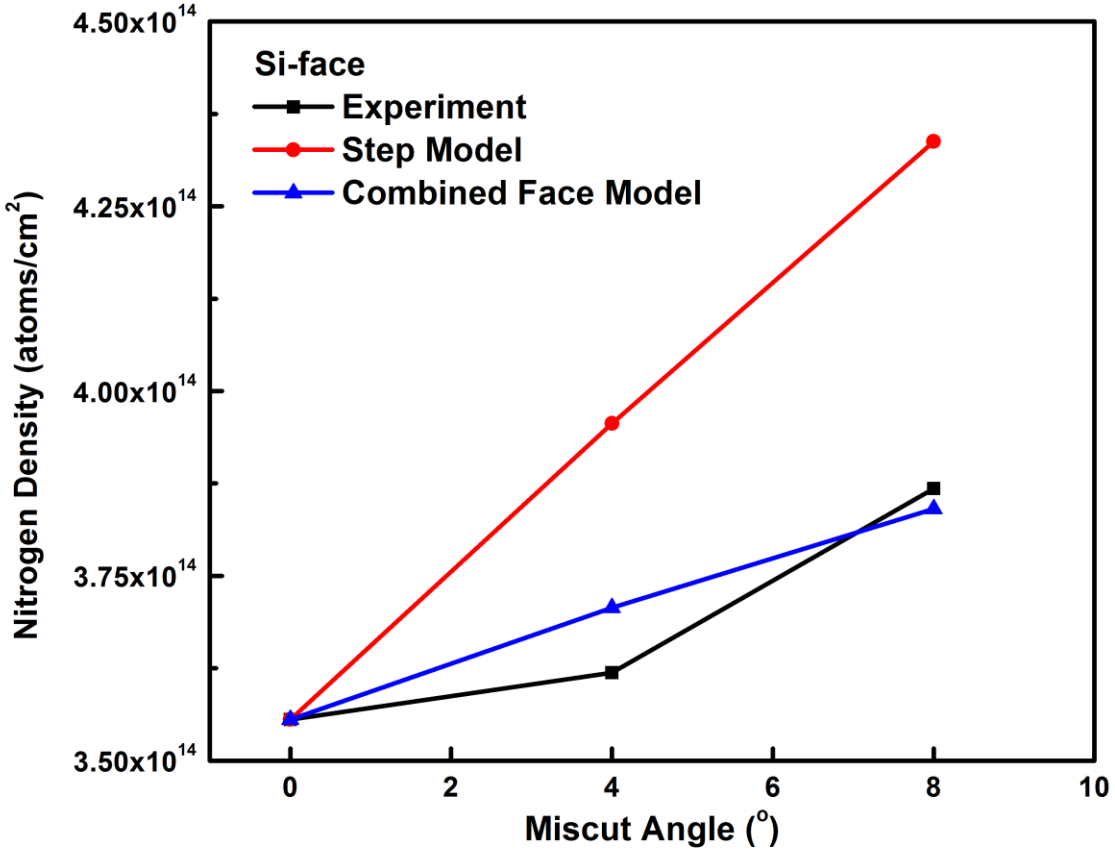

Fig. 4.9. N coverage data and models on the Si-face of SiC for different miscut angles.

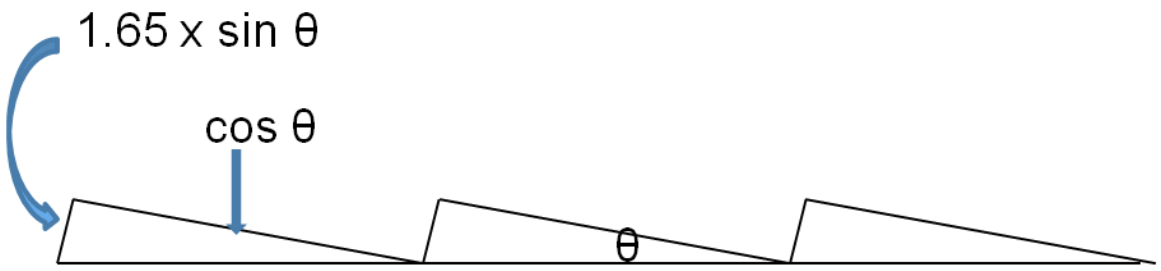

Fig. 4.10. The SiC miscut angle model; θ represents the miscut angle.

4.5. Kinetics model

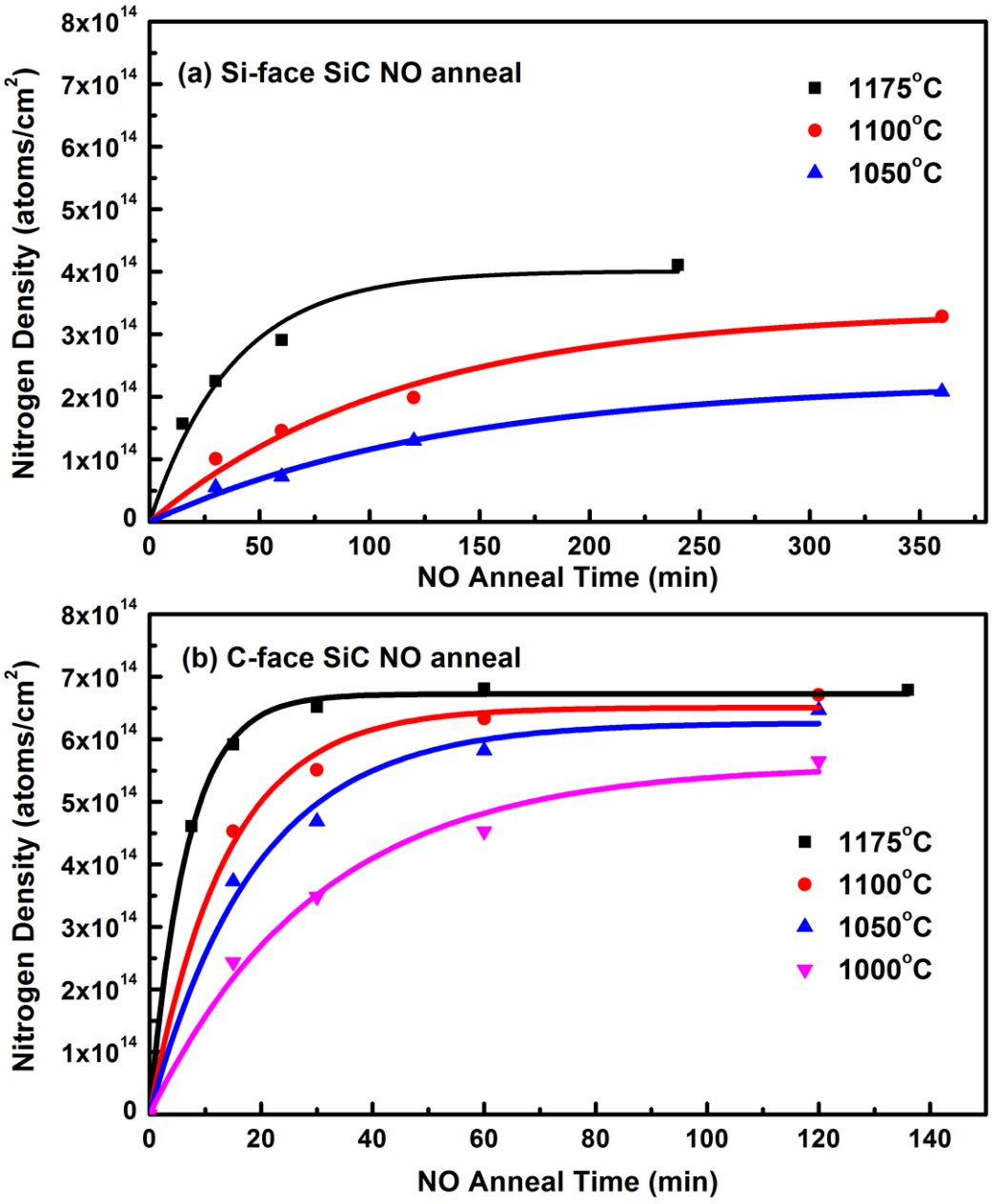

Fig. 4.11. Surface N coverage a function of the passivation time by XPS (again with an MEIS calibration). The (a) Si-face data, and (b) C-face data. The dots, squares and triangles are experimental measurements and the solid lines are fit curves using simple,

first order Langmuir kinetics. Note that different scales are used for the x-axes for the different faces.

We also investigate the N uptake at temperatures other than that used in the standard NO process. Fig. 4.11 shows the nitrogen areal density as a function of the annealing time and temperature. The reaction kinetics of NO with the C-face surface and the associated interfacial nitridation are significantly faster than with the Si-face. This result is consistent with an earlier report on nitrogen concentration by nuclear reaction analysis (NRA).[19] However, our new results show higher nitrogen concentrations for both faces, probably because the NRA samples were nitrided in a static (non-flowing) mode to efficiently use the isotopically enriched NO.

The N uptake data were analyzed using a first order chemical kinetics model suggested in by Dhar et al.[17] In our work, the model was applied at multiple temperatures and all the data were obtained while annealing with NO introduced in the flowing mode, more relevant to device processing. By nitriding at different anneal temperatures, we are able to extract the temperature dependence of the process.

McDonald *et al.*[12] reported that dry oxidation reduces the nitrogen content at the SiO_2/SiC interface. It is also known that NO decomposes into a mixture of NO, N_2, O_2, NO_2, N_2O, etc. at high temperatures.[12] This suggests that there are multiple factors that should be considered in understanding and predicting N uptake.[20] Not only should the nitrogen incorporation rate (from all sources) be understood, but the removal of nitrogen by reaction with oxygen or other species is essential, as the two processes occur in parallel and in some sense compete with each other. There is also interfacial oxidation,

the movement of the interface caused by oxidation during the NO anneals is not considered, and the focus is the change in nitrogen coverage at the interface.

If we consider that the change in the nitrogen areal density at the interface can be expressed most simply by one nitridation process (from NO) and one loss process (from reaction with O_2), then to first order:

$$\frac{dA_N(t)}{dt} = k_+ C_{NO}(t) - k_- C_{O2}(t) A_N(t), \qquad (3)$$

where $A_N(t)$ [atoms/cm^2] stands for the nitrogen areal density at the interface, k_+ [cm/min] and k_- [cm^3/(atoms-min)] stand for the rate of nitrogen incorporation and nitrogen removal, respectively, $C_{NO}(t)$ and $C_{O_2}(t)$ represent the concentration of NO (g) and O_2 (g) in the tube.

Nitrogen (N_2) could react with SiC to incorporate N in the form of Si_3N_4 given appropriate pressure and temperature.[21] The N_2 comes from the NO decomposition and at this temperature has a gas phase concentration of roughly 10%.[12] Therefore at atmospheric (total) pressure, the partial pressure of N_2 is about 0.1atm. In the temperature range of our experiment, the production of Si_3N_4 by pure N_2 can be ignored.[21] Therefore, no N_2 related term is included in this equation.

The solution can be expressed as $A_N(t) = \frac{K_+}{K_-}(1 - e^{-K_- t})$, where $K_+ = k_+ C_{NO}(t)$ and $K_- = k_- C_{O2}(t)$. The fit curves are also shown in Fig. 4.11. K_+ and K_- can be extracted from the fitting curves.

The results have interesting implications to our general understanding of SiC oxidation and NO passivation processes. Clearly N accumulates on the C-face faster than it on the Si-face. Using the data from Fig. 4.11 we can determine the ratio of N uptake on the C-face and Si-face in the linear regime, which is also the starting stage of N

incorporation, i.e. at low N coverage, or $\frac{dA_N}{dt}\Big|_{t=0} = K_+$. The work of Yamamoto[20, 22] and Kakubari[23] allow us to compare the actual oxidation rates under similar conditions. The N incorporation and oxidation rates in the linear regime are shown in Fig 4.12.

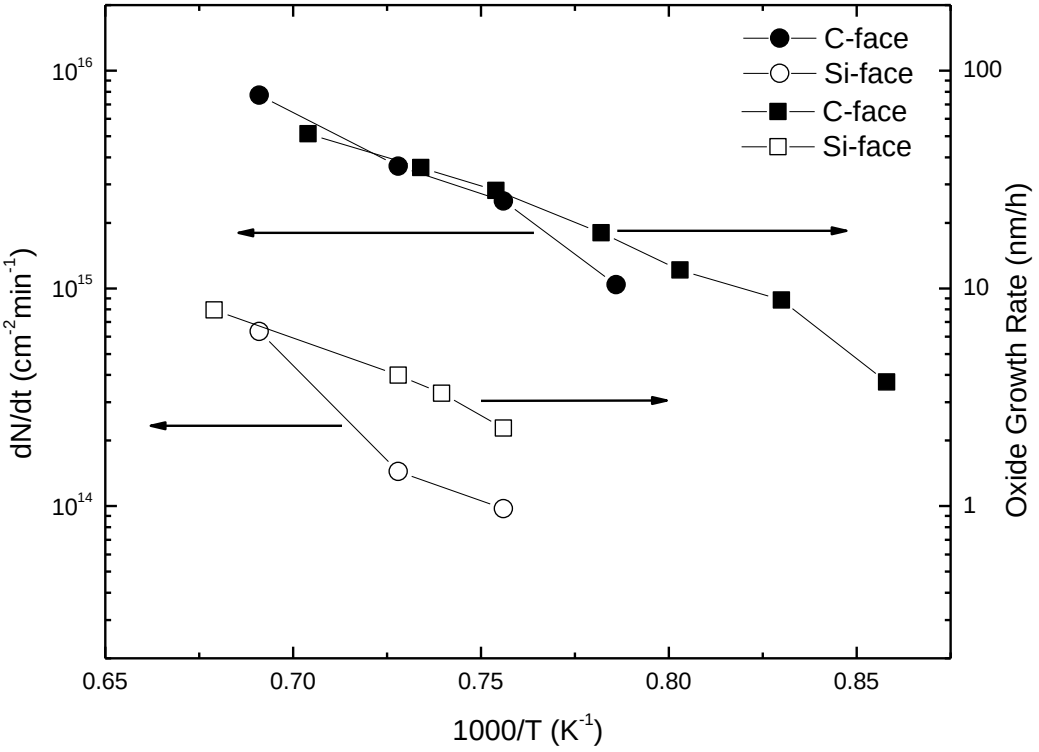

Fig. 4.12. Nitrogen incorporation rates at the SiO_2/SiC interface and the thermal dry oxide growth rate as function of temperature on the C-face and Si-face. The oxide growth rate data are from Yamamoto et al.[20, 22]

The most significant observation is that both nitridation and oxidation are faster on C-face at all measured temperatures. It is also clear that the rates of N uptake on the two surfaces follow the same trend in relative amount as the oxidation rates at all measured

temperatures. This figure suggests that in the NO annealing process, the nitrogen incorporation might be associated with (or follow a mechanism that is similar to) the simultaneous oxidation process: i.e. the faster the oxidation, the faster the N incorporation.

4.6. N uptake correlation with interface trap density

The N concentration in the films is also correlated to defect concentration and mobility as observed in electrical measurements on NO passivated SiO_2/SiC systems.

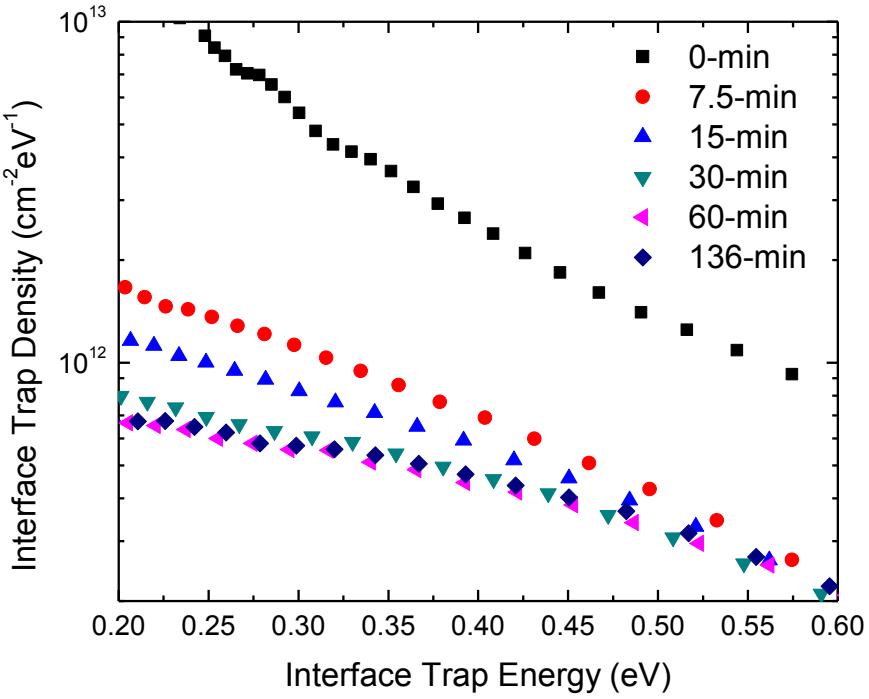

Fig. 4.13. Interface trap density of the carbon-face SiO_2/SiC passivated by NO at 1175^{o}C for different periods of time.

Interface state densities for the corresponding C-face MOS capacitors (1175°C NO annealed) are shown in Fig. 4.13. Comparing these results with Fig. 4.11 it is clear that the D_{it} reduces monotonically up to 30-min of NO annealing. Beyond 30 minutes, both the N coverage and the D_{it} become saturated. This 'scaling effect' was reported by Rozen et al. on the Si-face,[12, 13] and here we observed a similar scaling effect for the C-face. In this case, however, the lowest D_{it} obtained for the C-face is significantly higher than observed on the NO annealed Si-face,[3] even with higher saturation N coverage. The higher D_{it} in C-face MOS capacitors with a higher saturated N coverage is most likely associated with the existence of other defects which are not affected by N, possibly carbon containing species.

Rozen *et al.* have also shown that other than D_{it} scaling with the interfacial N content, the channel mobility for the Si-face also scales with the interfacial N content.[24] The mechanism by which N improves device performance is not fully understood. It is clear through the earlier works by Jamet et al.[6] and Shirasawa[16], and theoretical work by Pantelides[7], that N can passivate the carbon-related interface states and oxide traps, thus give rise to lower D_{it}. Earlier work also suggests that N is able to dissolve C clusters near the interface, further reducing interface defects and hence increasing mobility.[6] However, experimental proof of the detailed atomic scale nature of the defects remains lacking. Another possible explanation for the mobility improvement is "counter doping" induced by interface passivation, as proposed by Liu et al[25]. In this model, N diffuse into vacancies that are created below the surface during oxidation, and acts as a dopant. The passivation mechanism and counter doping mechanisms are not contradictory to each other and can be working together to passivate interface states in parallel to forming a

counter-doped layer. It has also been reported that N may reduce the width of the interfacial transition regime[26] suggesting that it may reduce interface roughness.

Sharma *et al.*, successfully employed phosphorus with simultaneous oxidation to reduce the interface trap density and improve channel mobility[27]. The phosphorus passivation and mobility improvement will be discussed in chapter 5.

4.7. Summary

The interfacial nitrogen coverage at the Si-, C- and a-faces of the SiO_2/SiC interface have been measured at different temperatures and for various annealing times. The interface trap density of the nitrogen passivated C-face SiO_2/4H-SiC has been explored and a scaling between the interface trap density reduction and the N uptake is observed, consistent with the Si-face behavior. The nitrogen incorporation and oxidation rates are suggested to be associated in the NO anneal process on both C-face and Si-face SiC. A first-order kinetics model of the interfacial N uptake is proposed and is shown to fit the data quite well; the N coverage that results from NO annealing can be predicted with the model. The results of this study can be useful in both technological applications as well as developing new methods of nitridation.

References

[1] S. W. Wang, S. Dhar, S. R. Wang, A. C. Ahyi, A. Franceschetti, J. R. Williams, L. C. Feldman, and S. T. Pantelides, "Bonding at the SiC-SiO_2 interface and the effects of nitrogen and hydrogen," *Physical Review Letters*, vol. 98, Jan 12 2007.

[2] G. Chung, C. C. Tin, J. R. Williams, K. McDonald, M. Di Ventra, R. K. Chanana, S. T. Pantelides, L. C. Feldman, and R. A. Weller, "Effects of anneals in ammonia on the interface trap density near the band edges in 4H-Silicon Carbide metal-oxide-semiconductor capacitors," *Applied Physics Letters*, vol. 77, pp. 3601-3603, 2000.

[3] S. Dhar, L. C. Feldman, S. Wang, T. Isaacs-Smith, and J. R. Williams, "Interface trap passivation for SiO_2/(0001) C-terminated 4H-SiC," *Journal of Applied Physics*, vol. 98, pp. -, 2005.

[4] J. L. Cantin, H. J. Von Bardeleben, Y. Ke, R. P. Devaty, and W. J. Choyke, "Hydrogen passivation of carbon Pb like centers at the 3C- and 4H-SiC/SiO_2 interfaces in oxidized porous SiC," *Applied Physics Letters*, vol. 88, pp. 092108-092108-3, 2006.

[5] H. Yano, F. Katafuchi, T. Kimoto, and H. Matsunami, "Effects of wet oxidation/anneal on interface properties of thermally oxidized SiO_2/SiC MOS system and MOSFET's," *Electron Devices, IEEE Transactions on*, vol. 46, pp. 504-510, 1999.

[6] P. Jamet, S. Dimitrijev, and P. Tanner, "Effects of nitridation in gate oxides grown on 4H-SiC," *Journal of Applied Physics*, vol. 90, pp. 5058-5063, Nov 15 2001.

[7] S. T. Pantelides, S. Wang, A. Franceschetti, R. Buczko, M. Di Ventra, S. N. Rashkeev, L. Tsetseris, M. Evans, I. Batyrev, and L. C. Feldman, "Si/SiO_2 and SiC/SiO_2 interfaces for MOSFETs–challenges and advances," in *Materials science forum*, 2006, pp. 935-948.

[8] Y. Song, S. Dhar, L. C. Feldman, G. Chung, and J. R. Williams, "Modified Deal Grove model for the thermal oxidation of silicon carbide," *Journal of Applied Physics*, vol. 95, pp. 4953-4957, 2004.

[9] J. N. Shenoy, M. K. Das, J. A. Cooper, M. R. Melloch, and J. W. Palmour, "Effect of substrate orientation and crystal anisotropy on the thermally oxidized SiO_2/SiC interface," *Journal of Applied Physics*, vol. 79, pp. 3042-3045, 1996.

[10] K. Christiansen, S. Christiansen, M. Albrecht, H. P. Strunk, and R. Heibig, "Anisotropic oxidation of silicon carbide," *Diamond and Related Materials*, vol. 6, pp. 1467-1471, 1997.

[11] X. Zhu, H. D. Lee, T. Feng, A. C. Ahyi, D. Mastrogiovanni, A. Wan, E. Garfunkel, J. R. Williams, T. Gustafsson, and L. C. Feldman, "Structure and stoichiometry of (0001) 4H-SiC/oxide interface," *Applied Physics Letters*, vol. 97, p. 071908, Aug 16 2010.

[12] K. McDonald, L. C. Feldman, R. A. Weller, G. Y. Chung, C. C. Tin, and J. R. Williams, "Kinetics of NO nitridation in SiO_2/4H-SiC," *Journal of Applied Physics*, vol. 93, pp. 2257-2261, Feb 15 2003.

[13] J. Rozen, S. Dhar, M. E. Zvanut, J. R. Williams, and L. C. Feldman, "Density of interface states, electron traps, and hole traps as a function of the nitrogen density in SiO_2 on SiC," *Journal of Applied Physics*, vol. 105, pp. -, 2009.

[14] R. Kosugi, T. Umeda, and Y. Sakuma, "Fixed nitrogen atoms in the SiO_2/SiC interface region and their direct relationship to interface trap density," *Applied Physics Letters,* vol. 99, p. 182111, Oct 31 2011.

[15] Y. Xu, X. Zhu, H. D. Lee, C. Xu, S. M. Shubeita, A. C. Ahyi, Y. Sharma, J. R. Williams, W. Lu, S. Ceesay, B. R. Tuttle, A. Wan, S. T. Pantelides, T. Gustafsson, E. L. Garfunkel, and L. C. Feldman, "Atomic state and characterization of nitrogen at the SiC/SiO_2 interface," *Journal of Applied Physics,* vol. 115, pp. -, 2014.

[16] T. Shirasawa, K. Hayashi, S. Mizuno, S. Tanaka, K. Nakatsuji, F. Komori, and H. Tochihara, "Epitaxial silicon oxynitride layer on a 6H-SiC(0001) surface," *Physical Review Letters,* vol. 98, p. 136105, Mar 30 2007.

[17] S. Dhar, L. C. Feldman, K.-C. Chang, Y. Cao, L. M. Porter, J. Bentley, and J. R. Williams, "Nitridation anisotropy in SiO_2/4H–SiC," *Journal of Applied Physics,* vol. 97, pp. -, 2005.

[18] G. Pennington and C. R. Ashman, "Nitrogen passivation of (0001) 4H-SiC silicon-face dangling bonds," *Applied Physics Letters,* vol. 91, p. 072106, Aug 13 2007.

[19] H. J. von Bardeleben, J. Cantin, I. Vickridge, Y. W. Song, S. Dhar, L. C. Feldman, J. R. Williams, L. Ke, Y. Shishkin, and R. P. Devaty, "Modification of the Oxide/Semiconductor Interface by High Temperature NO Treatments: a Combined EPR, NRA and XPS Study on Oxidized Porous and Bulk n-type 4H-SiC," in *Materials Science Forum*, 2005, pp. 277-280.

[20] T. Yamamoto, Y. Hijikata, H. Yaguchi, and S. Yoshida, "Oxide Growth Rate Enhancement of Silicon Carbide (0001) Si-Faces in Thin Oxide Regime," *Japanese Journal of Applied Physics,* vol. 47, p. 7803, 2008.

[21] T. Lichko, Y. A. Kryl, and V. E. Rymar, "High-temperature reaction between silicon carbide and nitrogen under pressure," *Powder Metallurgy and Metal Ceramics,* vol. 32, pp. 281-285, 1993/04/01 1993.

[22] T. Yamamoto, Y. Hijikata, H. Yaguchi, and S. Yoshida, "Growth Rate Enhancement of (000-1) Face Silicon-carbide Oxidation in Thin Oxide Regime," *Japanese Journal of Applied Physics,* vol. 46, p. L770, 2007.

[23] K. Kakubari, R. Kuboki, Y. Hijikata, H. Yaguchi, and S. Yoshida, "Real Time Observation of SiC Oxidation Using an In Situ Ellipsometer," in *Materials science forum*, 2006, pp. 1031-1034.

[24] J. Rozen, A. C. Ahyi, X. G. Zhu, J. R. Williams, and L. C. Feldman, "Scaling Between Channel Mobility and Interface State Density in SiC MOSFETs," *Ieee Transactions on Electron Devices,* vol. 58, pp. 3808-3811, Nov 2011.

[25] G. Liu, A. C. Ahyi, Y. Xu, T. Isaacs-Smith, Y. K. Sharma, J. R. Williams, L. C. Feldman, and S. Dhar, "Enhanced Inversion Mobility on 4H-SiC (1120) Using Phosphorus and Nitrogen Interface Passivation," *Ieee Electron Device Letters,* vol. 34, pp. 181-183, Feb 2013.

[26] J. A. Taillon, J. H. Yang, C. A. Ahyi, J. Rozen, J. R. Williams, L. C. Feldman, T. S. Zheleva, A. J. Lelis, and L. G. Salamanca-Riba, "Systematic structural and chemical characterization of the transition layer at the interface of NO-annealed

4H-SiC/SiO_2 metal-oxide-semiconductor field-effect transistors," *Journal of Applied Physics,* vol. 113, Jan 28 2013.

[27] Y. K. Sharma, A. C. Ahyi, T. Issacs-Smith, X. Shen, S. T. Pantelides, X. Zhu, L. C. Feldman, J. Rozen, and J. R. Williams, "Phosphorous passivation of the SiO_2/4H-SiC interface," *Solid-State Electronics,* vol. 68, pp. 103-107, Feb 2012.

Chapter 5. Phosphorus at the SiO_2/SiC interface

5.1 Phosphorus passivation

Recently, improved device performance has also been achieved by introducing phosphorous to the SiO_2/SiC interface.[1-4] It is shown that phosphorus passivation (P-passivation) is more effective than NO passivation in reducing interface trap density and increasing channel mobility.[1-4] In this chapter, we show that the interfacial P content is about 1/3 as much as interfacial N content in the NO passivated device, but the interface trap density near the conduction band edge (E_C - E = 0.2 eV) is reduced to around 2×10^{11}/eV cm^2, while it is about 7×10^{11}/eV cm^2 for the NO passivated case. The peak mobility of phosphorus passivated 4H-SiC MOSFET is around 85 $cm^2/V\,s$,[5] about twice as much as NO passivated device.

Phosphourous passivation is achieved by using a phosphosilicate glass (PSG). PSGs are polar materials, and using PSG as a dielectric layer in a device can result in instability.[1, 2, 4] A stabilized P-passivated SiC MOSFET device has been achieved by Sharma et al;[3] in that work, instead of using a thick PSG layer, a thin PSG layer capped with deposited SiO_2 was used as the dielectric.[3] This modified P-passivation process stabilizes the device while keep most of the passivating effect of P. The peak field effect mobility obtained using the thin PSG approach is around 72 $cm^2/V\,s$.[3]

In this chapter, we examine the chemical bonding of phosphorus and quantify the phosphorus content at the SiO_2/SiC interface, the mechanism by which phosphorus improves interface quality and device performance is also discussed. We present a brief overview of the motivation of the chapter in section 5.1. In section 5.2, the P-passivation

process is described. In section 5.3, the differences between the etching behavior of interfacial P on SiC and Si surfaces are studied. In section 5.4, we investigate the interfacial P and O bonding. In section 5.5, we present the interfacial P coverage on different crystal faces of 4H-SiC. The interfacial P content as measured by XPS and MEIS are in good agreement. In section 5.6, accurate P depth profiles at the SiO_2/SiC interface are studied using MEIS and angle resolved XPS, and the result is compared with the N depth profile at the interface. In section 5.7, we show the change of interfacial P content using a thin (stabilizing) PSG process. In section 5.8, the "counter doping" idea and mechanism is discussed.

5.2 Sample preparation

Si-face (4 ° off axis) and a-face (on-axis) n-type 4H-SiC samples were cleaned with a standard RCA process. After cleaning we explored two different PSG processes: the "thick PSG" and "thin PSG" processes. For the "thick PSG" process, samples underwent dry thermal oxidization at 1150 ℃ for different time periods depending on the crystal faces and desired oxide thickness. After the thermal oxidation, samples were annealed in Ar at 1150 ℃ for 30 min, and then the samples were annealed at 1000 ℃ with a planar diffusion source (PDS) for various lengths of time. The PDS provides P_2O_5 which diffuses into the thermo oxide and form PSG during the annealing. For the "thin PSG" process, samples underwent a dry thermal oxidation to grow about a 10 nm oxide, and then went through the phosphorus anneal for various time. After that, ~60 nm of SiO_2 was deposited using low pressure chemical vapor deposition.

All the thick PSG and thin PSG samples were analyzed by different techniques prior to and after HF etching.

5.3 Phosphorus etching behavior at the SiO_2/SiC and SiO_2/Si interface

Fig. 5.1 shows the SIMS profile of a thick PSG/SiC sample and demonstrates that the PSG chemical composition is approximately uniform throughout the entire PSG layer.

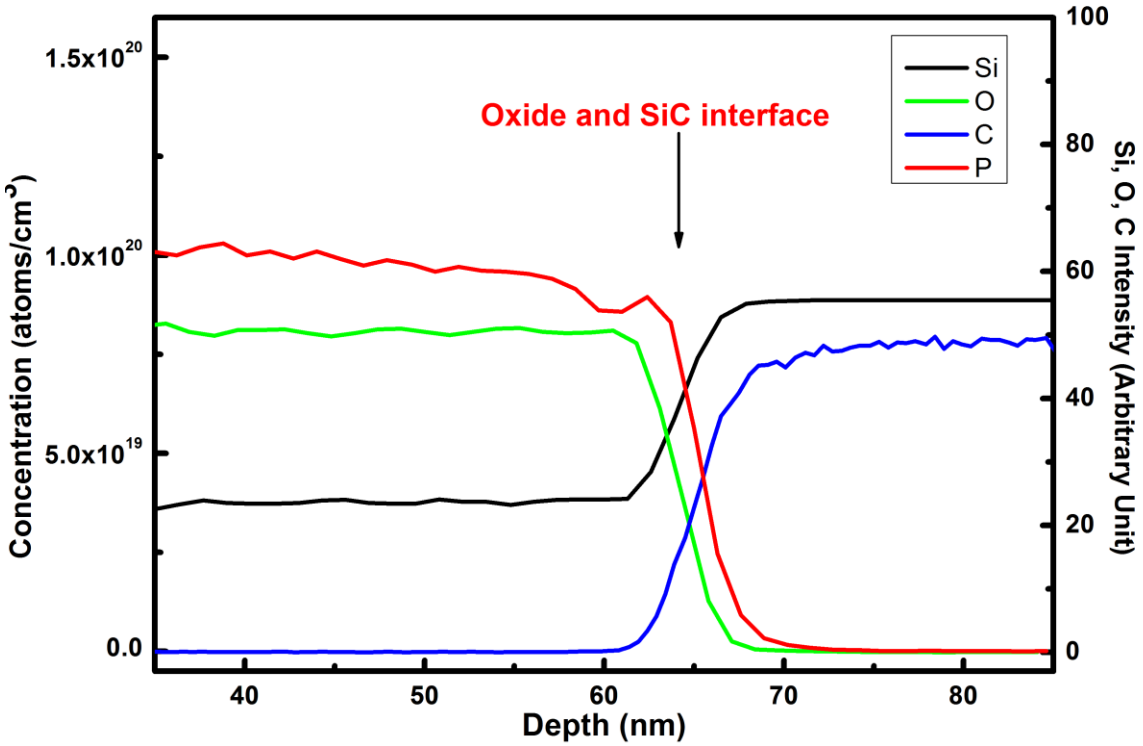

Fig. 5.1. SIMS profile of a thick PSG/SiC structure.

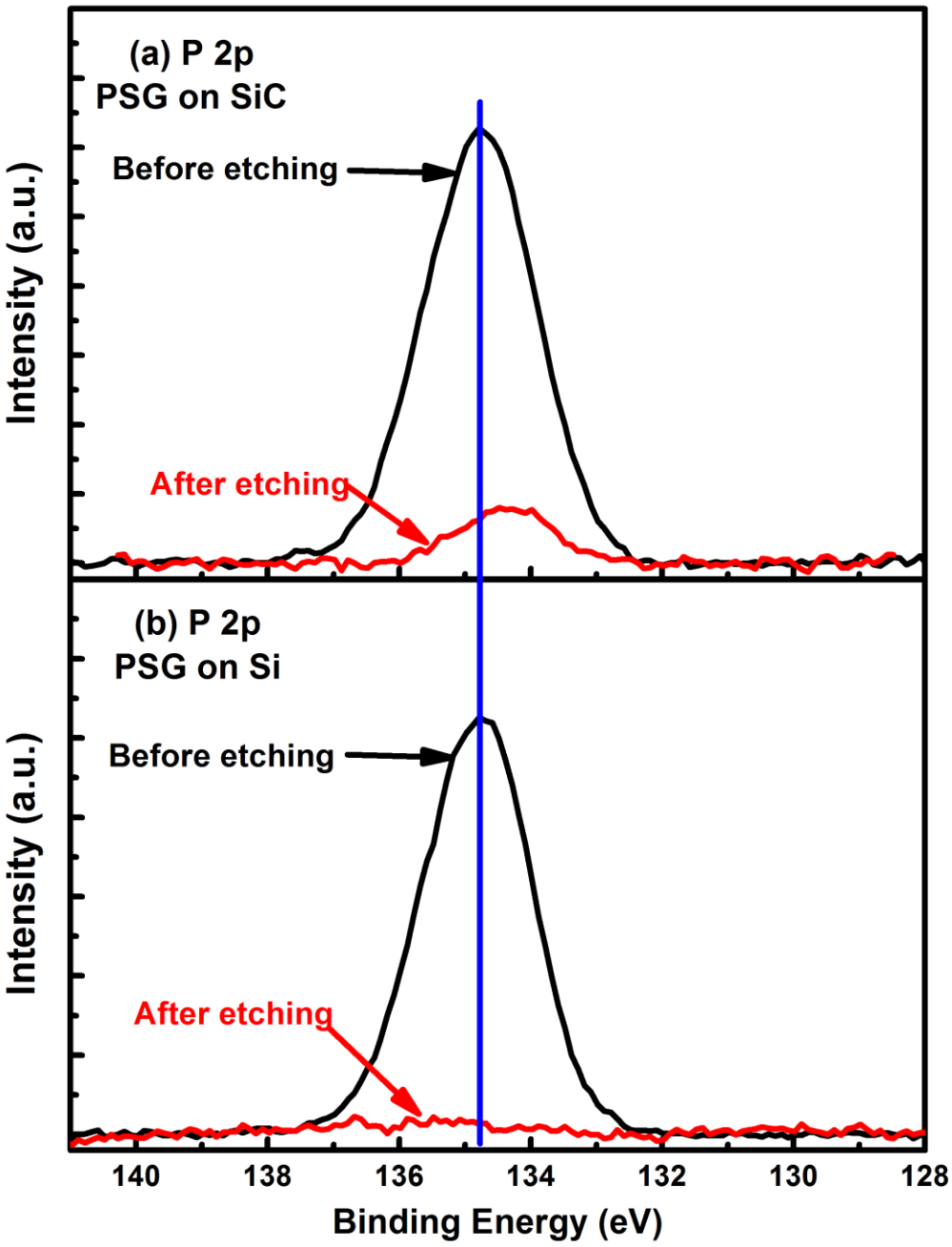

Fig. 5.2. XPS of P etching at PSG/SiC and PSG/Si interfaces.

Fig. 5.2(a) shows the P 2p XPS spectrum from 4H-SiC with ~60 nm PSG grown on the surface, before (black) and after (red) an etch in BOE. N^{+}-4H-SiC with 60nm

thermal oxide was annealed with a planar diffusion source (PDS) at 1000 ℃ for 3hr.[4] The figure shows that there is a significant amount of P remaining on the SiC surface after HF etching. The XPS spectrum indicates that the phosphorous and oxygen ratio is around 1:13 before etching and 1:15 after etching. The PSG chemical composition is about the same through the entire oxide layer and HF etching leaves about a layer of PSG. Fig. 5.2(b) shows the before and after etching P 2p XPS spectrum from Si(100) with phosphosilicate glass (PSG) grown on the surface using the same method as SiC. To compare the P 2p peaks on Si, the secondary plasmon peaks of Si 2p from elemental Si have to be considered. One XPS spectrum in this energy range taken from a clean Si sample is subtracted from the experimental data. The XPS spectrum shows no detectable phosphorous left on the Si after HF etching. The etching behavior of phosphorous is similar to N on both SiC and Si; both nitrogen and phosphorous at the SiO_2/SiC interface cannot be completely etched in HF while they can be removed from the Si surface.

5.4 Phosphorus bonding at the interface

Phosphorous is pentavalent, usually bonding to 3, 4 or 5 other atoms in molecules. In bulk PSG, P only bonds with oxygen atoms in the stable PSG network structure (Fig. 5.3),[6, 7] and has a 2p (XPS) binding energy of around 135-137 eV (the absolute number depends on the energy reference used).[8] In highly doped Si[9] or in phosphorus doped carbon films phosphorous has a 2p binding energy about 6 eV lower than that in PSG.[10] Note that the P 2p peak is shifted to a 0.6eV lower binding energy after etching (Fig. 5.2a), implying that phosphorous atoms at the interface are still primarily bound to oxygen atoms. This binding energy shift is likely caused by the different chemical

environment at the PSG/SiC interface than in the bulk; the shift may result from one of the P atoms being bound to C or Si, a secondary nearest neighbor effect, or increased final state screening by the substrate.

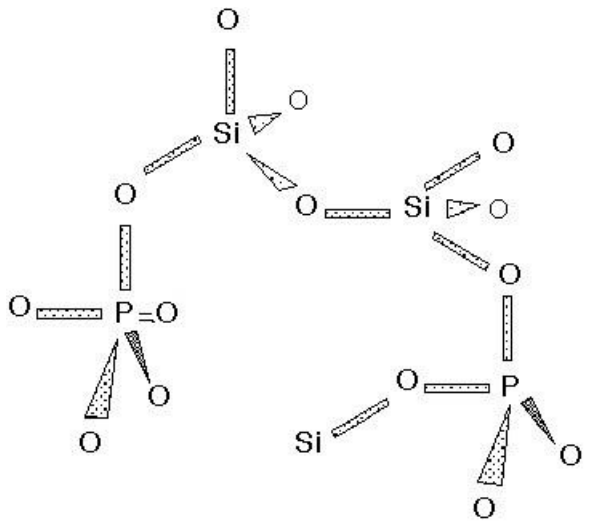

Fig. 5.3. Schematic two-dimensional model of the phosphosilicate glass structure. (Adapted from Daniel M. Dobkin)[11]

Note that we did not observe an analogous binding energy shift in the nitrogen case; this difference may be explained as follows. Nitrogen, from NO, is directly bonded to the SiC, hence shows no shift before and after etching because we are looking at the same N layer before and after etching. There is a shift in the N peak position relative to its position in the SiON layer formed on silicon. P, on the other hand, shows a chemical shift to lower binding energy after the etching, relative to the bulk PSG glass. Note that the phosphorus atoms are uniformly distributed through the oxide, and we observe the P in the bulk PSG before etching and P in the proximity of the interface after etching. Although the shift is relatively subtle, we believe it represents a significant change in

bonding which results in its lack of removal via etching and the improvement in the electronic properties of the interface.

5.5 Phosphorus incorporation and quantification on different crystal faces

The P coverage on an etched PSG/SiC surface is determined to be 1.2×10^{14} atoms/cm^2 based on XPS measurement using the photoelectron mean free path calculated in chapter 3, and about 1.3×10^{14} atoms/cm^2 based on MEIS measurement (Fig. 5.4). The two different techniques agree on the coverage of the passivating agent left on the SiC surface.

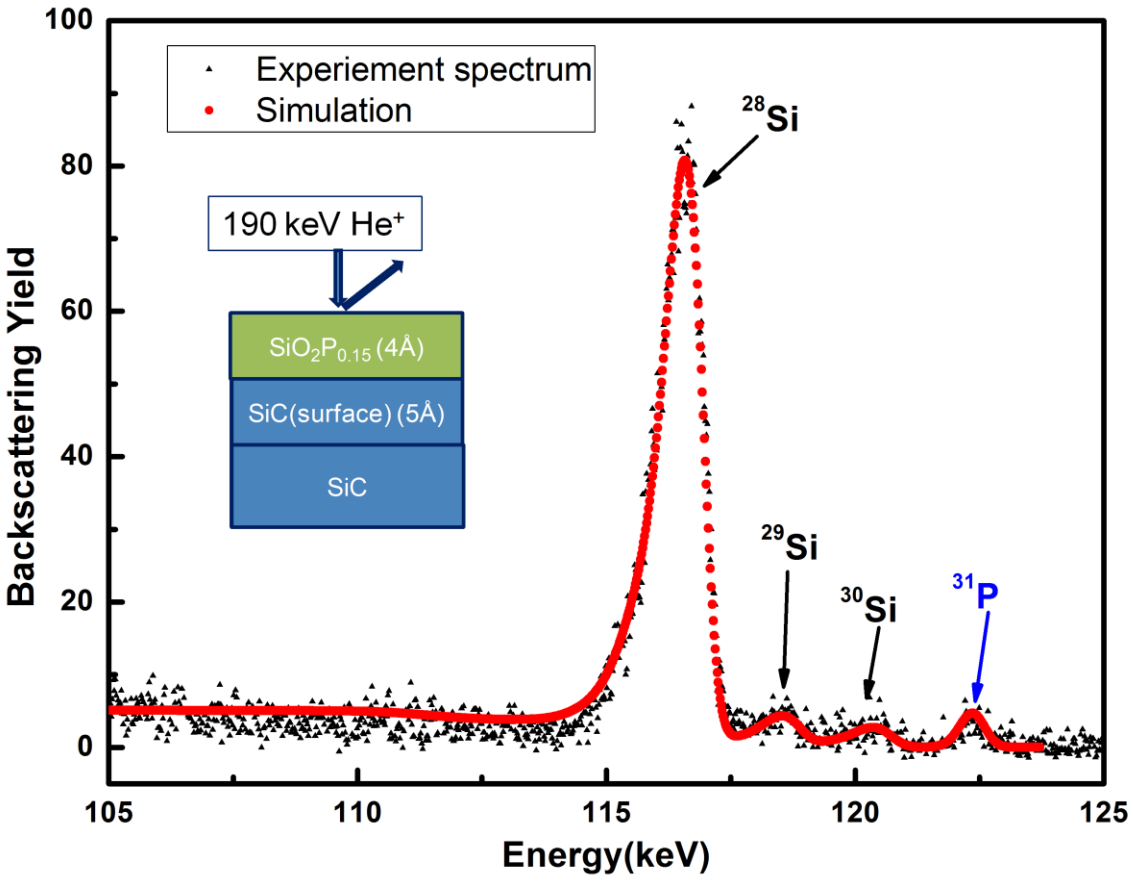

Fig. 5.4. MEIS data of etched etched PSG/SiC

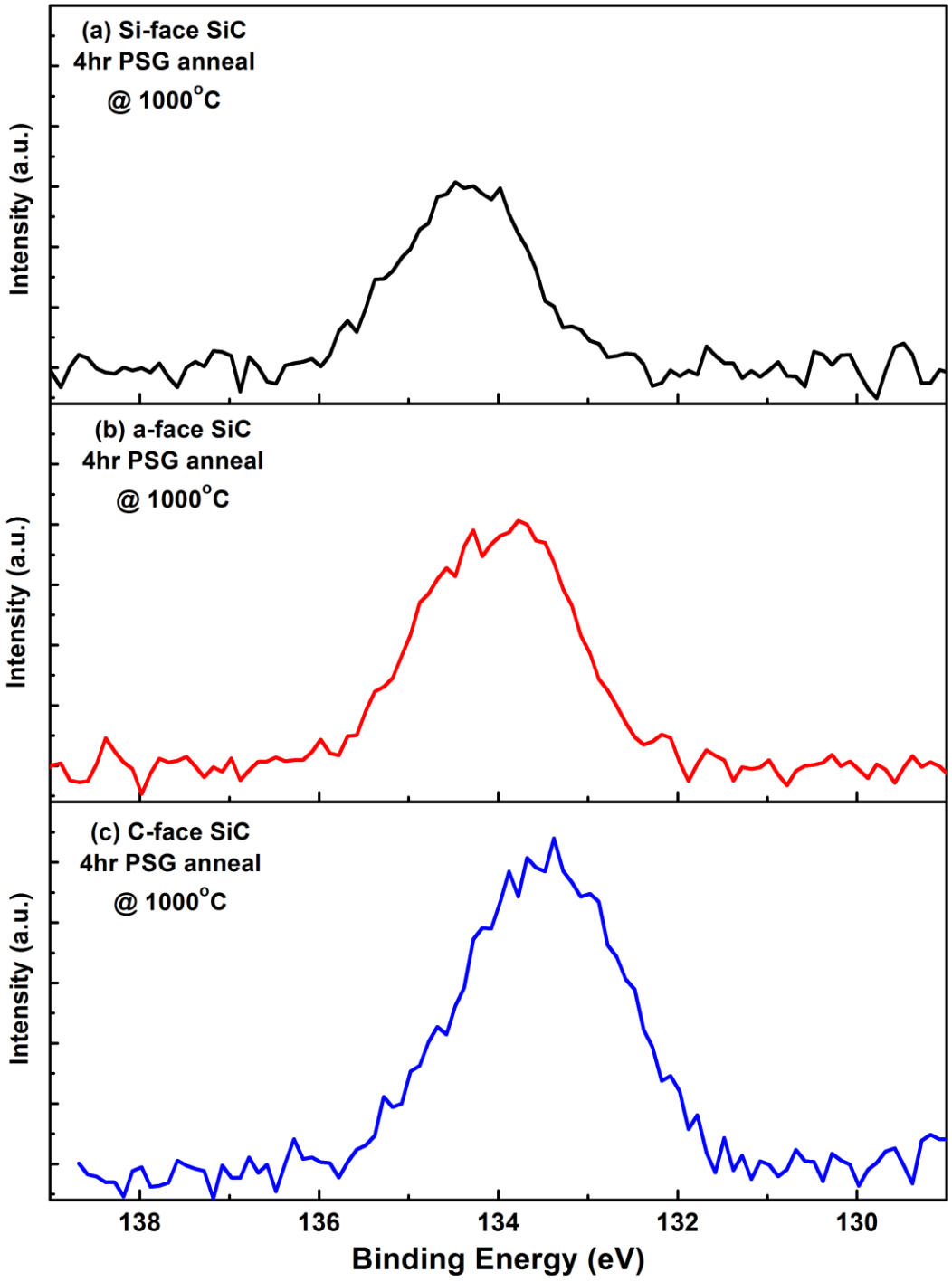

Fig. 5.5. P 2p XPS spectra of etched PSG/SiC on the (a) Si-face, (b) C-face and (c) a-face. Samples were annealed with a PDS source at 1000°C for 4 hr.

The P 2p XPS spectrum from all three crystal faces are shown in Fig. 5.5. All 3 samples were annealed with a PDS source at 1000^{o}C for 4 hr. The phosphorus coverages were determined to be 0.8×10^{14} atoms/cm^2 on Si-face, 1.2×10^{14} atoms/cm^2 on a-face and 1.6×10^{14} atoms/cm^2 on C-face. The Si-, C- and a-faces display a similar P 2p peak shape, and the peak binding energies fall in the range 133.5 eV ~ 134.5 eV, which is 0.6-1.6 eV lower than P from bulk PSG, suggesting that P atoms on all 3 crystal faces are still primarily bound to oxygen atoms which are themselves bonded to Si or C atoms. The differences of the P 2p binding energies between the different crystal faces is not well understood. One possible reason is the different structure and symmetry on the different crystal faces. On the a-face, there are 50% Si atoms and 50% C atoms on the surface, and both the P binding energy and interface coverage are intermediate to those of Si-face and C-face, as might be expected.

5.6 Phosphorus concentration profile across the SiO_2/SiC interface

The mechanism of how P generally improves device electrical performance, especially how P achieves a lower interface trap density and higher mobility than N, but with a lower interface coverage than that of N, are not fully understood. One possible argument is that similar to N,[12-14] P also acts as an efficient passivating agent for the interface traps,[12-15] which gives rise to a lower D_{it} value for devices. It is possible that P is more efficiently than N as a passivating agent. Another possible mechanism is "counter doping", proposed by Liu *et al.*,[16] which suggest that a small fraction of the passivating agent moves into near interface substitutional sites in the SiC substrate forming a counter-doped layer. If the counter-doping model is correct, it implies the formation of a

higher carrier concentration in the inversion mode of the device and leads to a higher inversion layer mobility. The counter doping mechanism will be discussed in more detail in section 5.8. It is important to note that the passivation and counter doping concepts are not contradictory to each other, and both N and P can function in both ways at the same time.

Having more information about the P depth profile at the interface would help us to better understand the role that phosphorus plays at the interface of a SiC device and how it is similar to or different from N. P atoms are distributed evenly in the PSG layer. Unfortunately, SIMS analysis does not have the depth resolution to provide a very accurate P depth profile across the interface region. In this case, MEIS (w/channeling) and angle resolve XPS are used to provide better interface P profiling.

The MEIS result (Fig. 5.4) not only provides accurate quantification but also indicates that the phosphorus is confined in a 4 Å thick un-etchable PSG layer above the SiC surface. Although the MEIS result rules out the possibility that all the P atoms are buried within the SiC substrate, it is still unclear that if the P passivated interface has the same or different structure as the N passivated interface. In order to obtain more information about the interfacial P position and chemistry, angle-resolved XPS measurements were performed. The experiment is performed with the same technique and experimental setup and parameters as in the angle-resolved experiment on N passivated SiC.

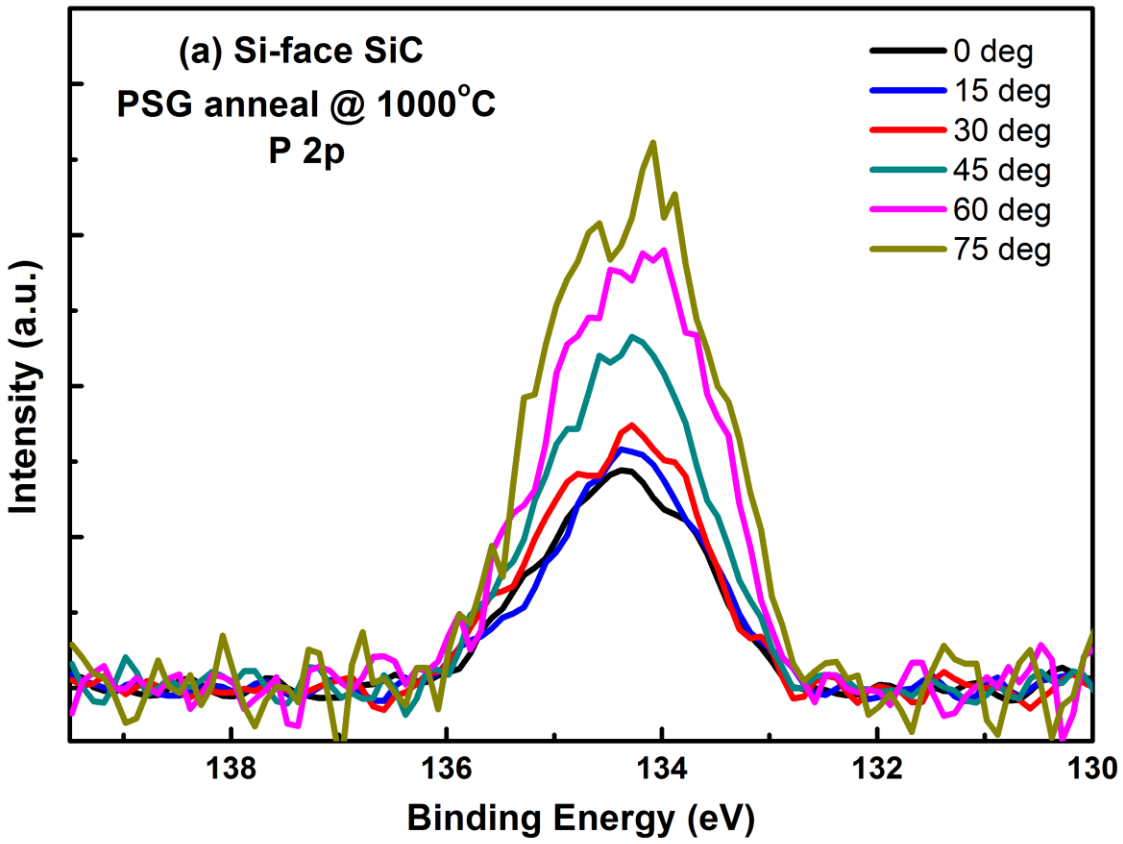

Fig. 5.6 (a) angle resolved XPS of the N 1s peak on an etched phosphorus passivated SiC. The P 2p peak intensities were normalized to a constant Si 2p peak intensity.

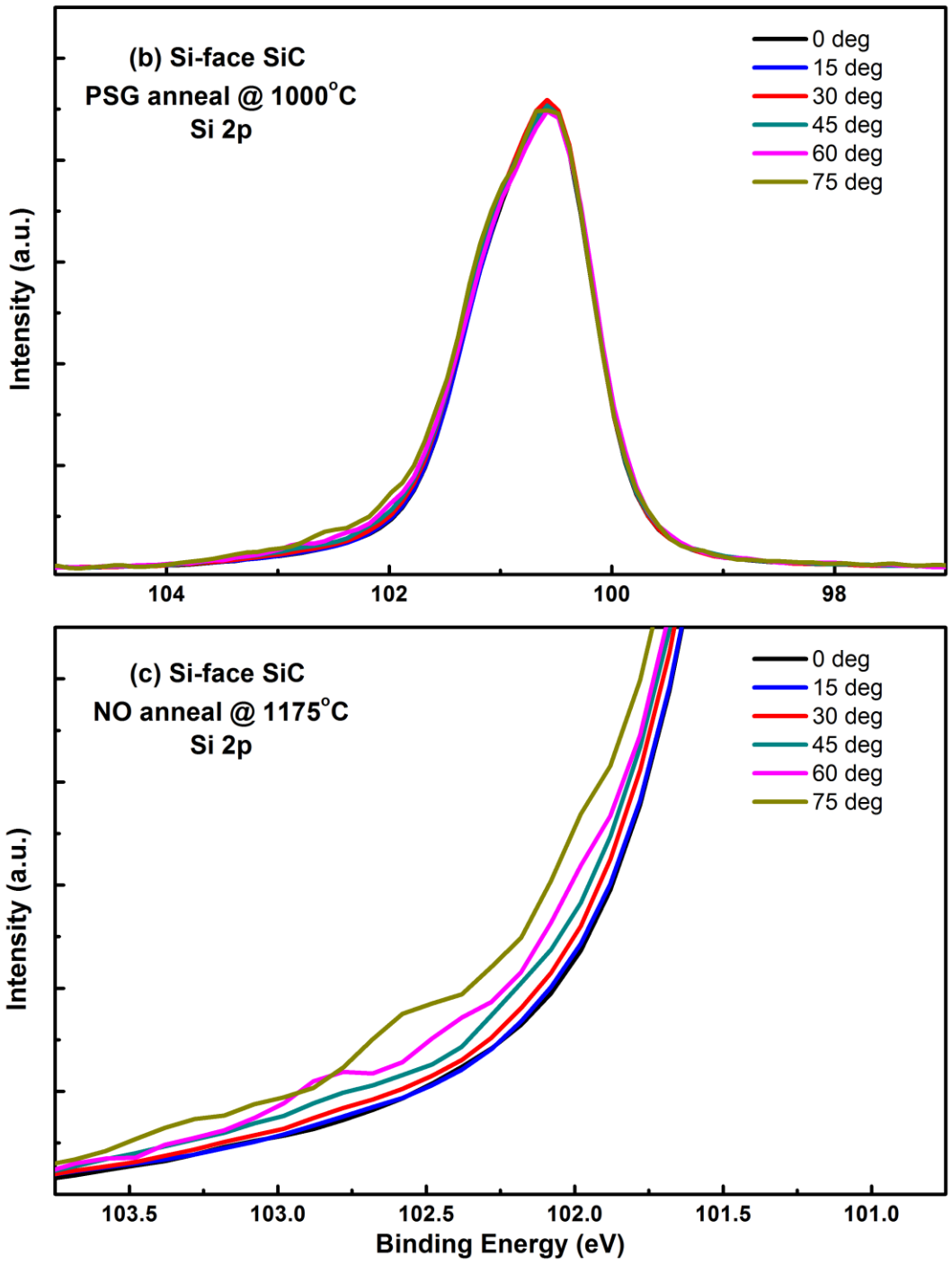

Fig. 5.6 (b). The Si 2p spectrum (normalized intensities) and (c) zoomed Si 2p spectrum of angle resolved XPS measurement on an etched phosphorus-annealed SiC.

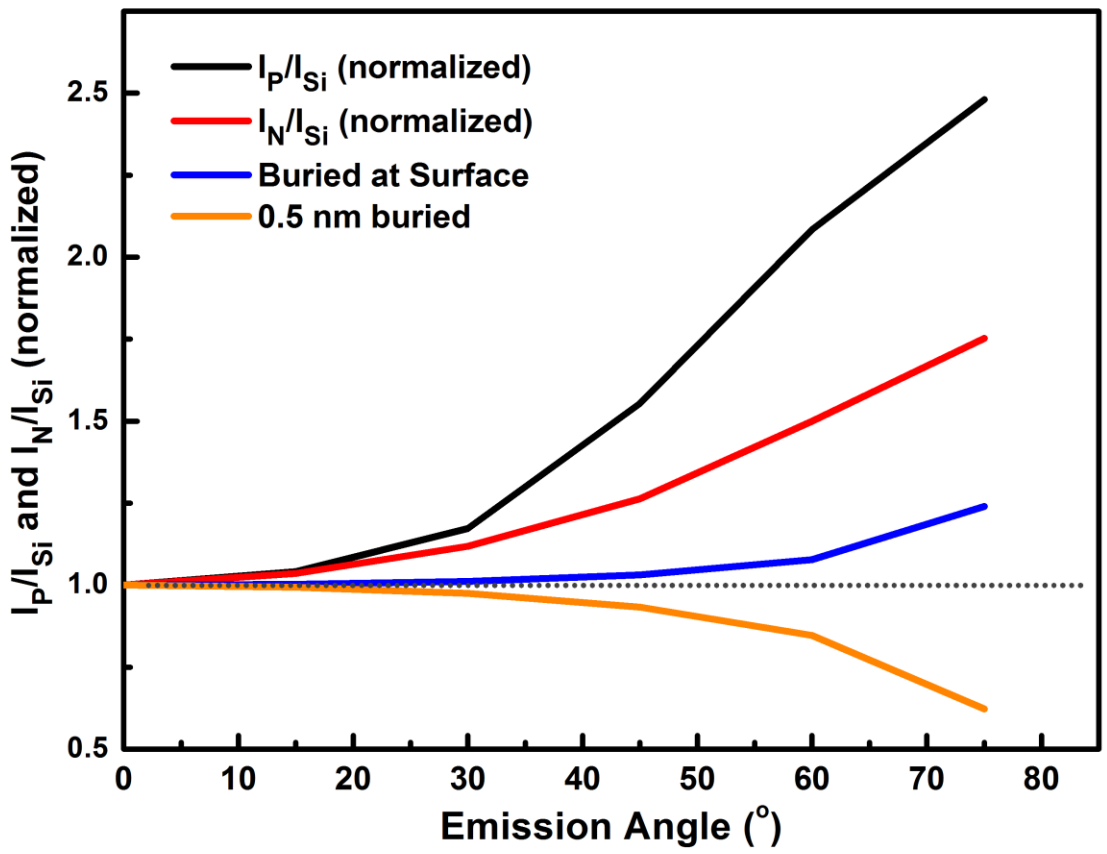

Fig. 5.7. Normalized peak intensity ratio of P and Si and normalized peak intensity ratio of N and Si.

Fig. 5.6 (a) shows the P 2p XPS spectrum of the angle resolved measurement with P peak intensities normalized to the Si 2p peak intensities. Data in Fig. 5.6 (a) shows that the P 2p peak intensity increases with increasing angle with respect to the constant Si 2p intensity; in other words, the photoelectrons from the SiC substrate are attenuated more than those of P, indicating that P atoms sit predominantly above/on top of the SiC substrate.

Fig. 5.6 (b) shows that the normalized Si 2p XPS spectrum from the angle resolved measurement, and Fig. 5.6 (c) zooms in on the peak tail region at higher binding energy.

The peak tail is identified in Fig. 3.11 as partially oxidized Si. There is a hint in Fig. 5.6 (c) that the peak tail increases with respect to the main substrate peak as the emission angle increases, indicating that these partially oxidized Si atoms sit on top of the SiC substrate, similar to the P atoms. This also supports our conclusion in section 5.3 that the HF etching leaves a layer of un-etchable PSG.

To get more insight into the structure of P-passivated SiC, we compare the angle resolve XPS result from P-passivated SiC and N-passivated SiC. We define the ratio of P 2p (or N 1s) peak intensity and Si 2p peak intensity at $0°$ emission angle (to the sample normal) as 1, and compare how they change with emission angle. The result is shown in Fig. 5.7. The orange curve shows the case that if the passivating agent is buried 5 Å inside the SiC substrate and the blue curve shows the case that the passivating agent is buried at the surface of the SiC substrate. The red curves shows the N angle resolve data acquired from an etched NO annealed SiC sample (section 3.8). In that section we concluded that the N atoms are located above the SiC substrate, passivating the Si dangling bonds in both the SiC substrate and the SiO_2. The black curve shows the P angle resolved data from an etched PSG/SiC sample. Comparing the black and red curve, it is clear that the P peak intensity is increasing more aggressively than the N peak with the increasing emission angle. This indicates that the P atoms are located at a larger distance from the SiC substrate than that of N. Considering the fact that in the PSG film, P is bound only with O, and there is no known stable compound as silicon phosphide (Si_xP_y), it is quite possible that at the P-passivated interface, oxygen atoms bond with the Si atoms and P bonds with oxygen atoms on top of Si. If the P atoms are not directly bonded to the Si, the mechanism of P passivating the interface may be an indirect one. By

bonding with the oxygen atoms on top of Si, P atoms are re-arranging the critical interfacial dielectric layer and possibly allowing oxygen to better passivate the interface dangling bonds. If true, the P may reduce the interface trap density more than N, and do so with a lower concentration.

5.7 Phosphorus uptake at the SiO_2/SiC interface

To better control device performance, one would greatly like to control the extent and location of P introduced during the passivation process. Knowing the fact that the phosphorus percentage is approximately the same in the bulk of the PSG layer and in the un-etchable PSG layer at the interface, the first approach would be to alter the P concentration in the bulk of the PSG. The blue line in Fig. 5.8 shows the bulk P concentration with respect to different PDS anneal time, and the black curve in Fig. 5.8 shows the interfacial P coverage (after etching) for the same sample. It appears that both the bulk P concentration and the interfacial P coverage saturates before 30 min. and does not increase with the longer annealing time. The red curve in Fig. 5.8 shows the interfacial P coverage of etched thin PSG samples, and it shows some variation with different PDS anneal times. It is possible that during the SiO_2 deposition step, some of the P diffused into the deposited oxide from the PSG layer giving rise to a lower interfacial P coverage. Note that the lower interfacial coverage gives a lower inversion layer mobility than the thick PSG device,[3] thus showing a correlation between the interfacial P coverage and device mobility.

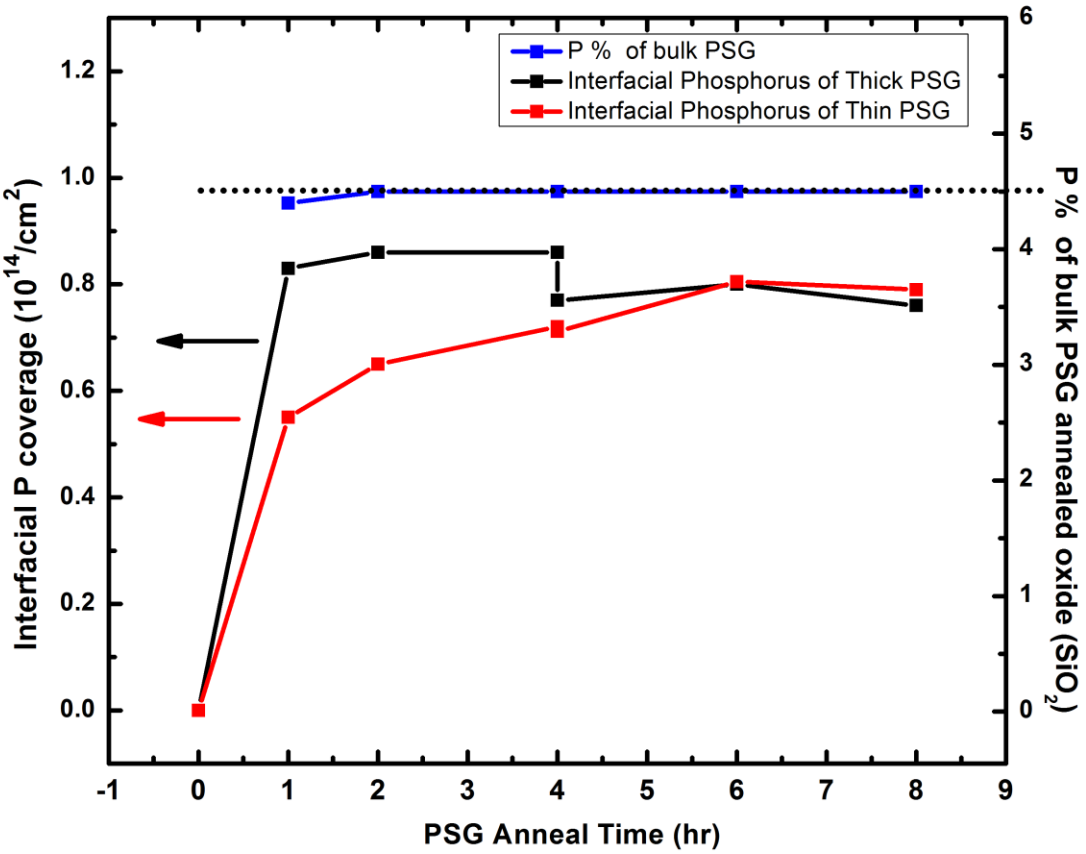

Fig. 5.8. Bulk phosphorus percentage (blue) and interface phosphorus coverage of thick (black) and thin PSG (red).

5.8 Counter-doping of SiC by phosphorus and nitrogen.

Aside from passivating defects such as Si dangling bond at the SiO_2/SiC interface, it is also possible that a small portion of the passivating agent diffuses into the bulk SiC and acts as an n-type donor. Fiorenza, et al. reported the doping concentration at the passivated and un-passivated surface measured by scanning capacitance microscopy.[17] At the SiO_2/SiC interface of un-passivated SiC, the doping concentration is measured to be $5\times10^{15}/cm^3$, same as the doping level of the SiC epi-layer.[17] In the NO-annealed system, the interfacial doping concentration reaches $5\times10^{17}/cm^3$, equivalent to $1.2\times10^{11}/cm^2$ N

atoms or 0.02% of the total interfacial N content. Finally, in the PSG/SiC interface, the interfacial doping concentration reaches $4.5\times10^{18}/cm^3$, equivalent to $1.1\times10^{12}/cm^2$ P atoms or 0.6% of the total interfacial P content.[17] In the two latter cases, the high doping concentration region is localized within the top ~3 nm of the SiC substrate. Unfortunately, the total P amount would below the detection limit of most direct physical analysis methods. The fact that the active counter dopant ratio is 30 times higher for P than N makes the counter doped P content higher than N, and consistent with the experiment result of P-passivated device (higher mobility and lower total P content).

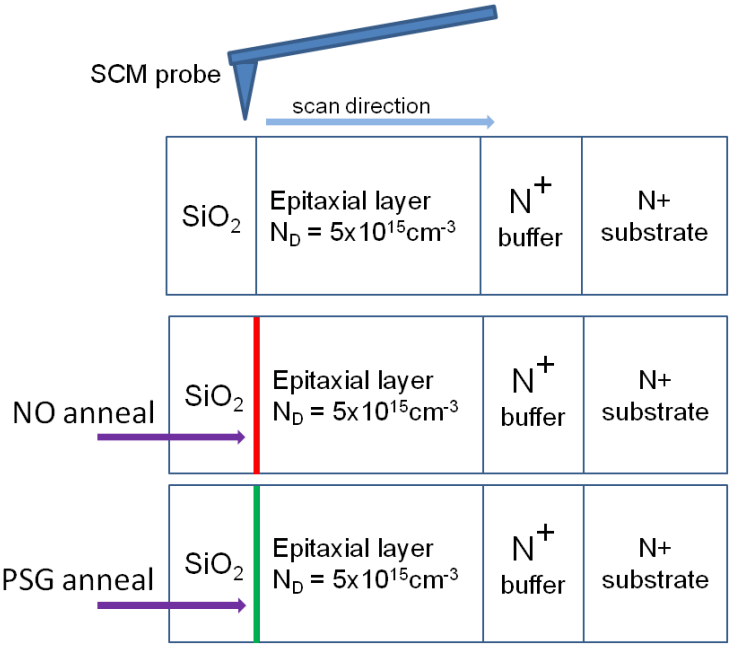

Fig. 5.9. Schematic of the cross section of a 4H-SiC MOS capacitor structure with and without passivation.[17]

5.9 Summary

In conclusion, the P-passivated SiO_2/SiC interface was examined by different techniques. P was bonded to oxygen at the interface and in the bulk SiO_2 layer. Both P and O remain after the HF etching on the SiC surface but are completely removed on the Si surface. The etching behavior of P is very similar to that observed for interfacial N on both SiC and Si surfaces. The analyses by angle resolved XPS and MEIS suggest that the majority of P atoms sit above the SiC substrate, even further away from the interface plane than N. The passivating agents, both N and P, reduced the interfacial traps, while a small portion may go into the SiC substrate and act as an n-type dopant (counter dopant).[16]

References

[1] D. Okamoto, H. Yano, T. Hatayama, and T. Fuyuki, "Removal of near-interface traps at SiO_2/4H-SiC (0001) interfaces by phosphorus incorporation," *Applied Physics Letters,* vol. 96, p. 203508, May 17 2010.

[2] D. Okamoto, H. Yano, K. Hirata, T. Hatayama, and T. Fuyuki, "Improved Inversion Channel Mobility in 4H-SiC MOSFETs on Si Face Utilizing Phosphorus-Doped Gate Oxide," *Ieee Electron Device Letters,* vol. 31, pp. 710-712, Jul 2010.

[3] Y. K. Sharma, A. C. Ahyi, T. Isaacs-Smith, A. Modic, M. Park, Y. Xu, E. L. Garfunkel, S. Dhar, L. C. Feldman, and J. R. Williams, "High-Mobility Stable 4H-SiC MOSFETs Using a Thin PSG Interfacial Passivation Layer," *Ieee Electron Device Letters,* vol. 34, pp. 175-177, Feb 2013.

[4] Y. K. Sharma, A. C. Ahyi, T. Issacs-Smith, X. Shen, S. T. Pantelides, X. Zhu, L. C. Feldman, and J. R. Williams, "Phosphorous Passivation of the SiO_2/4H-SiC Interface," *Solid-State Electronics,* vol. 68, pp. 103-107, 2012.

[5] J. Rozen, S. Dhar, S. K. Dixit, V. V. Afanas'ev, F. O. Roberts, H. L. Dang, S. Wang, S. T. Pantelides, J. R. Williams, and L. C. Feldman, "Increase in oxide hole trap density associated with nitrogen incorporation at the SiO_2/SiC interface," *Journal of Applied Physics,* vol. 103, Jun 15 2008.

[6] P. Balk and J. M. Eldridge, "Phosphosilicate Glass Stabilization of FET Devices," *PROCEEDINGS OF THE IEEE,* vol. 57, p. 1558, 1969.

[7] J. Eldridge and D. D. Kerr, "Sodium Ion Drift through Phosphosilicate Glass-SiO_2 Films," *J. Electrochem. Soc.,* vol. 118, p. 986, 1971.

[8] A. Tilocca, "Structure and dynamics of bioactive phosphosilicate glasses and melts from ab initio molecular dynamics simulations," *Physical Review B*, vol. 76, p. 224202, Dec 2007.

[9] W. B. Ying, Y. Mizokawa, Y. B. Yu, Y. Kamiura, M. Iida, and K. Kawamoto, "Annealing behavior of phosphorus in native oxide films on heavily phosphorus doped silicon," *Applied Surface Science*, vol. 100, pp. 556-560, Jul 1996.

[10] M. Rusop, X. M. Tian, S. M. Mominuzzaman, T. Soga, T. Jimbo, and M. Umeno, "Photoelectrical properties of pulsed laser deposited boron doped p-carbon/n-silicon and phosphorus doped n-carbon/p-silicon heterojunction solar cells," *Solar Energy*, vol. 78, pp. 406-415, 2005.

[11] D. M. Dobkin, "Gettering and Transport of Mobile Ion Contamination," *http://www.enigmatic-consulting.com/semiconductor_processing/selected_shorts/Gettering.html*.

[12] G. Y. Chung, C. C. Tin, J. R. Williams, K. McDonald, R. K. Chanana, R. A. Weller, S. T. Pantelides, L. C. Feldman, O. W. Holland, M. K. Das, and J. W. Palmour, "Improved inversion channel mobility for 4H-SiC MOSFETs following high temperature anneals in nitric oxide," *Ieee Electron Device Letters*, vol. 22, pp. 176-178, Apr 2001.

[13] P. Jamet, S. Dimitrijev, and P. Tanner, "Effects of nitridation in gate oxides grown on 4H-SiC," *Journal of Applied Physics*, vol. 90, pp. 5058-5063, Nov 15 2001.

[14] T. Shirasawa, K. Hayashi, S. Mizuno, S. Tanaka, K. Nakatsuji, F. Komori, and H. Tochihara, "Epitaxial silicon oxynitride layer on a 6H-SiC(0001) surface," *Physical Review Letters,* vol. 98, p. 136105, Mar 30 2007.

[15] K. McDonald, R. A. Weller, S. T. Pantelides, L. C. Feldman, G. Y. Chung, C. C. Tin, and J. R. Williams, "Characterization and modeling of the nitrogen passivation of interface traps in SiO_2/4H-SiC," *Journal of Applied Physics,* vol. 93, pp. 2719-2722, Mar 1 2003.

[16] G. Liu, A. C. Ahyi, Y. Xu, T. Isaacs-Smith, Y. K. Sharma, J. R. Williams, L. C. Feldman, and S. Dhar, "Enhanced Inversion Mobility on 4H-SiC (1120) Using Phosphorus and Nitrogen Interface Passivation," *Ieee Electron Device Letters,* vol. 34, pp. 181-183, Feb 2013.

[17] P. Fiorenza, F. Giannazzo, M. Vivona, A. La Magna, and F. Roccaforte, "SiO2/4H-SiC interface doping during post-deposition-annealing of the oxide in N2O or POCl3," *Applied Physics Letters,* vol. 103, Oct 7 2013.